sid.inpe.br/mtc-m21c/2021/01.13.15.06-TDI

SEASONALITY OF WATER AVAILABILITY, PLANT PHENOLOGY, AND PLANT TRANSPIRATION IN A BRAZILIAN CAATINGA ENVIRONMENT INVESTIGATED BY IN SITU AND REMOTE SENSING DATA

Rennan Andres Paloschi

Doctorate Thesis of the Graduate Course in Remote Sensing, guided by Drs. Laura De Simone Borma and Thales Sehn Körting, approved in December 18, 2020.

URL of the original document:
<http://urlib.net/8JMKD3MGP3W34R/43UHK8B>

INPE
São José dos Campos
2020

PUBLISHED BY:

Instituto Nacional de Pesquisas Espaciais - INPE
Gabinete do Diretor (GBDIR)
Serviço de Informação e Documentação (SESID)
CEP 12.227-010
São José dos Campos - SP - Brasil
Tel.:(012) 3208-6923/7348
E-mail: pubtc@inpe.br

sid.inpe.br/mtc-m21c/2021/01.13.15.06-TDI

SEASONALITY OF WATER AVAILABILITY, PLANT PHENOLOGY, AND PLANT TRANSPIRATION IN A BRAZILIAN CAATINGA ENVIRONMENT INVESTIGATED BY IN SITU AND REMOTE SENSING DATA

Rennan Andres Paloschi

Doctorate Thesis of the Graduate Course in Remote Sensing, guided by Drs. Laura De Simone Borma and Thales Sehn Körting, approved in December 18, 2020.

URL of the original document:
<http://urlib.net/8JMKD3MGP3W34R/43UHK8B>

INPE
São José dos Campos
2020

Cataloging in Publication Data

Paloschi, Rennan Andres.

P186s Seasonality of water availability, plant phenology, and plant transpiration in a Brazilian Caatinga environment investigated by in situ and remote sensing data / Rennan Andres Paloschi. – São José dos Campos : INPE, 2020.

xxviii + 99 p. ; (sid.inpe.br/mtc-m21c/2021/01.13.15.06-TDI)

Thesis (Doctorate in Remote Sensing) – Instituto Nacional de Pesquisas Espaciais, São José dos Campos, 2020.

Guiding : Drs. Laura De Simone Borma and Thales Sehn Körting.

1. Caatinga phenology. 2. Vegetation index. 3. Water availability. 4. Vegetation transpiration. I.Title.

CDU 630*1(213)(81)

MINISTÉRIO DA CIÊNCIA, TECNOLOGIA E INOVAÇÕES

INSTITUTO NACIONAL DE PESQUISAS ESPACIAIS

Serviço de Pós-Graduação - SEPGR

Pós-Graduação em Sensoriamento Remoto

DEFESA FINAL DE TESE DE RENNAN ANDRES PALOSCHI

No dia 18 de dezembro de 2020, as 08h 30min, por teleconferência, o(a) aluno(a) mencionado(a) acima defendeu seu trabalho final (apresentação oral seguida de arguição) perante uma Banca Examinadora, cujos membros estão listados abaixo. O aluno foi APROVADO pela Banca Examinadora, por maioria simples, em cumprimento ao requisito exigido para obtenção do Título de Doutor em Sensoriamento Remoto. O trabalho precisa da incorporação das correções sugeridas pela Banca Examinadora e revisão final pelo(s) orientador(es).

Título: "SEASONALITY OF WATER AVAILABILITY, PLANT PHENOLOGY, AND PLANT TRANSPIRATION IN A BRAZILIAN CAATINGA ENVIRONMENT INVESTIGATED BY IN SITU AND REMOTE SENSING DATA"

Observações da Banca:

Os membros da banca gostariam de deixar registrado que o aluno realizou um bom trabalho, compatível com uma tese de doutorado, mas que isso não está refletido no documento de tese que foi entregue para a banca, e portanto o aluno foi aprovado na condição de obrigatoriamente melhorar o documento escrito. O aluno deverá revisar o documento da tese de acordo com as sugestões e comentários dos membros da Banca. Deverá entregar uma nova versão do documento de tese, em 30 dias, para avaliação de seus dois orientadores, e depois terá mais 30 dias para entregar o documento final que passará por nova avaliação dos orientadores.

O aluno foi REPROVADO pelo membro Ieda Del' Arco Sanches, e APROVADO por todos os outros membros.

Eu, Ieda Del' Arco Sanches, como Presidente da Banca Examinadora, assino esta ATA em nome de todos os membros.

Membros da Banca

Dra Ieda Del' Arco Sanches - Presidente - INPE
Dra Laura de Simone Borma - Orientadora - INPE
Dr. Thales Sehn Körting - Orientador - INPE
Dra Magna Soelma Beserra de Moura - Convidada - EMBRAPA/Semiárido
Dr. Rodolfo Marcondes Silva Souza - Convidado - TEXAS A&M University

Documento assinado eletronicamente por **Ieda Del Arco Sanches**, **Pesquisadora**, em 18/05/2021, às 08:47 (horário oficial de Brasília), com fundamento no art. 6º do Decreto nº 8.539, de 8 de outubro de 2015.

A autenticidade deste documento pode ser conferida no site http://sei.mctic.gov.br/verifica.html, informando o código verificador **7340685** e o código CRC **58D106A4**.

Referência: Processo nº 01340.008652/2020-56 SEI nº 7340685

"Nothing is small if done with Love".

St. Therese of Lisieux
in *"Story of a Soul"*, 1898

For the Glory of ***God Father*** *our Creator,* ***Jesus Christ*** *our Redeemer, and the* ***Holy Spirit*** *our Paraclete.*

ACKNOWLEDGEMENTS

I thank the INPE post-graduate in Remote Sensing Sensing for the institutional and financial support, as well to all INPE professors and colleagues.

I thank the funding institutions: Higher Education Personnel (CAPES, Finance Code 001) for the scholarship granted; to the São Paulo Research Foundation (FAPESP NE/N012488/1) for the resources provided to the Nordeste project.

I thank the Government Company of Agricultural Research from the Semi-arid (Embrapa semi-árido); the Academic Unit of Serra Talhada (UAST); the Academic Unit of Garanhuns (UAG) from Rural Federal University of Pernambuco (UFRPE); the National Observatory of Water and Carbon Dynamics in the Caatinga Biome-NOWCDCB, for, among others, allowing the use of tools, academic installations, providing technical assistance and labor to carry out the installation of sensors and maintenance of equipment; Luciano Paganucci de Queiroz and his team, for leading the work of the Herbarium at State University of Feira de Santana in the species identification; Jonathan Lloyd for assisting in the management of financial and human resources and for his contributions in developing the methods.

At last but not least, I am grateful for the support of my parents, all my family, and friends.

ABSTRACT

The vegetation water use was investigated in three experimental areas in Caatinga, the largest seasonally dry forest in South America. In one of the sites, environmental drivers on phenology of woody species and their relationship with transpiration were identified and analyzed. In the other sites, the relationship between Remote Sensing data with the phenological response and the water condition of the soil was evaluated. To monitor the phenological evolution with Remote Sensing, vegetation indices were used: normalized difference vegetation index (NDVI); soil-adjusted vegetation index (SAVI) and; green chromatic coordinate (GCC). The GCC extracted from automated digital camera images in the field was used as a representative of phenology and ground truth. Were obtained NDVI, SAVI and GCC indexes from the Sentinel-2A and 2B satellites data, NDVI MYD13Q1 and MOD13Q1 from the MODIS sensor on the Terra and Aqua platforms and the NDVI calculated from the WFI camera data of the CBERS-4 satellite. Environmental factors included rain, air temperature, soil moisture, liquid radiation and vapor pressure deficit. To monitor the water condition we have installed sensors for humidity and soil matric potential. To monitor vegetation water use sap flow sensors were installed. Our study demonstrated that GCC data close to the surface played an important role in allowing individual species monitoring, while species flow data were better correlated with orbital NDVI, SAVI and GCC than with GCC close to the surface of the species. The plants wood density seemed to affect the transpiration cessation times in the dry season, since species with less wood density reach negligible transpiration values earlier, in the beginning of the dry season, than those with high density. The results show that the availability of water in the soil is the main limiting factor for transpiration for more than 80 % of the year, and that both the phenological response given by the vegetation indices and the use of water given by the sap flow are directly related to water availability when the relative saturation in the soil profile is below 0.25.

Keywords: caatinga phenology. vegetation index. water availability. vegetation transpiration.

SAZONALIDADE DA DISPONIBILIDADE DE ÁGUA, FENOLOGIA VEGETAL E TRANSPIRAÇÃO VEGETAL EM UM AMBIENTE DA CAATINGA BRASILEIRA INVESTIGADA POR DADOS IN SITU E DE SENSORIAMENTO REMOTO

RESUMO

O uso da água pela vegetação foi investigado em três áreas experimentais da Caatinga, a maior floresta sazonalmente seca da América do Sul. Em um dos sítios, foram identificadas e analizadas as infuências ambientais na fenologia de espécies lenhosas e sua relação com a transpiração. Nos demais sítios foi avaliado a relação de dados de Sensoriamento Remoto com a resposta fenológica e a condição hídrica do solo. Para monitorar a evolução fenológica com Sensoriamento Remoto foram utilizados os seguintes índices de vegetação: índice de vegetação por diferença normalizada (NDVI); índice de vegetação ajustado ao solo (SAVI) e; coordenada cromática verde (GCC). Como representante da fenologia e verdade de campo, foi utilizado o GCC extraído de imagens de câmeras digitais automatizadas em campo. Foram utilizados os índices NDVI, SAVI e GCC obtidos de dados dos satélites Sentinel-2A e 2B, os produtos de NDVI MYD13Q1 e MOD13Q1 do sensor MODIS nas plataformas Terra e Aqua e o NDVI calculado de dados da camera WFI do satélite CBERS-4. Os fatores ambientais incluíram chuva, temperatura do ar, umidade do solo, radiação líquida e déficit de pressão de vapor. Para monitorar o estado da água no solo e o uso da água na vegetação, instalamos sensores de umidade e potencial mátrico do solo e sensores de fluxo de seiva. Nosso estudo demonstrou que os dados de GCC próximos à superfície desempenharam um papel importante em permitir o monitoramento individual das espécies, enquanto os dados de fluxo de seiva das espécies foram melhor correlacionados com NDVI, SAVI e GCC orbitais do que com GCC próximos à superfície das espécies. A densidade da madeira das plantas pareceu afetar os tempos de cessação da transpiração na estação seca, uma vez que as espécies com menor densidade de madeira atingem valores insignificantes de transpiração mais cedo, no início da estação seca, do que aquelas com alta densidade. Os resultados mostram que a disponibilidade de água no solo é o principal fator limitante da transpiração durante mais de 80 % do ano, e que tanto a resposta fenológica dada pelos índices de vegetação quanto o uso da água dado pelo fluxo de seiva, estão diretamente relacionados à disponibilidade de água quando a saturação relativa no perfil do solo fica a abaixo de 0,25.

Keywords: Fenologia da Caatinga. índice de vegetação. diponibilidade hídrica. transpiração da vegetação.

LIST OF FIGURES

Page

LIST OF TABLES

Page

LIST OF ABBREVIATIONS

AWC	–	Available Water Capacity
CBERS	–	China-Brazil Earth-Resources Satellite
DBH	–	Diameter at Breast Height
EC	–	Eddy covariance
EMBRAPA	–	Empresa Brasileira de Pesquisa Agropecuária
EP	–	Earth Observation
ESA	–	European Space Agency
ET	–	Evapotranspiration
EVI	–	Enhanced vegetation index
FTSW	–	Fraction of trasnpirable Soil Water
GCC	–	Green Chromatic Coordinate
IBGE	–	Instituto Brasileiro de Geografia e Estatística
LE	–	Latent Heat
LGE	–	Lagoa grande
MODIS	–	MODerate-resolution Imaging Spectroradiometer
NDVI	–	Normalized Difference Vegetation Index
NIR	–	Near Infrared
RS	–	Remote Sensing
SAVI	–	Soil Adjusted Vegetation Index
SDTF	–	Seasonally Dry Tropical Forest
SJO	–	São João
STA	–	Serra Talhada
VPD	–	Vapor Pressure Deficit
WRC	–	Water Retention Curve

LIST OF SYMBOLS

F_d	–	Sap flow density
F_{dn}	–	Sap flow density normalized
F_{dnc}	–	Community sap flow density normalized
GCC_{ns}	–	GCC derived from near-surface camera data
GCC_{s2}	–	GCC derived from Sentinel-2 data
$NDVI_{cbers}$	–	NDVI derived from CBERS-4 data
$NDVI_{modis}$	–	NDVI derived from MODIS data
$NDVI_{s2}$	–	NDVI derived from Sentinel-2 data
s_e	–	Soil water relative saturation
$s_{e,prof}$	–	Soil water relative saturation on soil profile
Sw	–	Soil moisture storage
R_n	–	Net radiation
ΔT	–	Temperature difference
ΔT_{max}	–	Maximum temperature difference on period
Ψ	–	Soil matric potential
θ	–	Soil water moisture
θ_r	–	Residual soil water moisture
θ_s	–	Soil Water moisture on soil saturation
$\theta_{r,proof}$	–	Residual soil water moisture of soil profile
$\theta_{s,proof}$	–	Soil water moisture on soil profile saturation point
θ_{pwp}	–	Soil profile wilting point

CONTENTS

Page

1 INTRODUCTION

Monitoring and evaluating changes in vegetation water use under climatic variations is extremely important, as it allows understanding the response of ecosystem functions to climate change, such as sensitivity, resilience, speed of adaptation, and, concerning climate change, it is also a key aspect (FRANCESCONI et al., 2016; PUGNAIRE et al., 2019).

When analyzing dry forests, the water assessment is critical, since all environment is highly dependent on the water availability. At the Caatinga forest, the biggest Seasonally Dry Tropical Forests (SDTF) in South America, the high dependence on vegetation phenology (LIMA; RODAL, 2010; LIMA et al., 2012) turns evident that specific plant water use strategies are crucial to plant development and survival (TROVÃO et al., 2007).

Despite being the dominant vegetation of northeastern Brazil, with an area greater than 844,000 km^2 and more than 60% of native vegetation (MAPBIOMAS, 2019), the Brazilian Caatinga is highly fragmented, anthropized, and has only 1.2% of its total extension included within effective protected areas (ANTONGIOVANNI et al., 2020).

The Caatinga region is characterized by a warm and semi-arid climate, strongly seasonal. Most of its extension has a rainfall regime of less than 800 mm per year, spread over a period of three to six months that vary widely spatially and temporally (VELOSO, 2001). As a result, the vegetation is subject to seasonal water deficiency, being vulnerable to current climate variability and extremes, mainly in the form of intense rain and floods or dry spells, as can be seen in the analysis made by Torres et al. (2017) of the Intergovernmental Panel on Climate Change (IPCC) projections for Caatinga region. This region, compared to other Brazilian regions, presents many extreme characteristics among the meteorological parameters: the highest solar radiation, the highest average annual temperature, the lowest relative humidity rates, the highest potential evapotranspiration, and, above all, lower and irregular rainfall (REIS, 1976). This vegetation consists of trees and/or shrubs of varying height, with almost all woody as deciduous species and with an abundant presence of cacti.

Vegetation water use can be analyzed at various scales, which include canopy or leaf level, ecosystem level, regional and global level. Each of these scales involves different methodologies, that differ mainly about data acquisition. Monitor spots and individuals is possible with soil and sap flow sensors (PING et al., 2004; PASQUALOTTO

et al., 2019; REN et al., 2020). A broader view of the environment can be made using Eddy Covariance (EC) technique (COAGUILA et al., 2017; SOUZA et al., 2018) and wide aperture cameras (phenocam) (GONÇALVES et al., 2020; RICHARDSON, 2019), installed above the canopies. However, monitoring the vegetation of large regions and extracting important information, such as vegetation resilience concerning environmental conditions, or "climate forcing", is still a challenge. This challenge has been overcome in the last decade thanks to the development and popularization of Remote Sensing (RS) techniques. Part of this popularization is due to the availability of new image processing and acquisition tools, such as Google Earth Engine and the Brazil Data Cube (SIDHU et al., 2018; PICOLI et al., 2020), and free satellite image distribution. Such imagery, obtained by the actual great amount of new Earth Observation (EO) satellites, allows more refined monitoring, both spatially and temporally (RICHARDSON et al., 2018; FERREIRA et al., 2020; MIRANDA et al., 2020).

However, the use of RS techniques requires terrestrial truth data, since they indirectly measure the processes occurring on the surface or provide data to feed models that estimate these processes. As a result, many studies take advantage of combining RS with data obtained by other monitoring techniques, such as the Eddy covariance (EC) technique, soil moisture sensors, and sensors capable of measuring transpiration flow, the sap flow sensors (RICHARDSON, 2019; ALBERTON et al., 2019; GONÇALVES et al., 2020).

Although there are few studies for the caatinga region that investigate vegetation/surface processes, i.e. transpiration, evapotranspiration and carbon exchange, (TEIXEIRA, 2010; COAGUILA et al., 2017; SOUZA et al., 2018; MARQUES et al., 2020; MENDES et al., 2020), surface energy balance and components (FERREIRA et al., 2020; BORGES et al., 2020; SANTOS et al., 2020) and vegetation phenology patterns (ALBERTON et al., 2019), so far, no work brings together, under the same perspective, the different observation methodologies, comparing them with RS data and making it possible to analyze the limits of the relationships between each variable, providing a broad view of the Caatinga vegetation response from these different perspectives.

The purpose of this study is to investigate the relationship between RS derived products and the Caatinga ambient condition, represented by vegetation transpiration soil water condition. The hypotheses are: (1) Caatinga phenology at the community scale (represented by RS data) and individual scale (represented by near proximal RS data) are fully explained by soil water availability; (2) time series of optical RS

data, for the Caatinga vegetation, are strongly correlated to variations in individual's species water use; (3) variations in the sap flow signal are fully explained by changes in water availability; (4) the RS data relations with Caatinga environment identified in the previous hypotheses are consistent and applicable over different regions with different rainfall regimes and soil characteristics.

To verify the hypotheses raised, the study was divided into two parts. The first part comprises hypotheses 1, 2, and 3, presented in Chapter 4. This chapter is presented the plant water use analysis at an experimental Caatinga site, at species and community level, and phenology observed at different scales: those representatives of moderate orbital RS spatial resolution, high spatial resolution RS and near-surface cameras. Besides, the investigation on environmental drivers of and factors that limit phenology (leaf flush and senescence) and transpiration is presented. The second part, presented in Chapter 5, comprises the last hypothesis. In this chapter are provided tests on the relations described in Chapter 4 with different satellites over three experimental sites from different Caatinga regions.

2 LITERATURE REVIEW

2.1 Brazilian Caatinga

The term Caatinga is originally from Tupi-Guarani and means white forest, term that refers to the typical predominantly deciduous vegetation that exhibits whitish trunks in the dry season. However, Caatinga region can be considered as an Biome, exclusively Brazilian (OLIVEIRA et al., 2016). The Caatinga is the largest Seasonally Dry Tropical Forest (STDF) in the world, and the STDF most rich in biodiversity (QUEIROZ et al., 2017), covering several types of vegetation in the Northeast Region and occupying a approximately 10% of the Brazilian territory, mainly in the hinterland depression, with an area greater than 840,000 km^2 (MAPBIOMAS, 2019). It includes the states of Ceará, Rio Grande do Norte, Paraíba, Pernambuco, Alagoas, Sergipe, Piauí, Minas Gerais and Bahia.

In the last decade authors have proposed different borders for the Caatinga region, being the main factor the vegetative formation characteristics (VELOSO, 2001; SILVA et al., 2017). Taking into account the various factors pointed out by the specialists such as vegetation and climate properties, including aided by specialists field visits, the Brazilian Institute of Geography and Statistics (Instituto Brasileiro de Geografia e Estatística - IBGE) presented in 2019 the last biomes maps including the new Caatinga shape with detail on a scale 1: 250,000 (INSTITUTO BRASILEIRO DE GEOGRAFIA E ESTATÍSTICA - IBGE, 2019).

This least IBGE Caatinga shape (Figure 2.1) is already used by the project Annual Mapping of Land Cover and Land Use in Brazil (MapBiomas), an initiative produced by a collaborative network of co-creators formed by NGOs, universities and technology companies that, as the name says, map coverage and land use in Brazil (MAPBIOMAS, 2019). Throw the project products is possible to track the land cover and land use in Caatinga region and the others Brazilian biomes from 1985 to 2019.

Figure 2.1 - Caatinga region map.

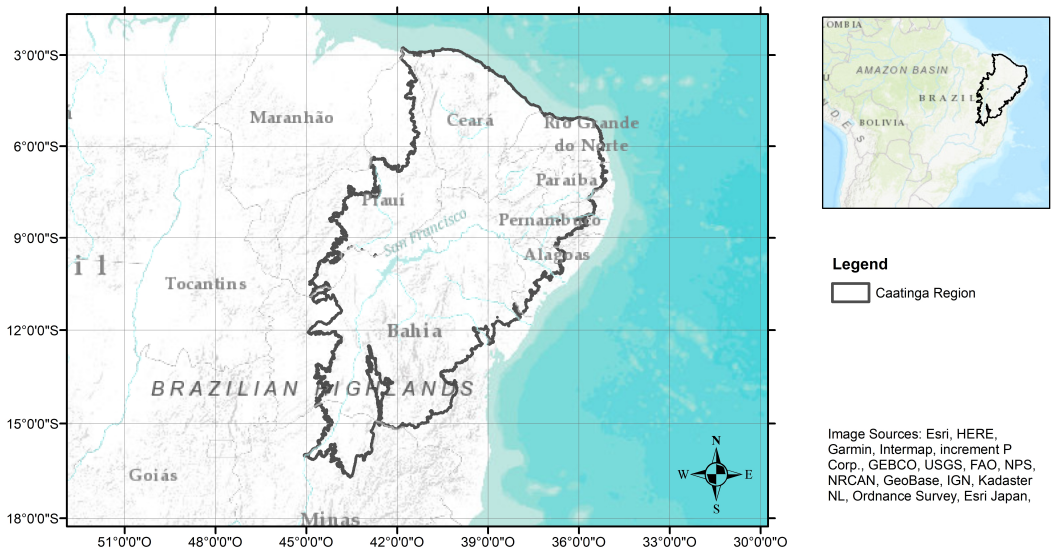

Although the Caatinga region is located in an area of semi-arid climate, it presents a wide variety of landscapes, relative biological wealth and endemic species (MESQUITA et al., 2017). However, the considered typical Caatinga vegetation is mainly found in the hinterland depressions, that consists of generally deciduous, xerophilous and sometimes prickly (VELOSO, 2001). The different types of this vegetation also extend to higher altitude regions of varying relief, varying with the soil mosaic and the water availability. Its include the arbustive/arboreal caatinga, dry and wet forest, the carrasco (very dense savanna) and open formations with domain of cacti and bromeliads (VELOSO, 2001).

In this work are used the terms "Caatinga region" as referring to the Caatinga shape presented by IBGE in 2009 (Figure 2.1) and "Caatinga vegetation" as referring to the typical caatinga vegetation found in the hinterland depressions. The Caatinga vegetation is the dominant vegetation of northeastern Brazil and Caatinga region still has more than 60% of its native vegetation (MAPBIOMAS, 2019), whoever only 1.2% of its total extension included within effective protected areas (ANTONGIOVANNI et al., 2020).

2.1.1 Caatinga climate

As mentioned, the Caatinga is characterized by a warm and semi-arid climate, most of its cover has a rainfall regime lower than 800 mm per year, spread over a period of three to six months and varying spatially. As a semi-arid climate, most BSh (arid steppe hot) and Aw (tropical savannah) climate, Figure 2.2.a, Köppen system. Caatinga is among the regions that will be most impacted by current climate changes. Torres et al. (2017) analyzed the impacts of climate change in different scenarios presented by the Intergovernmental Panel on Climate Change (IPCC) and pointed Caatinga as being vulnerable to current climate variability and extremes, mainly in the form of intense rain and floods or dry spells, with its biodiversity at risk. These authors point that for some modeled studies, future climate show desertification of the Caatinga region (BWh - arid desert hot), just as shown in the future projection derived from an ensemble of 32 climate model projections made by Beck et al. (2018) (Figure 2.2.b)

Figure 2.2 - Caatinga Kopper classification, present climate (a) and future projection (b).

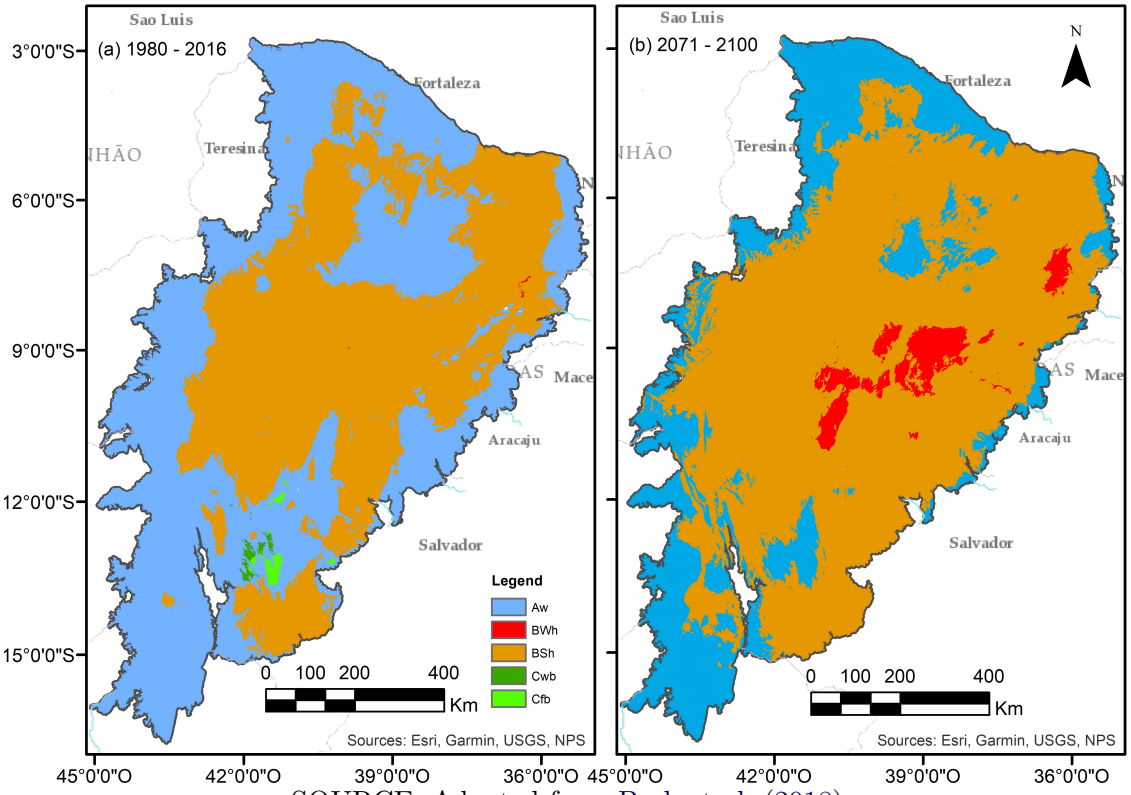

SOURCE: Adapted from Beck et al. (2018).

2.1.2 Caatinga soils

Not only is the climate important for the development of biodiversity, the soil characteristics are very important, mainly in the vegetation formation (QUEIROZ et al., 2017). Queiroz et al. (2017) point that the collected data over past 10 years support the hypotheses that recognized two major biotas in Caatinga: the Crystalline Caatinga, mostly associated with medium to highly fertile soils in the wide hinterland Depression; and the Sedimentary Caatinga, mostly associated with poor sandy soils derived from patchy sedimentary surfaces. However, the soils of the Caatinga region form a complex mosaic, ranging from shallow and stony soils to sandy and deep soils. Mostly consisting of Neosolos, Argisolos and Latossolos 2.3, as described by Brazilian soil classification System (EMPRESA BRASILEIRA DE PESQUISA AGROPECUÁRIA - EMBRAPA, 2018).

Figure 2.3 - Caatinga soil maps according to EMBRAPA classification.

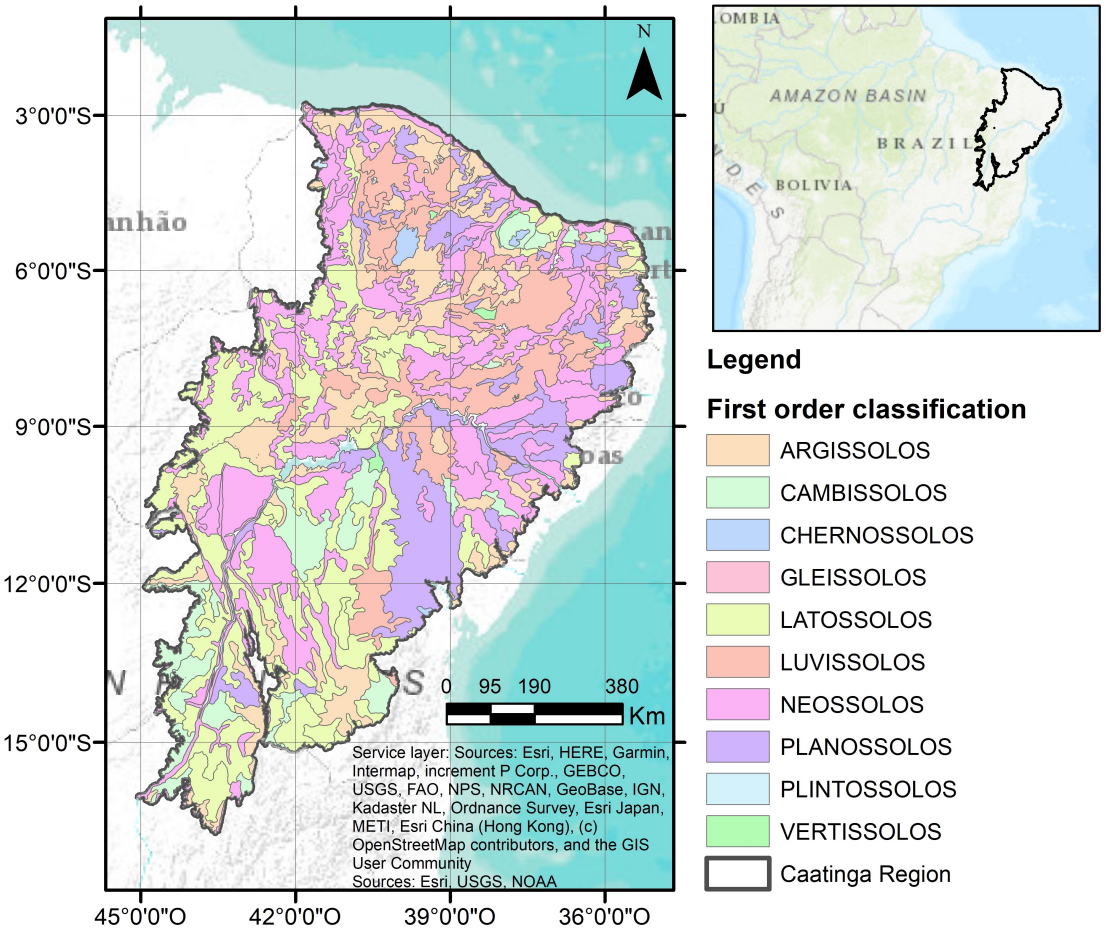

2.2 Soil water retention and soil water availability

As the soil dries, roots need to apply a higher 'suction' to extract water from the soil. Thus, the plant's capacity to extract water from the soil is more closely related to the soil matric potential (with the term 'suction' denoting the absolute value of the matric potential) than to the volumetric water content (θ, m^3 m^{-3}) (VERHOEF; EGEA, 2014). The relationship between the moisture content retained in the soil, θ, and its concurrent matric potential (Ψ, kPa), (the so-called soil water retention curve, WRC) depends on the structural characteristics of the soil (as determined by texture and pore-size distribution). This curve can be constructed from laboratory or field measurements, and its shape subsequently described by a mathematical model equation that fits the WRC.

One of the models to fit WRC is the Durner's model (DURNER, 1994). Durner's model allows to identify multi-modal systems, to adjust to soils that have more than one behavior depending on the water saturation level, it's equation is given by

$$S_e = \sum_{i=1}^{k} W_i [\frac{1}{1 + (\alpha_i \left|\Psi\right|)^{n_i}}]^{m_i} \tag{2.1}$$

where S_e is the relative saturation (dependent on the actual θ, the residual moisture content, θ_r, and the saturated moisture content, θ_s, see Equation 2), Ψ is the suction, α_i and n_i are curve fitting parameters (where m_i is derived from n_i), k is the number of "subsystems" that form the total pore-size distribution, and W_i are weighting factors for the sub-curves, subject to $0 < W_i < 1$ and $\sum W_i = 1$. For the present study $k = 2$ was used (bi-modal pore-system), separating between micro- and mesopore flow, and macropore flow. Parameter W_i was found to range from 0.32 to 0.85, depending on the soil layer.

2.3 Earth observation

With the launch of the first ERTS satellite, renamed Landsat 1, on July 23 1972, with MultiSpectral Scanner (MSS), one of those early studies was directed toward examining the spring vegetation green-up and subsequent summer and fall dry-down (STANLEY et al., 1973). Since then, many studies have been developed in an attempt to relate the phenological behavior observed by satellites to the biophysical conditions of vegetation and various space programs and satellites have been launch to increase the earth observation capability, such as Sentinel and CBERS programs.

2.3.1 Sentinel-2

Sentinel is a space program from the European Space Agency (ESA), which has been working on a constellation with various orbital satellites. The Sentinel-2 platform has spectral radiometers aimed at the visible, near and medium infrared spectrum. Having two satellites launched so far, Sentinel-2A (launch on 23 June 2015) and Sentinel-2B (7 March 2017), with a designed life time of 7 years, offering spectral bands in the visible and near infrared spectrum, with spectral bands from 10m spatial resolution (Blue 492.4 nm B2, Green 559.8 B3 nm, Red 664.6 nm B4 and NIR 832.8 nm B8). The two identical satellites operate simultaneously, phased at 180° to each other, in a sun-synchronous orbit at a mean altitude of 786 km. Together the satellites operate in with a revisit time of up to 5 days in areas close to the equator (EUROPEAN SPACE AGENCY - ESA, 2015).

2.3.2 CBERS-4

CBERS-4 satellite is part of the program China-Brazil Earth Resources Satellite (CBERS), a cooperation between Brazil and China, successfully launches a series of satellites with multispectral instruments. CBERS-4 was launched on 7 December 2014 with a original designed life of 3 years. Among the instruments on board, CBERS-4 has a Wide FIeld (WFI) camera, with spatial resolution of 64 m, revisit time of 5 days and the bands: Blue 450-520 nm B13; Green 520-590 nm B14; Red 630-690 nm B15 and; NIR B16 770-890 nm (INSTITUTO NACIONAL DE PESQUISAS ESPACIAIS - INPE, 2018).

2.3.3 MODIS

The Moderate-Resolution Imaging Spectroradiometer (MODIS) is an instrument that provides high radiometric sensitivity (12 bit) in 36 spectral bands ranging in wavelength from 400 nm to 14,400 nm (NATIONAL AERONAUTICS AND SPACE ADMINISTRATION - NASA, 2020a). Having two identical sensors were launched over different platforms, Terra (launched on 1999) with 10:30 am crossing time, and Aqua (launched in 2002) with 1:30 pm crossing time. With a original designed life of 6 years, the MODIS has 20 years of operation, performing more than 100,000 orbits, with Terra and Aqua sensors data over 20,000 journal papers (WOLFE et al., 2019). Despite the long life, Aqua will end its extended mission on 2022 due to the fuel ending (PARKINSON; GUIT, 2019) and Terra platform will get out of its operational altitude range from march 2021, losing altitude and starting to crossing no longer at 10:30 am, but at an increasingly delayed time until crossing at 9 am in 2026, when

will start the "deorbit burn trajectory" (WOLFE et al., 2019).

MOD13Q1 and MYD13Q1 products are among the various products derived from MODIS sensors. They provide NDVI in 16-day compositions, where the best pixel is chosen from each image position in this time interval. Together with the NDVI, pixel quality information and the day of the year (DOY) corresponding to the capture of each selected pixel are also provided (DIDAN, K., 2015a; DIDAN, K., 2015b).

2.3.4 Vegetation indices - VIs

The Vegetation Indices (VIs) are generally computed using simple ratios between specific bands in the electromagnetic spectrum. They are calculated from digital intensity values of electromagnetic radiation in order to assess, among others, biomass or vegetative vigor. Some relationships between bands have been defined by applying knowledge of the spectral behavior of living vegetation. This strategy can be especially effective in view of the existence of an inverse relationship between the reflectance in the spectral regions of the red and the infrared. These indices are generally used in the search to quantify the response of vegetation to a given water availability (RESTREPO-COUPE et al., 2013).

The VIs minimize the interference related to variations from the solar angle and atmospheric effects (HUETE et al., 1994), which is essential when analyzing vegetation variations over time, such as seasonal analysis.

Each index is designed according to the objective of extracting biophysical properties of the plant (i.e. vegetative vigor). Therefore, each index has a different capacity to represent the attributes of a given vegetation. For example, while Normalized Difference Vegetation Index - NDVI is sensitive to chlorophyll, Enhanced Vegetation Index - EVI is more sensitive to variations in the structural response of the canopy, including the leaf area, the physiognomy of the plant and the canopy architecture (HUETE et al., 2002).

2.3.4.1 Green chromatic coordinate - GCC

The RGB chromatic coordinates (RGBcc) indices are the most suitable type of index to detect leaf color changes, such as changes caused by leaf development and photosynthetic dynamics, and the most efficient type of index to minimise the effects of light variations (ALBERTON et al., 2019; ALBERTON et al., 2017; RICHARDSON et al., 2009; RICHARDSON, 2019; AHRENDS et al., 2009; WOEBBECKE et al., 1995). A great advantage of this approach is that it can be extracted from ordinary cameras, which

normally only cover the RGB spectrum. The green chromatic coordinate (GCC) is calculated according to the following equation:

$$GCC = \frac{Green_{avg}}{Red_{avg} + Green_{avg} + Blue_{avg}} \tag{2.2}$$

2.3.4.2 Normalized difference vegetation index - NDVI

Developed in the early 1970s (STANLEY et al., 1973), the Normalized Difference Vegetation Index (NDVI) was and still is widely used, among others, as a descriptor of vegetative vigor and other properties of vegetation (TEIXEIRA, 2010; SANTANA, 2018; SEO et al., 2019; LI et al., 2019) and as discriminator of the type of land cover (ALMEIDA et al., 2016; DINIZ et al., 2020). The NDVI is computed by the normalized difference between the reflectance in the red (Red) and near infrared (NIR) parts of the spectrum:

$$NDVI = \frac{NIR - Red}{NIR + Red} \tag{2.3}$$

2.3.4.3 Soil-adjusted vegetation index - SAVI

The SAVI is an improved NDVI with a soil effect factor (L) (HUETE, 1988). In the SAVI equation, the L is the adjustment factor of the original NDVI equation to correct soil brightness. The value of L varies according to the presence of vegetation, very high (L = 0) to no vegetation (L = 1), but in most cases L = 0.5 is used to minimize variations in soil brightness and eliminate the need for additional calibration for different soil (HUETE, 1988).

$$SAVI = \frac{(1 + L) \times (NIR - Red)}{L + NIR + Red} \tag{2.4}$$

Miranda et al. (2020) compared several indexes with the leaf area index (LAI) for the Caatinga region. In this work the authors adjusted the L factor as 0.37. This SAVI (with L=0.37) performed better as LAI predictor than others VI.

2.4 Transpiration estimation

The transpiration is the evaporation given by the physiologic process. In the vegetables this process occurs mainly through stomata. Since it is part of the photosyn-

thesis process, transpiration is highly related to plant production and it's reduction is associated to hydric stress due to lack of available soil water (JABLOUN; SAHLI, 2008).

In a environment, the transpiration is part of evapotranspiration, process that comprises evaporation others than transpiration, such as soil evaporation and intercepted rain by canopy (RAFI et al., 2019). Evapotranspiration is, in quantitative terms, the main process by which water is removed from the watershed. When it is lower than precipitation, it gives rise to rivers, lakes and groundwater formation. In arid or semi-arid climates, such as in the Caatinga, evapotranspiration may be equivalent or greater than precipitation over large periods of the year (TEIXEIRA et al., 2008). The developed methods to assess transpiration on environment level often consist in derive the transpiration from evapotranspiration such as soil water balance using instruments as lisymeters or moisture sensors, and micrometeorological techniques (RAFI et al., 2019; WILLIAMS et al., 2004)

At individual level there are techniques developed such as leaf gas exchange instruments (SÁNCHEZ-CARRILLO et al., 2001; ANYIA, 2004), plant chamber (BURKART et al., 2007) and sap flow sensors.

2.4.1 Sap flow sensors

Sap flow is a feasible way to quantify plant water use and provide insights into field-scale water consumption (DUGAS et al., 1994; FENG et al., 2019). This technique is used in detection of crop water stress (FERNÁNDEZ et al., 2001), in determining the effect of elevated CO2 on plant water use (DUGAS et al., 1994) and also to aid evaluate evapotranspiration components by improving evapostranspiration models (RAFI et al., 2019; WILLIAMS et al., 2004).

Sap flow technique have been improved (MINER et al., 2017; PASQUALOTTO et al., 2019; REN et al., 2020) and applied on diverse plant types including agriculture and natural/urban forest (ČERMÁK et al., 2004; KUME et al., 2011; PATAKI et al., 2011; MINER et al., 2017; PATAKI et al., 2011).

There are two general approaches to measuring sap flow, continuous heat balance (HB) methods and apparent heat pulse velocity methods (HP) (MINER et al., 2017). Both techniques apply heat to the stem and detect the rate of sap flow by monitoring the stem's thermal changes (MINER et al., 2017). The HB method involves solving the heat balance over a stem section by applying constant or variable power to

continuously heat the tissue. The HP sap flow techniques determine the apparent heat pulse velocity (V). The heater probe releases a heat pulse of short duration that is carried via convection and conduction as a tracer in the transpiration stream. The HP velocity is then calculated by measuring temperature differences at defined locations around the heater (MINER et al., 2017).

The majority of methods developed measuring sap flow density utilize heat pulse (HP) methods (MINER et al., 2017). However the Granier's continuous heat sap-flux density method (GRANIER, 1985), is probably the most applied method to compute transpiration fluxes (PASQUALOTTO et al., 2019) due to its simplicity and effective compromise between theory and data availability (PING et al., 2004; PASQUALOTTO et al., 2019; BAIAMONTE; MOTISI, 2020).

While the HB method has the cited advantages over HP techniques, it requires significant power inputs, which can be a particular disadvantage at remote sites (MINER et al., 2017). However recently sap flow HB devices can reduce the power consumption by reducing power loss by the use of higher efficiency power controllers, such as switched-mode power supplies.

According to the Granier's TDP method, two probes are installed in each tree trunk in contact with the xylem, separated by 10-15 cm. The upper probe was equipped with an electric resistance, heated at a constant power, while the lower probe remained at tree temperature.

The working principle is that the sap flow cools the upper probe, thereby decreasing the temperature difference between the heated and non-heated probes (ΔT, $^{\circ}C$), so that F_d is inversely proportional to the temperature difference. Sap flow density is empirically given by Granier (1985):

$$F_d = 118.99 \times 10^{-6}[(\Delta T_{max} - \Delta T)/\Delta T]^{1.231} \tag{2.5}$$

where ΔT_{max} corresponds to the maximum temperature difference, for which $F_d = 0.0$.

Due to changes in the thermal equilibrium conditions of the xylem, ΔT_{max} may differ between days and hence will vary throughout the monitoring period (PING et al., 2004). Therefore, some adjustments may be necessary, such as improving the thermal insulation of the probes with thermal blankets (BUTZ et al., 2018) and adjusting the

ΔT_{max} as time goes by (PING et al., 2004).

These techniques are easily applied in controlled experiments, but the number of sensors necessary to measures sap flow at field scale, the high cost of commercial devices coupled and the need for replication can make it impractical to adequately quantify SF in many cases (MINER et al., 2017). Therefore authors have been recurring to own crafted probes (LOPEZ, 2015; MINER et al., 2017) and developed they own low-costs logger and power control devices, mainly based on accessible and open source Arduino Platform (MINER et al., 2017; CÁRDENAS et al., 2019; JOHN et al., 2020).

3 GENERAL METHODOLOGY

3.1 Study area

To carry out the study, three monitoring regions were stipulated, called in this work as study sites. Both study sites are areas of Caatinga vegetation in the state of Pernambuco (Figure 3.1), in the municipalities of Lagoa Grande (LGE), Serra Talhada (STA) (7°58'12"S, 38°23'06"W, 455 m a.s.l.) and São João (SJO). Our study took place from April 2018 to March 2019.

Figure 3.1 - Map of study area site locations.

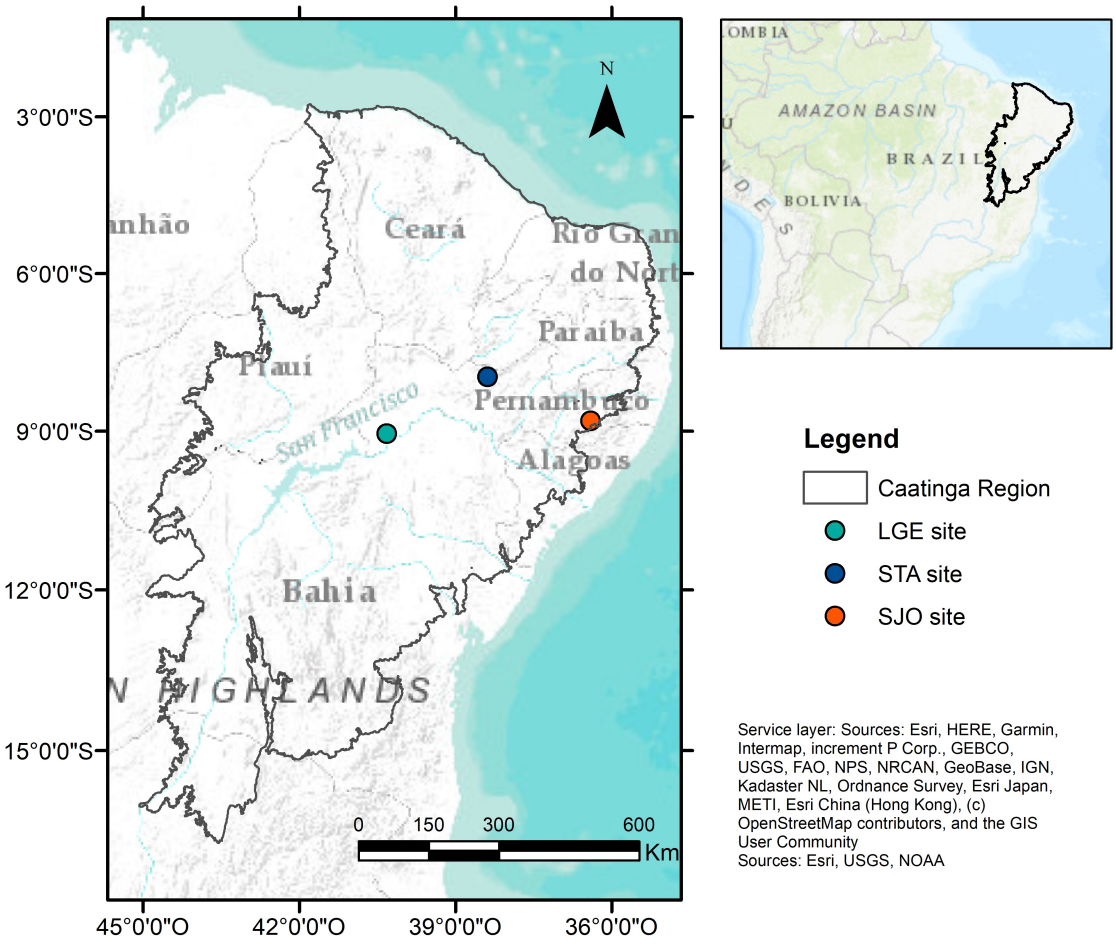

About the climatic characteristics of each site we used here the nearest cities that have information about their climatic normal's.

The city of Petrolina, about 45km from the LGE site, is located in the center of the Caatinga, in the ecoregion of the Meridional Sertaneja Depression, and is popularly considered as the capital of the "Sertão". Its dominant vegetation is the shrub-to-tree, hyperxerophytic Caatinga. The average annual rainfall is 435mm, the average annual temperature is 24.8 °C, and is 381m above sea level (CLIMATE-DATA.ORG, 2019). Compared with the other 3 sites, it has the lowest annual rainfall, highest average temperatures, and lowest altitude.

The city of Serra Talhada, about 10km from the STA site, slightly less arid than Petrolina, also in the Meridional Sertaneja Depression, presents annual precipitation of 686mm, an average temperature of 23.8 °C, and altitude of 438m (CLIMATE-DATA.ORG, 2019).

São João city, about 12km of SJO site, is the least arid region chosen. It is already located in Agreste Pernambucano, the limit of the Chapada Diamantina ecoregion also considered a transition region between the Sertão and the Zona da Mata. It has an average annual temperature of 20.4 °C, an altitude of 717m, and an annual rainfall of 885 mm (CLIMATE-DATA.ORG, 2019). The native vegetation is made up of Subperennial Forest, with parts of the Hypoxerophilous Forest.

3.1.1 Experimental strategy

The experimental design is shown in the flowchart (Figure 3.2). In terms of ground data, the experimental strategy consists of (i) measuring the sap flux density (F_d) on individual tree species found within the monitoring plot and normalizing it among the sampled species (F_{dn}); (ii) upscaling the normalized flux density (F_{dn}) to the level of the plot (or community; F_{dnc}); (iii) comparing the F_{dn} with the soil water availability. The purpose of these measurements was to evaluate the main drivers affecting the physiological response of Caatinga trees (i.e., the plant-water availability and VPD). To test the relationship between plant physiology patterns (sap flow) and leaf phenology, we used VIs obtained from different datasets.

Figure 3.2 - Flowchart of the experimental design.

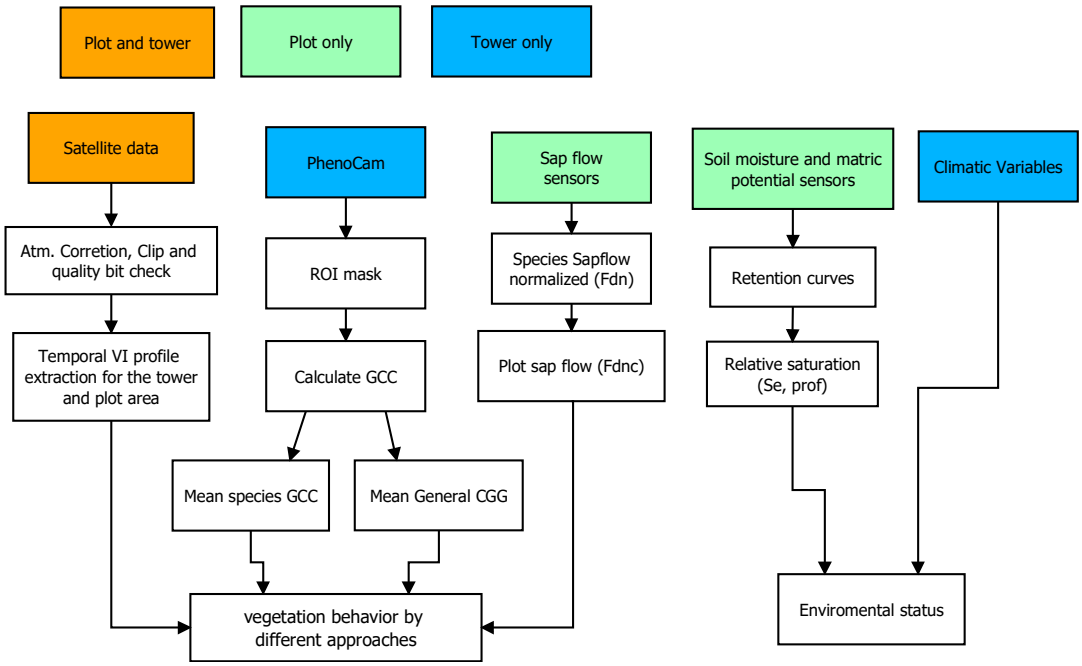

3.2 Meteorological data

Meteorological variables for this study were collated from May 2018 onwards. The variables analyzed were rainfall (P), evapotranspiration (ET), Net radiation (R_n), air temperature (T_{air}) and vapor pressure deficit (VPD).

In STA, rainfall was measured with a rain gauge. R_n was measured with a net radiometer (NRLITE, Kipp & Zonen, Delft, Netherlands). To calculate ecosystem ET, half-hourly turbulent fluxes of latent heat (LE) above the canopy were estimated continuously using the EC technique consisting of a three-dimensional sonic anemometer (model CSAT3, Campbell Scientific Inc., Logan, UT, USA) and a fast-response CO_2/H_2O infrared gas analyzer (model LI7500DS LI-COR Inc., Lincoln, NE USA). The raw data were recorded at a rate of 10 Hz and processed using the software EddyPro v. 7.0.4 (LI-COR Inc.) where coordinate rotation and Webb-Pearman-Leuning corrections were performed. The gaps in the dataset, due to system malfunctions, extreme rain events, and power failure, were filled using the REddyProc package (WUTZLER et al., 2019), using the R programming language (R CORE TEAM, 2019). Sensible flux (H, Wm^{-2}) was also measured in the tower. For more details about site instrumentation, please see (SILVA et al., 2017).

3.3 Soil moisture and soil matric potential

To monitor soil moisture and soil matric potential, inside both monitoring plots (LGE, STA and SJO), were installed profiles with soil moisture sensors (5TM, Decagon Devices, Pullman, WA, USA) and matric potential sensors (MPS-6, Decagon Devices, Pullman, WA, USA) were installed. Data were recorded every 20 minutes on a self-manufactured data logger based on the Arduino Platform (see Appendix A), powered by solar panels and batteries and programmed with the standard calibration equation that describes the relationship between the dielectric constant and volumetric soil moisture content for mineral soils (TOPP G.C.AND DAVIS; P.ANNAN, 1980), recommended by Decagon Devices (DEVICES, 2017).

The total profile soil moisture content (θ_{prof}) was computed taking into account the thickness of the soil layer represented by each sensor. Each sensor was assumed to be at the center of a layer that started and ended half-way in between the two nearest sensors. The distance between these pairs of sensors defined the thickness of the layers, which was multiplied with the soil moisture content and summed, generating a total soil moisture storage value for each profile. So despite the depth where the sensor was installed, the total depth of the monitored soil moisture was 77.5 cm. Subsequently, the values of the three profiles were averaged to obtain a single total soil moisture storage value for the monitoring plot (S_w), expressed in mm of water. S_w was then normalized between 0.0 and 1.0, taking into account the minimum S_w and maximum S_w values in the period.

At LGE site three profiles were installed (P1, P2 and P3) with sensors located at depths of: 5, 15, 25, 40 and 50 cm; the total soil depth considered was 55cm. At STA site 3 profiles were installed with sensors at depths of: 5, 15, 25, 40 and 65 cm were installed; the total soil depth considered was 77,5cm. At SJO 2 soil profiles, one with sensors located at depths of: 5, 15, 25, 40 and 65 cm; and in the other with sensors at depths of: 60, 80, 90 and 100 cm. A summary of depths of soil moisture and matric potential sensors are presented on Table 3.1.

For this study, the equations that describe the WRCs for each depth, based on field observed data of θ and Ψ, were determined with the Durner model (DURNER, 1994), using the software SWRC Fit (SEKI, 2007). To avoid the effect of the hysteresis on the measured data, we only used data (θ and Ψ) for periods when the soil was drying out.

The residual moisture content θ_r and the saturated moisture content θ_s values for

Table 3.1 - Sensors depth in field profiles, soil water moisture (w) and matric potential (p) sensors, into LGE, STA and LJO sites.

	LGE prof. depths (cm)			STA prof. depths (cm)			SJO prof. depths (cm)	
Depth	P1	P2	P3	P1	P2	P3	P1	P2
1	5-w,p	5-w	5-w	5-w	5-w,p	5-w	5-w,p	40-w
2	15-w,p	15-w	15-w	15-w	15-w,p	15-w	15-w,p	60-w
3	25-w,p	25-w	25-w	25-w	25-w,p	25-w	25-w,p	80-w
4	40-w,p	40-w	40-w	40-w	40-w,p	40-w	40-w,p	90-w
5	50-p	50-w,p		65-w	65-w,p	65-w	65-w,p	100-w

each layer, fitted parameters of the Durner equation, were used to calculate a layer thickness-weighted profile-average $\theta_{r,prof}$ and $\theta_{s,prof}$. Together with the profile averaged volumetric soil moisture, θ_{prof}, these values were used to calculate the relative saturation of the entire soil profile ($S_{e,prof}$):

$$S_{e,prof} = \frac{\theta_{prof} - \theta_{r,prof}}{\theta_{s,prof} - \theta_{r,prof}} \tag{3.1}$$

The data presentation and discussion were conducted in terms of the relative soil moisture content (S_{prof}) because it allows for a better comparison among sites. However, we also provide the Available Water Capacity (AWC) ($\theta_{s,prof} - \theta_{r,prof} \times soildepth$) because this information can be useful to other researchers working on Caatinga vegetation, and related soil environment.

Perhaps, a more meaningful normalization of the volumetric soil moisture content would be achieved using θ_{fc} and θ_{wp} (VERHOEF; EGEA, 2014), as their difference theoretically represents the soil moisture range over which vegetation can extract water from soil, i.e., the plant-available water; this normalized soil moisture content is called the fraction of transpirable soil water (FTSW).

However, since in the measured time-series there are θ_{prof} values lower than soil profile wilting point (θ_{pwp}), it would imply negative values of FTSW. Zeroing the negative values, as suggested by (BEST et al., 2011), would be inappropriate in our case, since the period corresponding to the driest part of the dataset is important in the context of our research questions, e.g. in relation to the (rate of) response of the vegetation at the beginning of a new rainy season to the initial increase in soil moisture content.

3.4 Remote sensing data

3.4.1 Green chromatic coordinate

To obtain the individual GCC, a downward-facing digital hemispherical Mobotix Q 25 lens camera (Mobotix AG-Germany) was placed in the EC flux tower attached to an extension arm facing south (northeast of the monitoring plot) at a vertical distance of 6 m from the top of the canopy. The camera was powered by a 12 V battery that was charged by solar panels. The camera was set to automatically take a sequence of five JPEG images (with a size of 1280 × 960 pixels) in the first 10 minutes of each hour, from 6h00 to 18h00 (UTC-3), on a daily basis, as described in Alberton et al. (2014) and Alberton et al. (2017).

Field surveys were conducted to identify and compile a list of the main plant species captured by the field of view of the camera. Next, the identified individuals were matched with the crowns observed in the images. Raw images were initially screened visually to remove the saturated ones, showing evidence of some digital registration failure, or when the lens had been removed for cleaning. The remaining images were analyzed in terms of the contribution of the relative brightness of red, green, and blue color channels (RGBcc – (WOEBBECKE et al., 1995)), as described by Richardson et al. (2009), Ahrends et al. (2009), Alberton et al. (2014), Alberton et al. (2019).

Orbital GCC (GCC_{s2}) was calculated using Sentinel-2 data in order to verify differences between the proximal GCC and satellite GCC. GCC_{s2} was calculate with bands: 490 (blue-B2), 560 (green-B3) and 665 nm (red-B4), all bands with 10 m resolution.

3.4.2 NDVI

To capture the community-wide phenological response through the use of satellite data, the NDVI was used. The enchanted vegetation index (EVI) was previously tested, however since the initial tests the NDVI showed better correlations and that is why it was selected. The NDVI was derived from orbital images was obtained by using data from three different satellite missions, each with different spatiotemporal resolutions. The one with the highest spatial resolution and a relatively recent launch date concern the Sentinel-2 A and B satellites, S2A and S2B. The second multispectral data source relates to an already consolidated and widely used sensor, the Moderate-Resolution Imaging Spectroradiometer (MODIS), aboard the Terra and Aqua satellites. And the third, from the CBERS-4/WFI, obtained from the Brazil

Data Cube. For the MODIS sensor, we used the NDVI provided by the MOD13Q1 and MYD13Q1 products (DIDAN, K., 2015a; DIDAN, K., 2015b). Thus, different pixels present in the same NDVI image composition may have been acquired on different days. Instead, we considered the acquisition date of each pixel, dates that are provided with the product, and not the composition date.

The Sentinel-2 NDVI ($NDVI_{S2}$) was calculated from the bands 665 and 842 nm, Red-B4 and NIR-B8, respectively, of the 10 m spatial resolution. The CBERS NDVI ($NDVI_{cbers}$) was calculated from the two bands 660 nm and 830 nm, Red-B3 and NIR-B4, respectively, of the 64 m spatial resolution.

As the pixel size of the NDVI MODIS product is greater than the size of the monitoring plot (Figure 3.3), only the pixel that coincided with the monitoring area was considered. We assumed that the monitoring plot is homogeneous and without border effects. In Sentinel-2 images, the pixels were cut out using the monitoring plot shape, and all the pixels of the monitoring plot were selected. In the case of CBERS-4, pixels with an overlap area in the plot area were selected. After the central pixels representing the monitoring plot were extracted, GCC and NDVI were calculated. Next, an average of the values was extracted for the monitoring plot.

Figure 3.3 - Modis, CBERS/WFI and Sentinel-2 pixel area coverage over STA site.

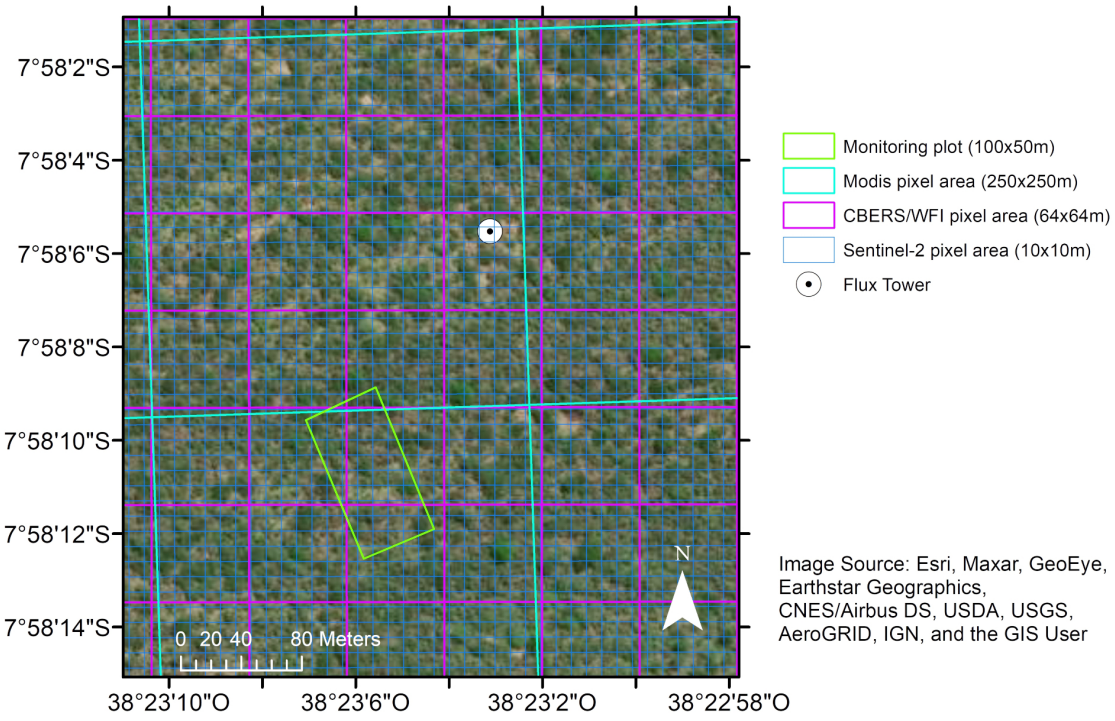

To compare satellite data (i.e., orbital RS data) with data from phenocam (i.e., near-surface RS data), we calculated the SAVI, NDVI and GCC from Sentinel-2 for the tower region, where the phenocam is installed. For this calculation, a 50 m radius circle around the EC flux tower was considered as the footprint for the phenocam view.

3.4.3 Satellite data correction

The atmospheric correction procedure relies on each sensor characteristics. The $NDVI_{modis}$ from product MOD13Q1 and MYD13Q1 was filtered by the pixel quality information provided with the product.

The Sentinel-2 images were corrected to represent surface reflectance using the sen2cor plugin that is part of the Snap software. A cloud filter was applied in Google Earth Engine using the cloud mask generated by the sen2cor plugin; however, a second visual analysis was necessary because some cloudy images were not automatically detected by the algorithm. The atmospheric correction was performed for Sentinel-2/MSI images using the Sen2cor with cirrus correction (LOUIS et al., 2016).

The CBERS-4/WFI images were obtained from Brazil Data Cube (BDC) project (PICOLI et al., 2020), that applies the atmospheric correction by using MS3 (SILVA; ANDRADE, 2013).

3.5 Sap flow

3.5.1 Sap flow measurement

Granier's thermal dissipation method (GRANIER, 1985) was used. In order to assess the sap flow density (F_d, $g\ m^{-2}\ min^{-1}$) in twenty plant individuals belonging to 5 different species in each site (LGE, STA and SJO), about a hundred of sap flow sensors built.

In a natural environment, the distance between trees of the same species is uncertain and the loss or interference of signal in the wires can compromise it. Because of this, a logger for each monitored individual was used, reducing the maximum wire length necessary to connect the probes. However, the cost of commercial sap flow loggers in relation to the limited budget makes the experiment unfeasible. Therefore, a low-cost logger based on the Arduino platform was developed.

The sensor probes were handcrafted using copper and constantan wires (thermocouples type T), cooper wires to make the heating resistance, needles as the external probe, and aluminum tubes to protect the heating resistance (Figure 3.4). A manual published by Lopez (2015) shows the process used to craft the probes.

The power (W) applied to an electric resistance (R) is given by:

$$P = I^2 \times R \tag{3.2}$$

where P is adjusted to 0.03 W by a current (I, A) regulator according to the heating resistance (R, Ω).

I vary according to the voltage (V) applied to the resistance as follow:

$$I = V/R \tag{3.3}$$

since the equipment was supplied by solar panels and batteries, V supplied vary along the day, affecting the power applied to the heating resistance and being nec-

Figure 3.4 - Diagram of the heat dissipation probes.

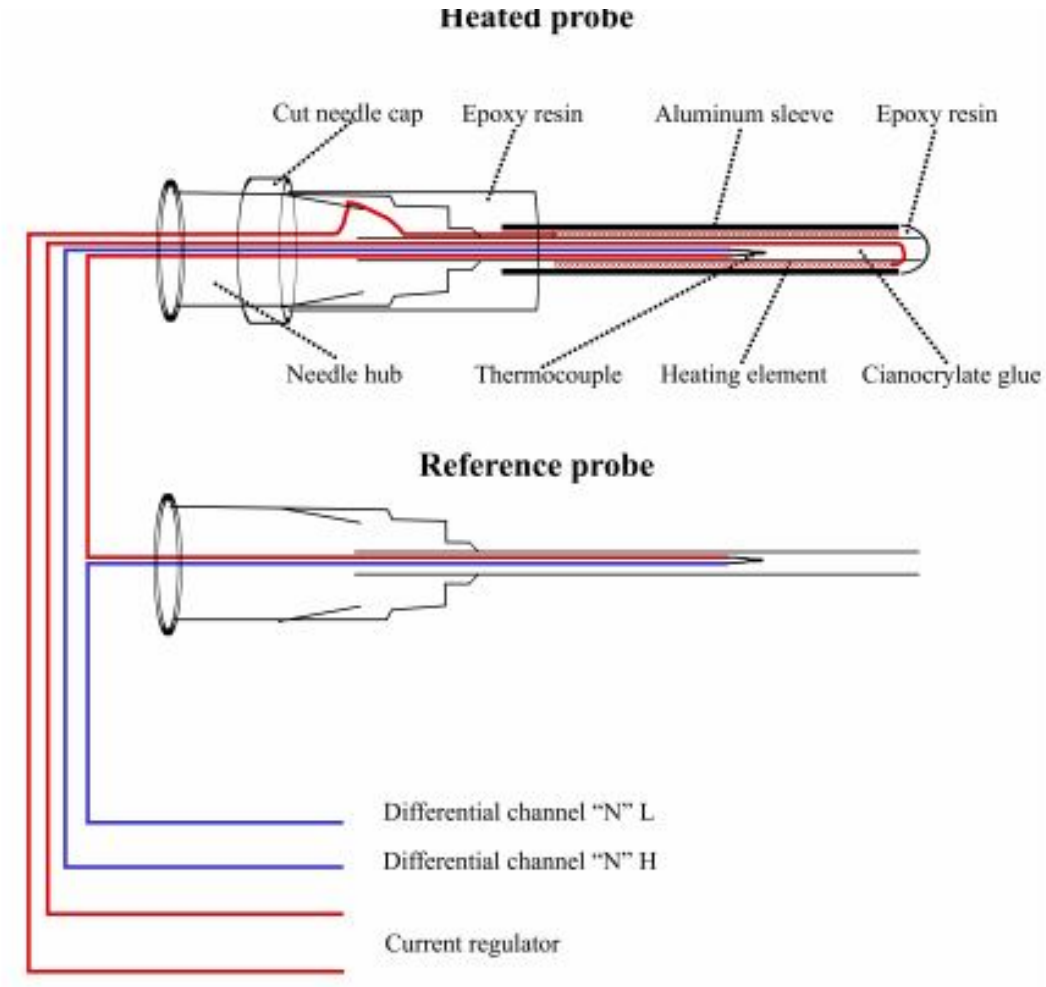

SOURCE: Lopez (2015).

essary a current regulator (PING et al., 2004; CÁRDENAS et al., 2019). However, since the heating resistances were handcrafted, their R may vary from probe to probe. Therefore, to guarantee the same electric power to each heated probe, a power regulator was design instead of a current regulator. Because it's not possible to measure power directly the adjustment was made varying the voltage and measuring at the same time the V and I to match the specified P as follows:

$$P = V \times I \tag{3.4}$$

Since R is unknown, a calibration algorithm was created to calculate P by check

both V and I while varying V by Switched-mode power supplies with a digital potentiometer (Figure 3.5). As supply battery voltage varies during the day, the power calibration was applied every 10 minutes.

Figure 3.5 - Diagram of the heating probe power calibration.

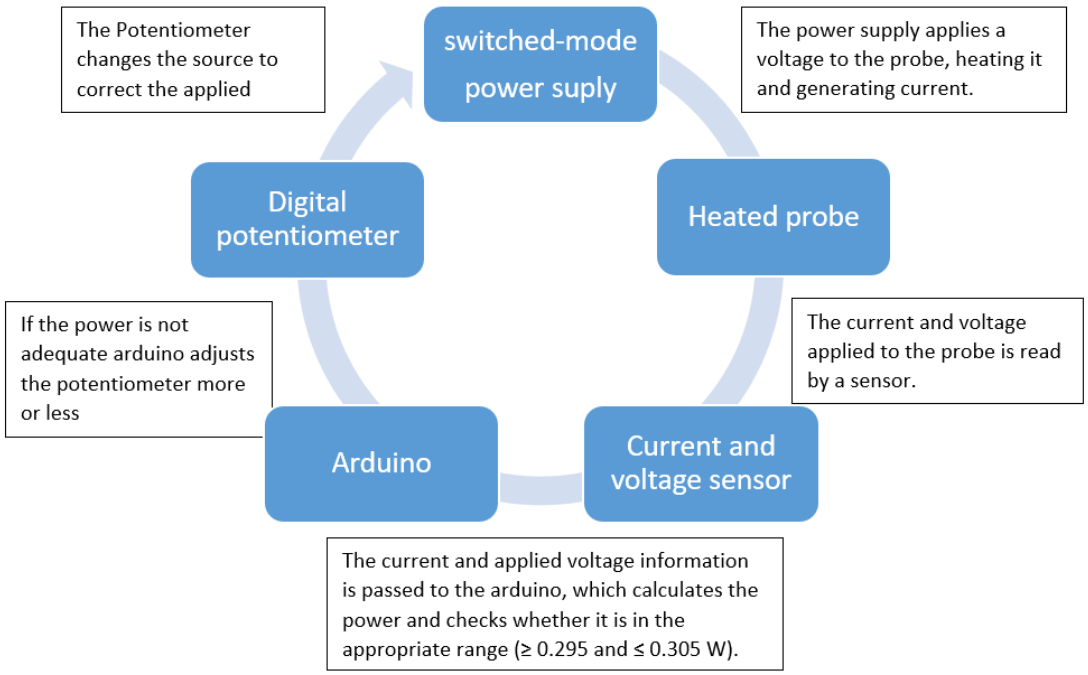

The thermocouples type T temperature Sensitivity is 0.045 mV/C and the voltage related to the temperature difference of the probes, which is read in the differential channels 3.4), varies in the order of micro volts (PING et al., 2004). The ordinary analogical to digital circuit ports used to work on a voltage of 5 or 3.3V, incapable to measure such small voltage variations. Therefore an amplification system is necessary for the logger system to be able to convert and record the signals (CÁRDENAS et al., 2019). The logger circuit designed with the integrated thermal power control can be seen in Appendix C.

Due to changes in the thermal equilibrium conditions of the xylem, ΔT_{max} may differ between days and hence will vary throughout the monitoring period, is recommended to take the maximum daily value or establish a function to capture the ΔT_{max} variation over time (PING et al., 2004). However, in the dry period of the study, the

sap flow becomes very low and the natural gradient starts to influence almost all the temperature difference registered by the sensor, so the ΔT_{max} may no longer represent the thermal equilibrium point, but the hottest time of the day. In the Figure 3.6 is shown the signal variation of a tree monitored in Serra Talhada at a rainy season day and at a dry season day.

Figure 3.6 - Sap flow probe signal variation (mV) in relation to Latent (LE) and sensible (H) heat fluxes (W/m^2) to: rainy season (a/top) and dry season (b/bottom).

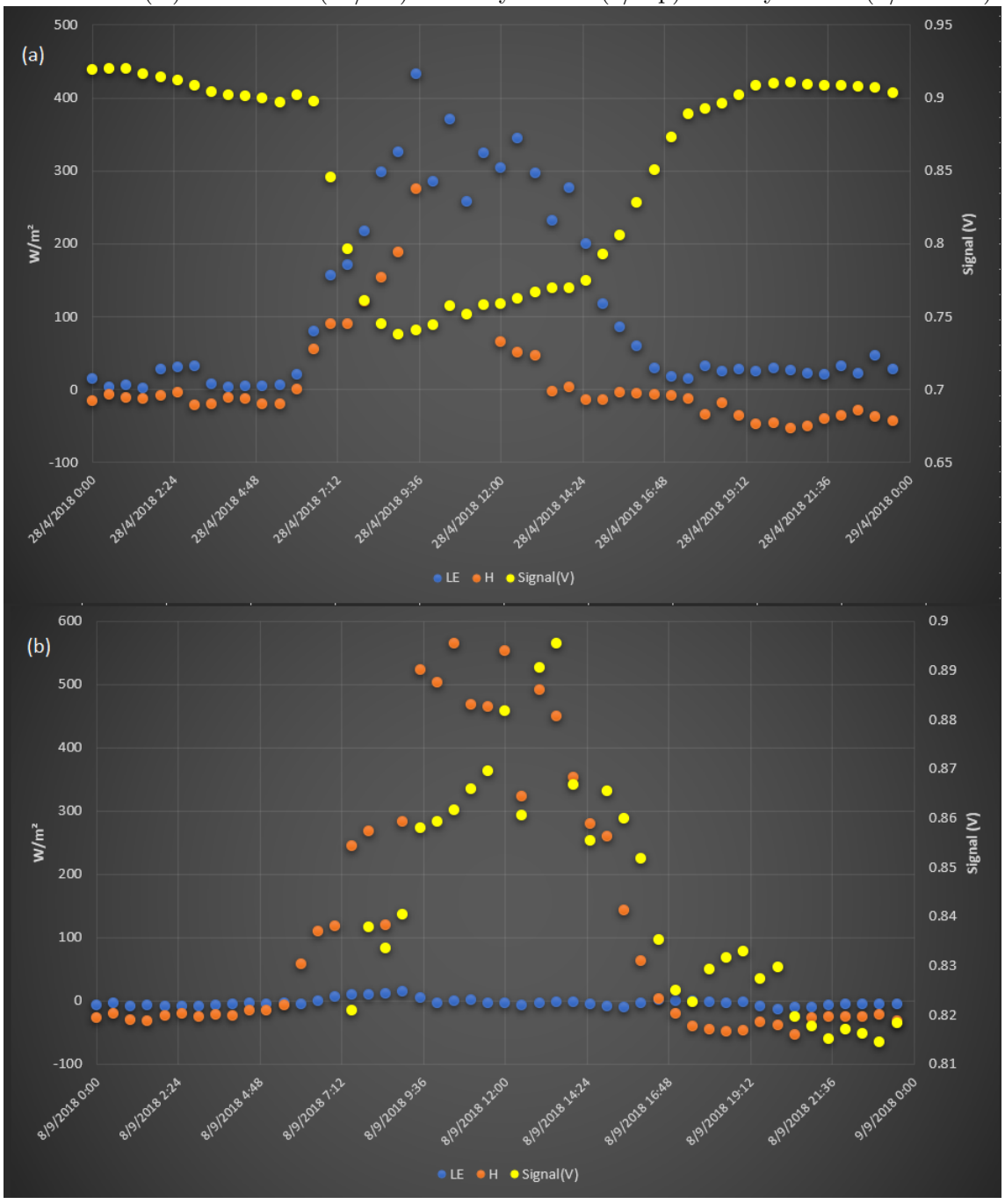

Therefore, in our study, the value of ΔT_{max} was assumed to equal the maximum value of ΔT registered by the sap flow system during the nocturnal period of each day (i.e. 10 pm to 4 am; UTC-3 Universal Time Coordinated). For the days where power failures occurred during the night, the night value of the previous day was considered. An average value of F_d per species was calculated (by averaging values for the 4 individuals) and this species-average was normalized from 0.0 to 1.0 taking into account the minimum and maximum F_d for each species; this normalized average for each species is referred to in this study as F_{dn}.

We considered only the intra-annual course of sap flow and not the exact amount of water used. Therefore, for analysis of the relationship between sap flow and measured environmental variables only the typical flow density of the morning period, at 10h30 (UTC-3), was considered as representative of the flow of the day. The choice of 10h30 was not entirely arbitrary, since i) this time is close to the MODIS Terra, Sentinel-2 and CBERS-4 overpass time, and ii) the sap flow at this time of the day exhibits a very strong correlation with the total daily sap flow – so that it represents an approximate estimate of daily water use.

3.5.2 Sap flow upscale

To represent the community-scale transpiration of the monitoring plot, a weighted average considering the total sapwood contribution by each species was calculated. The total amount of plot transpiration was normalized between 0.0 and 1.0, and referred to as normalized flux density of the monitored species community (F_{dnc}).

The sapwood area for all individuals belonging to the monitored plant species was estimated based on the linear relationship between the radial diameter of the sapwood and the diameter at breast height (DBH, cm) (LUBCZYNSKI et al., 2017). Cylindrical cross-section samples were collected from all monitored trees using a drill typically used for dendrochronology (Figure 3.5.2 A). The sapwood area of the samples was measured using dye-aided visual analysis (Figure 3.5.2 B). This simple technique is cheap and objective, yielding results that are appropriated for the proposed analysis.

Figure 3.7 - Sapwood sampling: (A) collecting wood sample and; (B) measuring sample.

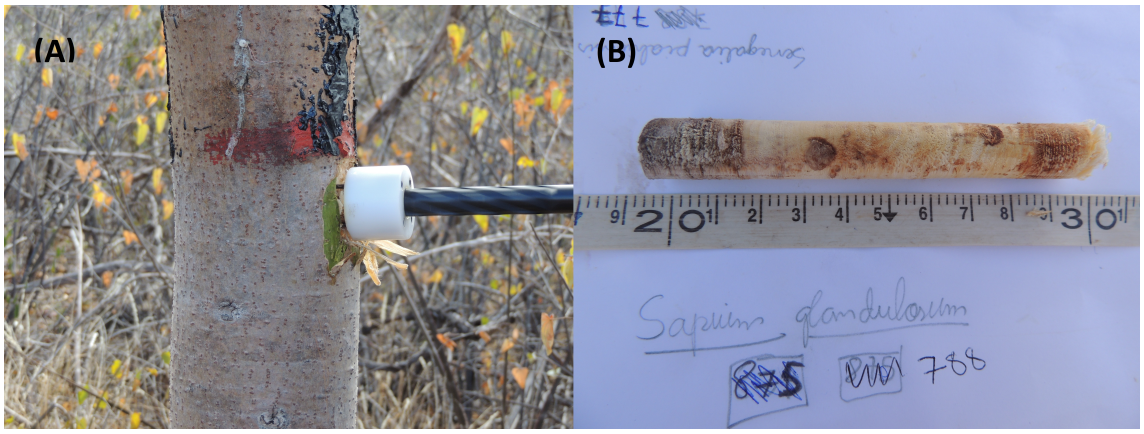

Due to low DBH variation same species individuals was not possible to estimate a dendrometric relationship to each species. Therefore a linear equation was derived to estimate the sapwood of all samples collected from monitored species from LGE and STA (Figure 3.5.2). The statistical parameters can be seen in Appendix A.

Figure 3.8 - Scatter plot between DBH and sapwood depth sampled.

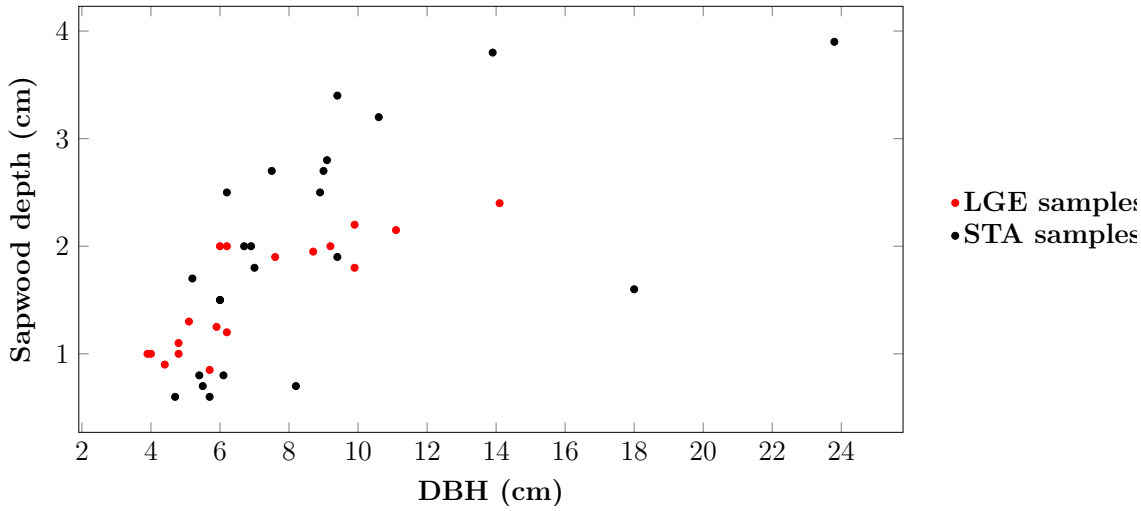

The sapwood area was than calculated to each individual using the estimated sapwood radial diameter and the standard equation used to calculate the area of a circle, by subtraction of the estimated core area and estimated bark area from the total measured tree cross-sectional area.

4 ENVIRONMENTAL DRIVERS OF WATER USE FOR CAATINGA WOODY PLANT SPECIES: COMBINING REMOTE SENSING PHENOLOGY AND SAP FLOW MEASUREMENTS[1]

4.1 Introduction

A better understanding of plant water availability and water use is of great importance for reliable assessments of ecosystem's resilience to droughts (PUGNAIRE et al., 2019). Water availability is critical for plant growth, inducing phenological transitions and, ultimately, plant survival. Additionally, information on plant water balance also allows the development of more realistic soil water assessment tools and land surface models, which is a widely acknowledged requirement for research related to the plant–soil–atmosphere continuum (FRANCESCONI et al., 2016).

Plant species have their own specific adaptive mechanisms to cope with droughts (LIMA et al., 2012; ALBERTON et al., 2019), which are particularly important in water-limited ecosystems such as seasonally dry tropical forests (SDTFs).

The SDTF is a unique biome that occurs in low-latitude areas of fertile soils with a low annual precipitation (ranging from about 250 to 1500 mm year^{-1}) and a prolonged dry season that extends for five to six months (MURPHY; LUGO, 1986; SÄRKINEN et al., 2011; PENNINGTON et al., 2009). The vegetation ranges from tall forests with closed canopies to scrublands rich in succulents and thorn-bearing plants (PENNINGTON et al., 2009; PENNINGTON et al., 2018). The long water-limited period has been shown to be selective

for deciduous, thorny, and succulent plant species that show a marked leaf senescence during the dry season followed by synchronous leaf flushing at the beginning of the rainy season (LIMA et al., 2012; ALBERTON et al., 2019; PENNINGTON et al., 2009; PENNINGTON et al., 2018; MACHADO et al., 1997). The deciduity and absence of a grassy layer are important characteristics that distinguish SDTFs from other mild seasonally dry tropical biomes such as the savannas (PENNINGTON et al., 2018).

In South America, SDTFs are largely represented by the Caatinga vegetation, the predominant vegetation in northeast Brazil and located in a semi-arid region that

[1]This chapter is an adapted version of the paper: PALOSCHI, R. A.; RAMOS, D. M.; VENTURA, D. J.; SOUZA, R.; SOUZA, E.; MORELLATO, L. P.; NÓBREGA, R. L. B.; COUTINHO, Í. A. C.; VERHOEF, A.; KÖRTING, T, S.; BORMA, L. D. S. Environmental drivers of water use for Caatinga woody plant species: combining remote sensing phenology and sap flow measurements. **Remote Sensing**, n 13 v 1, 75, 2020. DOI: https://doi.org/10.3390/rs13010075

extends over 800.000 km^2 (SOUZA et al., 1992; SAMPAIO, 1995; LEMOS; RODAL, 2002). The climate is predominantly hot and dry, with temperatures around 26 °C and high evapotranspiration (1500 to 2000 mm year^{-1}) coupled with low annual rainfall (400 to 800 mm year^{-1}) (REDDY, 1983; SAMPAIO, 1995). This results in high water deficits, which are aggravated by the short rainy season that usually lasts three to five months and show erratic rain episodes (REDDY, 1983; SOUZA et al., 1992). The water deficit is even more severe during catastrophic severe droughts that may last three to five years (SAMPAIO, 1995).

For most Caatinga plant species, vegetative and reproductive structures develop exclusively during the rainy season (LIMA; RODAL, 2010; LIMA et al., 2012). In fact, the fast metabolic response, which is unique to the Caatinga, allows species to produce a synchronous leaf flush with the onset of the rainy season (LIMA; RODAL, 2010; LIMA et al., 2012).

Caatinga tree species are able to cope with long periods of drought by exhibiting different transpiration-reducing leaf morphological and photosynthetic characteristics. They also display a considerable variability in wood density and related water storage properties (LIMA; RODAL, 2010; LIMA et al., 2012). Lima et al (2012) show a high correlation between wood density and water storage in Caatinga vegetation and relate these characteristics to a seasonal phenology. Several studies have shown that high wood density and thick cell walls tend to protect plants from cavitation but, in general, both are associated with low water storage in stem tissues (SOBRADO, 1993; STRATTON et al., 2000; HACKE et al., 2001; REICH et al., 2003; SWENSON; ENQUIST, 2007). On the other hand, low wood density and thin cell walls increase the chances of cavitation but water storage may be higher and the maintenance of a high water potential may be prolonged (SOBRADO, 1993; STRATTON et al., 2000; HACKE et al., 2001). The combination of these diverse plant traits produce different phenological evolutions throughout the growing season that depend on different plant water use strategies (REICH et al., 2003; SWENSON; ENQUIST, 2007; CHAVE et al., 2009).

Eddy covariance (EC) and remote sensing (RS) techniques have been used to evaluate terrestrial environments because they allow vegetation systems to be studied at different scales: from local to global scales. The use of RS is gaining importance as satellites provide low-cost products and images with increasing spatial and temporal resolutions. The advances in technology have allowed several RS vegetation indices (VIs) to be used, improving our understanding of temporal and spatial changes in plant communities (RICHARDSON et al., 2018; FERREIRA et al., 2020; MIRANDA et al.,

2020). The direct relationship between water use and phenological response observed by RS has been used in models that seek to estimate evapotranspiration (ET) and gross primary production (COAGUILA et al., 2017), mainly through the use of empirical or semi-empirical parameterisations, taking advantage of vegetation indices such as normalized difference vegetation index (NDVI) (TEIXEIRA, 2010). This approach is particularly successful in the Brazilian semi-arid regions due to the strong synchronicity between phenology and plant-water availability (LIMA et al., 2012).

An alternative approach to monitor vegetation phenology is near-surface RS, which uses in-situ automated cameras (phenocams) (ALBERTON et al., 2017). This technique, in combination with EC measurements and remote sensing, has been applied in Brazilian SDTFs (ALBERTON et al., 2019) to investigate the drivers that regulate phenological patterns and vegetation responses to seasonal and severe droughts.

Regarding water use, EC and RS can be used to estimate ET (TEIXEIRA, 2010), a flux that encompasses processes other than transpiration, such as evaporation of soil water, canopy-intercepted water, and other free water surfaces. However, RS generally provides discontinuous time series of ET (e.g., due to cloudy conditions) (KANDASAMY et al., 2012). Moreover, none of these tools allow direct measurements of transpiration at the individual tree or species level. Hence, these techniques cannot explain species-specific strategies that are strongly dependent on individual structural, phenological, and physiological traits. For such, in-situ or near-surface methods make monitoring possible.

Continuous in-situ estimation of transpiration is possible with sap flow sensors. Among the methods used to estimate sap flow, thermal dissipation probes (TDP) have been widely used and improved throughout the years (REN et al., 2020). Information on transpiration is essential for studies related to plant water use, including those in SDTFs (GOLDSTEIN et al., 2008; BUTZ et al., 2018). Sap flow measurement techniques can provide time series of diurnal and seasonal water fluxes to estimate plant water use. The TDP method, suggested by Granier (GRANIER, 1985; GRANIER, 1987), is widely applied to estimate tree transpiration because the sensor system is simple to construct, easy to install, and relatively inexpensive (PING et al., 2004; PASQUALOTTO et al., 2019).

When analysing time series and patterns of water use, vapor pressure deficit (VPD) has been considered as the main environmental driver of plant transpiration under most conditions, representing the atmospheric demand (GROSSIORD et al., 2019). performed continuously-logged sap flow monitoring experiments in humid tropical

forests and observed that sap flow was highly dependent on VPD. However, for the less humid regions studied, very high VPD led to a reduction in transpiration as a result of the strong negative dependence of stomatal opening on VPD Grossiord et al. Similarly, Butz et al (2018) monitored sap flow of both deciduous and non-deciduous species and showed that evergreen species have a stronger relationship with seasonal VPD variation than deciduous ones, and a slightly higher dependence of sap flow on soil moisture than on VPD. Overall, these studies indicate that in more water-limited systems, species will be more dependent on soil water availability.

Here, we combine several datasets and approaches, as well as ground truth data, in order to test the efficiency of remote sensing data to monitor a significant physiological process such as water use. We aim to investigate the relationship between plant water use and phenology for Caatinga woody plant species at both the species and community level using different scales: moderate RS spatial resolution, high RS spatial resolution, and near-surface cameras. In addition, we intend to evaluate the environmental drivers and factors that limit plant phenology (leaf flush and senescence) and transpiration. We hypothesize that: (1) phenology at the community level (represented by RS data) and at the species level (represented by near surface remote sensing data) are fully explained by soil water availability; (2) RS data for the Caatinga vegetation are strongly correlated to variations in water use strategies among species; (3) variations in the sap flow signal are fully explained by changes in water availability.

4.2 Materials and methods

4.2.1 Study Site

The study site (Figure 4.1) is located in central-northern part of the Brazilian state of Pernambuco, in the municipality of Serra Talhada (7°58'12"S, 38°23'06"W, 455 m a.s.l.). The soils are predominantly Aridisols Argid and Entisols orthents (SOIL-SURVEY-STAFF, 1999). The area has a relatively smooth relief and comprises various xerophilous vegetation types (JACOMINE et al., 1973). The local climate is Bsh (arid-steppe-hot arid) according to the Köppen system in a transition region to the Aw (winter dry season) (KOTTEK et al., 2006; RUBEL et al., 2017; CLIMATE-DATA.ORG, 2019), with a mean annual rainfall of 680 mm yr^{-1} and a mean temperature of 23.8 °C (CLIMATE-DATA.ORG, 2019). The experimental site includes a 50 × 100 m monitoring plot (Figure 4.1) which is part of the Nordeste project plot network (MOONLIGHT et al., 2020), and a 10 m tall eddy covariance (EC) flux tower (site ID BR-CST in AmeriFlux network; 7.9682°S, 38.3842°E) located 200 m away from the

monitoring plot.

Figure 4.1 - Study site: Map of the study area showing eddy covariance (EC) flux tower location (where the phenocam is installed), and the monitoring plot (where sap flow and soil moisture sensors were installed); location of the study site in the context of the Brazilian Caatinga. Spatial resolution: 15 cm.

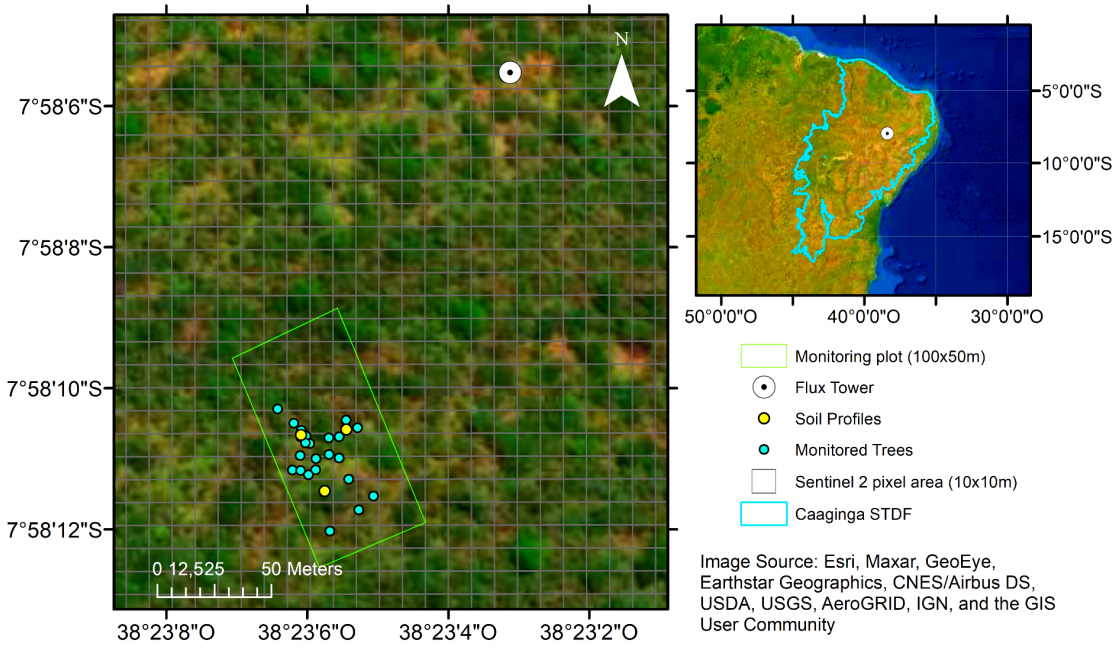

Our study was carried out from April 2018 to March 2019, during which the in-situ pluviometer registered a pronounced rainy season from December to April (total precipitation of 499 mm), whereas the dry period lasted from May to November (total precipitation of 40 mm). Regarding the total rainfall in April, which marked the beginning of our experiment, that month was considered the wet-to-dry transition period. These precipitation values and their timing are consistent with the normal climate found for this region (CLIMATE-DATA.ORG, 2019). Therefore, the results found in this work can be extended to other years with normal rainfall.

4.2.1.1 Plant species

A total of 24 species were found in the plot, of which 11 showed a dominance over 1.0: *Anadenanthera colubrina* (Vell.) Brenan, *Aspidosperma pyrifolium* Mart. & Zucc, *Astronium urundeuva* Engl., *Cenostigma nordestinum* Gagnon & G.P.Lewis, *Cereus jamacaru* DC., *Commiphora leptophloeos* (Mart.) J.B. Gillett, *Croton echioideus*

Baill., *Erythroxylum pungens* O.E.Schulz, *Mimosa acutistipula* Benth. *Piptadenia flava* Benth. and *Senegalia polyphylla* (DC.) Britton & Rose.

We selected five species to monitor sap flow density, which accounted for 80% of the total dominance: *C. leptophloeos*; *A. colubrina*; *S. polyphylla* and; *A. pyrifolium*; *C. nordestinum*. All selected species are deciduous and were selected based on their abundance registered in the inventory of the monitoring plot and the Nordeste project plot network (MOONLIGHT et al., 2020), and based on their relative abundance, as indicated in Table 4.1.

Table 4.1 - Tree species monitored, wood density (W_d, g cm^{-3}), mean diameter at breast height (DBH) mean species height (H.), dominance in the plot (D.), estimated sum of the sapwood area per species per species, percentage of the sapwood area in relation to the total sapwood area in the plot.

Species	W_d	DBH (cm)	H. (m)	D. (%)	Sap. Area (cm^2)	% of Total Sap.
Anadenanthera colubrina	0.59	13.4	7.2	4	175	6.2
Aspidosperma pyrifolium	0.54	8.1	4.9	30	772	27.3
Cenostigma nordestinum	0.66	13.8	5.4	30	1751	62.0
Commiphora leptophloeos	0.28	20.0	5.2	1	78	2.8
Senegalia polyphylla	−−	15	7.7	5.4	49	1.7
Total	−−	80	−−	−−	2824	100

W_d values obtained from (LIMA et al., 2012).

All plant specimens were collected and identified by botanists at the Herbarium of the State University of Feira de Santana (HUEFS) Bahia, Brazil. The inventory included all plant individuals with a diameter at breast height (DBH) over 5 cm; the average height of trees in the plot was 5.2 m. Abundance of each species was determined by establishing the frequency of individuals of a given species within the monitoring plot.

We estimated sapwood depth using the linear regression given by 0.377 * DBH -1.075, R^2 of 0.67 ($p < 0.05$ for both coefficients). Additionally, we estimated the total sapwood area for all individuals of a given species, calculated the sapwood area of each species, and estimated the percentage of the total active xylem area for each species Table 4.1.

4.2.1.2 Ground measurements

Sap flux density (F_d, $g\ m^{-2}\ min^{-1}$) for the selected individuals was measured using Granier's TDP method (see Supplementary Materials, Section 1.C). The sap flux

density at the individual level (F_d) was first normalized, yielding F_{dn}, and then scaled-up to the community level, F_{dnc}, considering the relative sapwood area of each species (Table 4.1). At the community level, F_{dnc} was calculated as the weighted average considering the relative contribution of the sapwood area for each species. The environmental drivers and plant traits used in the sap flow and phenology analysis are described in Table 4.2. The environmental drivers and plant traits used in the sap flow and phenology analysis were: vapour-pressure deficit (VPD) and plant water availability, expressed in terms of soil water content (S_w) and relative soil water saturation ($S_{e,prof}$; Table 4.2). S_w is the amount of water for the total soil profile of 77.5 cm. $S_{e,prof}$ is a fraction dependent between the actual profile soil moisture (θ_{prof}) and the difference between the saturated profile moisture content, $\theta_{s,prof}$, and residual profile moisture content, $\theta_{r,prof}$.

Table 4.2 - Summary of measured or derived environmental variables: category of the variable; name; description; units.

Category	Variable	Description	Unit
Atmospheric driving	R_n	Net Radiation	W m^{-2}
	T_{air}	Air temperature	°C
	VPD	Vapour-pressure deficit	hPa
	P	Rainfall	mm
Soil moisture status	$S_{e,prof}$	Relative saturation	-
	W_s	Soil Water Storage	mm
Transpiration and evapotranspiration	F_{dn}	Sap flow density normalized	-
	F_{dnc}	Community sap flow normalized	-
	ET	EC evapotranspiration	mm month^{-1}
Plant trait	W_d	Wood density	g cm^{-3}
	Dominance	Relative frequency abundance	%
	Sap. area	Sum of estimated species sapwood area	cm^2

4.2.1.3 Remote sensing data

Information on land surface phenology and vegetation indexes (VIs) was obtained from remote sensing (RS) sensors which operate at different spatial and temporal scales: remote sensors MODIS/Terra + Aqua (250 m products MYD13Q1 and MOD13Q1) and MSI/Sentinel-2A + B (10 m), and near-surface remotely sensed data, obtained by one phenocam (Mobotix AG-Germany) installed at the top of the EC flux tower (see Supplementary Materials, Section 1.A). The VIs derived from

these RS products are NDVI (MODIS and Sentinel-2A), GCC (Sentinel-2A and phenocam) and SAVI (Sentinel-2A), as presented in Table 4.3.

Because of the rapid dynamics of the Caatinga vegetation, which responds to rain and soil water content within a few days, a short revisit time satellite was necessary. The Sentinel-2 satellite was chosen because of its spatial resolution (10 m) and mainly because of its revisit time (3–10 days). The MODIS sensor was chosen for comparison purposes. Despite its moderate spatial resolution (250 m) considering the dimensions of our plot, the high revisit frequency and well known product quality provides a simple and effective way to compare the performance of the Sentinel-2 index. Since our objective is to analyze forest change over time, comparing the variables with a product resulting from a very low revisit time is essential (Terra and Aqua satellites cross every day, morning and afternoon, providing temporal VI products with much less cloud probability). The phenocam provided the field truth for the region and also enabled us to evaluate the phenology of each species separately.

Table 4.3 - Remote Sensing data: Variable; Sensor/Satellite, spatial resolution; temporal resolution; respective section. Please see the Supplementary Materials for more details.

Variable	**Sensor/Satellite**	**Spatial Resolution**	**Temporal Resolution**	**Section nr.**
$NDVI_{modis}$	MODIS/TERRA + AQUA	250 m	8 days *	1.D
$NDVI_{S2}$	MSI/Sentinel 2A + 2B	10 m	3–10 days	1.D
GCC_{S2}	MSI/Sentinel 2A + 2B	10 m	3–10 days	1.D
GCC_{ns}	Near surface camera/NA	**	daily	1.D
$SAVI_{S2}$	MSI/Sentinel 2A + 2B	10 m	3–10 days	1.D

* pixel composition from daily image acquisitions; ** camera spatial resolution depends on the distance from camera's nadir.

The proportion of canopy coverage in relation to soil exposure is also seen by Sentinel-2 and MODIS. The coverage was considered spatially homogeneous since no significant differences ($p > 0.5$) were found between the temporal behavior of the sentinel individual pixels and individual species. This was due to the proximity of trees from different species, sometimes less than two meters, but also due to the spatial autocorrelation of the pixels. Each pixel influences its neighborhood (VAJSOVÁ et al., 2020), reducing the effective pixel resolution. It is worth mentioning that the spatial miss-registration in the Sentinel-2 images series vary by around 12 m (more than one pixel) but can be greater than 3 pixels according to (YAN et al.,

2018). For all these reasons, it was not possible to analyze the temporal behavior of Sentinel-2 pixels individually. Thus, a temporal profile was extracted considering the pixel mean of the monitoring plot area.

Regarding the phenocam images, the regions of interest (ROIs) were selected at the species and at the community level. At the species level, we selected pixels corresponding to the tree crowns of the four species found within the phenocam's field of view (Figure 4.2). *S. polyphylla*, which represents only 1.7% of the total sapwood area, was not present within the camera's field of view. We then extracted the GCC for each ROI and calculated the mean GCC for each species ($GCC_{ns,e}$. At the community level, we selected the ROI pixels corresponding to the entire vegetated area in the image, excluding bare soil and the tower (Figure 4.3). The community ROI includes trees, shrubs, and eventual forbs if present. The GCC was extracted from the community's ROI. Conservatively, the same ROI was used for the community during the entire study period, including the dry and rainy seasons. Figure 4.3 shows the contrast between the seasons: the fully developed tree crowns in the rainy season and the leafless crowns during the dry season.

4.2.2 Data analysis

In order to establish relationships between plant water use and environmental drivers, we compared the temporal variability of F_{dnc} with the environmental data obtained from the micrometeorological flux tower (i.e., VPD, R_n and T_{air}) and with the relative saturation, $S_{e,prof}$. To identify the relationship at the community level, we used the same approach to compare F_{dnc} with NDVI (MODIS and Sentinel-2) and GCC_{S2}.

The VIs (GCC, SAVI, and NDVI) used to compare with the results obtained from the phenocams (GCC_{ns}) were calculated for the tower region; we assumed that the tower region consisted of a circle around the flux tower with a radius of 50 m, which is compatible with the camera field of view. The VIs (Table 4.3) used to compare with the sap flow (F_{dn} and F_{dnc}) data and with $S_{e,prof}$ were calculated using the pixels that covered the monitoring plot area (Figure 4.1).

To compare the VIs obtained from different scales, we used the transition dates of start (SOS) and end (EOS) of the growing season. The length of the growing season and associated phenological transitions, SOS and EOS (RICHARDSON et al., 2018), were calculated from the phenocam GCC and the RS vegetation indices GCC, SAVI, and NDVI based on Alberton et al. 2019.

Figure 4.2 - Example of a hemispherical image used for the proximal remote sensing phenological analyses at the study site, PE-Brazil. The areas selected in white represent tree crowns of individuals from four species: A, *Anadenanthera colubrina*; B, *Aspidosperma pyrifolium*; C, *Cenostigma nordestinum* and D, *Commiphora leptophloeos*.

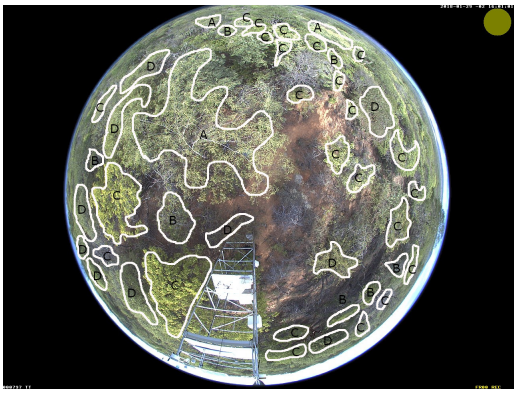

Figure 4.3 - Hemispherical image used for the proximal remote sensing phenological analyses at the study site, PE-Brazil; (**A**) In the rainy season day of year (DOY) 107, 2018. (**B**) In the dry season DOY 256, 2018; the area selected in white represents the entire vegetation sampled as the region of interest (ROI) of the community for the extraction of phenological indices.

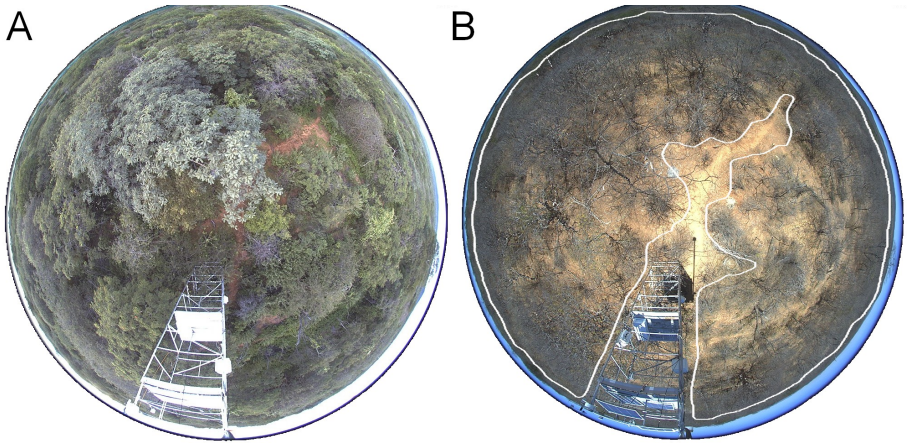

This method uses the confidence intervals of curve derivatives to identify changes in phenology (ALBERTON et al., 2019). First, we fitted a generalized additive model (GAM) using the species and community GCC as the response variable fitted by the sequence of consecutive days (time) of the phenological observations, which was used as an independent smoother variable to produce the phenological curves.

We then calculated which regions of the curve had derivatives and detected when the derivatives were increasing (to determine SOS) or decreasing (to determine EOS) (ALBERTON et al., 2019). We considered SOS as the first day detected on the derivative at the left side of the GCC curve and EOS as the last day of the derivative at the right side of the curve. The transition dates calculated from the phenocam GCC were verified by visual inspection of the digital images and adjusted when necessary (for more details see Supplementary Materials 1.D).

In addition, to evaluate whether variations in wood density could explain differences in water use and transition dates, we assessed species' wood density (W_d, g cm^{-3}) and the difference between F_{dn} time series and near-surface GCC for each species.

Finally, the F_{dnc} data were compared with the VI that showed the greatest correlation with F_{dnc}. Thus, we compared NDVI indices ($NDVI_{modis}$ and $NDVI_{S2}$) with $S_{e,prof}$ using scatter plots in order to explicitly assess the dependence between variables across their data range.

4.3 Results

4.3.1 Hydroclimatological drivers of sap flux density

Figure 4.4a shows that the net radiation, R_n, was relatively low between April and August. This is part of the dry and cooler period where shortwave and longwave incoming radiation are lower than during the wet period, while albedo and longwave outgoing radiation are relatively more frequent, as previously observed in the Caatinga (SILVA et al., 2017; FERREIRA et al., 2020). R_n remained approximately constant after September. The ET, shown in Figure 4.4b, varies between 0 and 125 mm month^{-1}, and the lowest values were found between August and November, when rainfall, (P) was negligible (see Figure 4.4a). Despite the low P in May and June, ET is still considerable because of the total water stored (S_w) in the soil profile (see Figure 4.4c), which allows transpiration to continue. It is worth noting that for leaves that are well-coupled to the atmosphere (i.e., with open stomata), the transpiration at the leaf level can be approximated by the product of the leaf-to-air VPD and the stomatal conductance according to Fick's law of diffusion (COSTA et al., 2010). However, in this region, our results show that intra-annual ET was inversely related to VPD ($p < 0.05$) (Figure 4.4b), most likely because, despite the higher VPD, plant species are mostly leafless from September to November.

Figure 4.4 - Climate variables, soil water availability, and community-level sap flow: (**a**) Net Radiation (R_n, W m^{-2}) and rainfall (P, mm $month^{-1}$); (**b**) vapour pressure deficit (VPD, hPa) and EC evapotranspiration (ET, mm $month^{-1}$); (**c**) soil water storage (S_w, mm) and monthly mean air temperature (T_{air}; °C); (**d**) Normalized sap flow for the plot community (F_{dnc}, dimensionless).

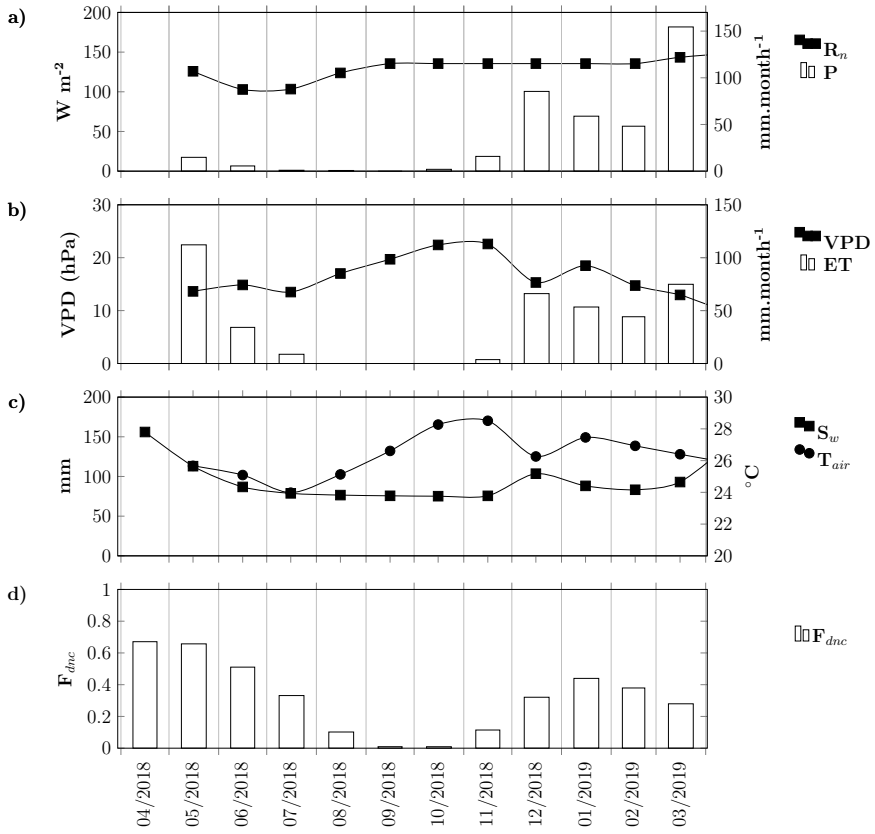

The ET is in phase with S_w. The latter varied from a maximum of 184 mm at the beginning of April to a minimum of 74 mm at the end of November. However, after September S_w remained fairly constant (approximately 75 mm) until November when the rains started (Figure 4.4c). The highest air temperatures, T_{air}, coincided with the lowest values of ET, underlining the harsh climatic conditions during the dry season. T_{air} varied between 24 °C in July and 28.5 °C in November.

The community-level sap flow, F_{dnc} (Figure 4.4d), is in phase with S_w and ET. However, ET increased rapidly during the first rainy month, while F_{dnc} increased gradually, suggesting that a large part of the ET recorded during the first rainy month may be due to the evaporation of intercepted water and/or to soil water evaporation. Furthermore, the F_{dnc} varies in synchrony with the vegetation indices GCC_{S2}, $NDVI_{S2}$, and $NDVI_{modis}$ (Supplementary Materials, Figure S2).

4.3.2 Transpiration, soil water condition, and remote sensing data

The normalized sap flux density at the species level, F_{dn}, was strongly affected by soil conditions when $S_{e,prof}$ was below 0.25 (Figure 4.5), indicating the high dependency of transpiration on stored water and demonstrating the threshold when plant water stress starts to limit transpiration. GCC and F_{dn} increased rapidly after the first rain, even with low water availability ($S_{e,prof}$ around 0.18), for all species except *A. pyrifolium*. After December 2019, the sap flow signal varied reasonably, but still followed the evolution of $S_{e,prof}$. This is due in part to climate variations, but also to the fact that a number of sensors failed during this period. Thus, the average F_{dn} for certain months was not based on all four sap flow sensors. All individuals from the studied species had a fully developed canopy at the beginning of the sap flow measurements. Therefore, our study period included two transition dates, the EOS of the ongoing growing season (2017–2018) and the SOS of the second growing season (2018–2019). Moreover, leaf fall still occurred after the EOS in the rainy season in 2018, and a SOS with new leaf flushing was detected at the beginning of the next rainy season in December of 2019. All species showed a negative correlation to daily VPD since all are deciduous and lost their leaves, halting transpiration precisely in the periods when VPD was highest.

Despite their approximate correspondence (Figure 4.5), as both variables exhibit a strong seasonality, the correlation between F_{dn} and GCC obtained from the proximal RS was poor (see Table 4.4, last column; the highest correlation (0.51) was found for *A. colubrina* and *C. nordestinum*, species with high wood density). In fact, F_{dn} and F_{dnc} have a stronger relationship with all RS indices, especially with NDVI (Table 4.4). $NDVI_{modis}$ data better explained the variation in F_{dnc} than $NDVI_{S2}$, Table 4.4 shows a Pearson correlation coefficient of 0.92 ($p < 0.01$) versus a value of 0.88 ($p < 0.01$).

Table 4.4 - Pearson correlation coefficient between F_{dn} and $NDVI_{modis}$, $NDVI_{S2}$, GCC_{S2}, $SAVI_{S2}$ and GCC_{ns}, respectively.

$\mathbf{F_{dn}}$	$\mathbf{NDVI_{modis}}$	$\mathbf{NDVI_{S2}}$	$\mathbf{GCC_{S2}}$	$\mathbf{SAVI_{S2}}$	$\mathbf{GCC_{ns}}$
A. colubrina	0.83 *	0.80 *	0.71 *	0.74 *	0.36 *
A. pyrifolium	0.76 *	0.78 *	0.67 *	0.79 *	−0.14
C. leptophloeos	0.31	0.49	0.55 *	0.56 *	0.06
C. nordestinum	0.85 *	0.71 *	0.68 *	0.63 *	0.51 *
S. polyphylla	0.82 *	0.73 *	0.71 *	0.62 *	–
F_{dnc}	0.92 *	0.88 *	0.84 *	0.81 *	

obs.: * = $p < 0.5$.

Figure 4.5 - (**a**) Rainfall (mm day^{-1}) and soil water profile relative saturation ($S_{e,prof}$, dimensionless); and normalized near surface species GCC (GCC$_{ns,e}$, dimensionless) , and species averaged sap flow density (F$_{dn}$, dimensionless), together with $S_{e,prof}$ for (**b**) *C. nordestinum* and $S_{e,prof}$; (**c**) *S. polyphylla*; (**d**) *A. colubrina*; (**e**) *C. leptophloeos*; (**f**) *A. pyrifolium*.

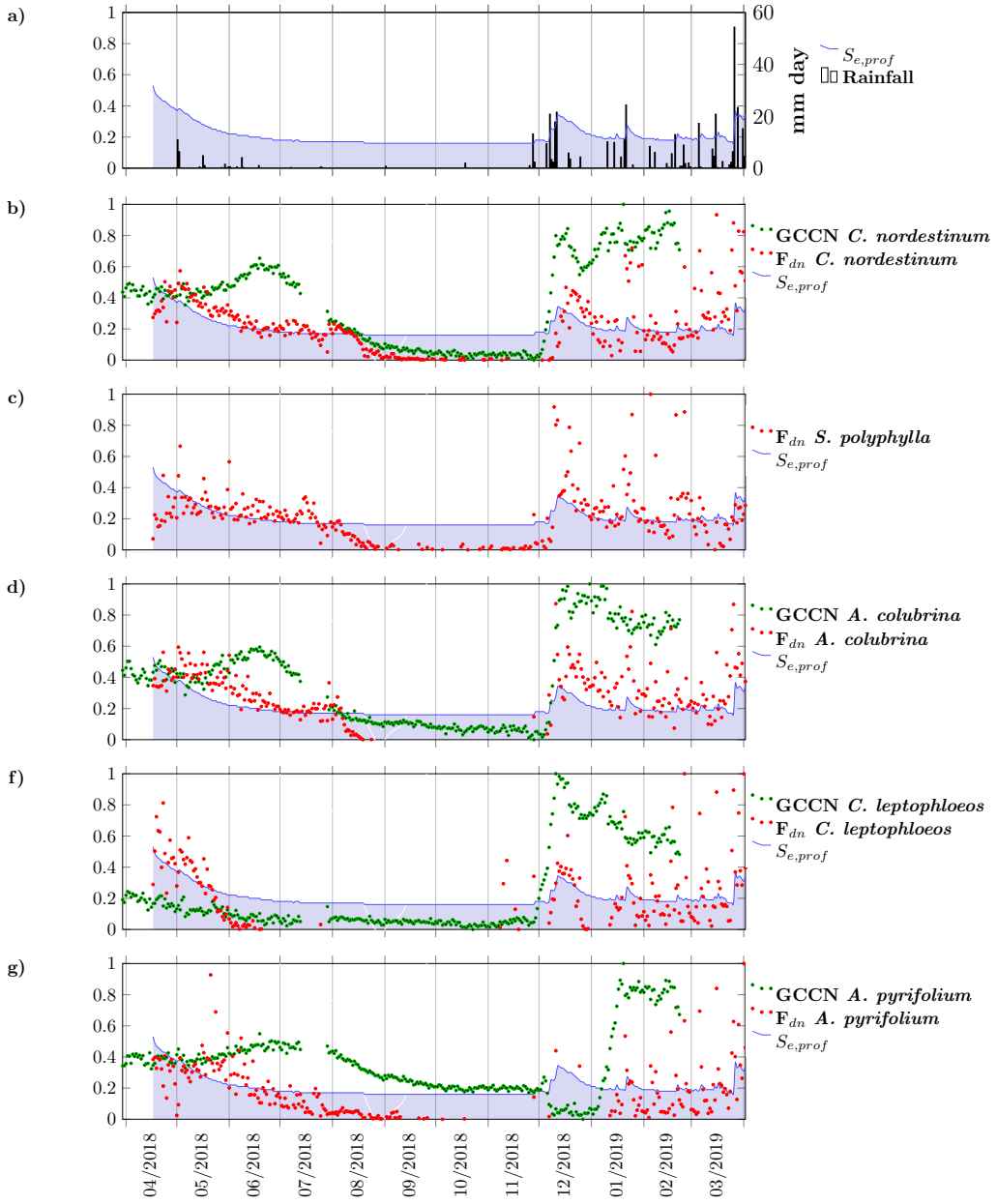

The transition dates (in format DD/MM/YY) calculated for each species were the following: *A. pyrifolium*: EOS = 10/08/18, SOS = 10/01/19; *C. nordestinum*: EOS = 05/08/18, SOS = 08/12/18; *C. leptophloeos*: EOS = 12/06/18, SOS = 11/12/18;

A. colubrina: EOS = 03/08/18, SOS = 07/12/18. Based on visual inspections of the images, we found that during the period between EOS and SOS, all individuals of the four species were leafless. The development dates for the tower region estimated by the sensors (Sentinel-2 and MODIS) can be seen in Table 4.5. We found that $NDVI_{modis}$ was the index with the highest correlation to species' water use, and its transition dates were the most similar to the GCC_{ns} results (Table 4.5).

Table 4.5 - VI Transition dates (day of year/year) and bias in relation to near-surface GCC.

Transition Dates	$\mathbf{GCC_{ns}}$	$\mathbf{GCC_{S2}}$	$\mathbf{NDVI_{S2}}$	$\mathbf{SAVI_{S2}}$	$\mathbf{NDVI_{modis}}$
EOS	238/18	220/18 (−18)	196/18 (−42)	191/18 (−47)	229/18 (−9)
SOS	339/18	306/18 (−33)	305/18 (−34)	321/18 (−18)	309/18 (−20)

Both the seasonal evolution of transpiration and the phenological response of the vegetation show an asymptotic limit in relation to $S_{e,prof}$ (Figure 4.6a,b), most likely because we are using $\theta_{s,prof}$ and $\theta_{r,prof}$ to normalise the data (please see the Supplementary Materials for an explanation of these parameters and of θ_{pwp} and θ_{fc} used below). During a considerable part of the year, the moisture content of the soil layers that contain most of the roots are below wilting point (θ_{pwp}), yet above the residual moisture content (θ_{fc}). Additionally, not all of the water stored in the soil pores is used for transpiration, as part of it is stored below the root zone or lost to soil evaporation.

Figure 4.6 - Scatter plots of (**a**) community level normalized sap flow (F_{dnc}) versus S_{prof} (dimensionless), (**b**) $NDVI_{modis}$ and $NDVI_{S2}$ versus S_{prof}, (**c**) $NDVI_{modis}$ versus F_{dnc}, (**d**) $NDVI_{S2}$ versus F_{dnc}.

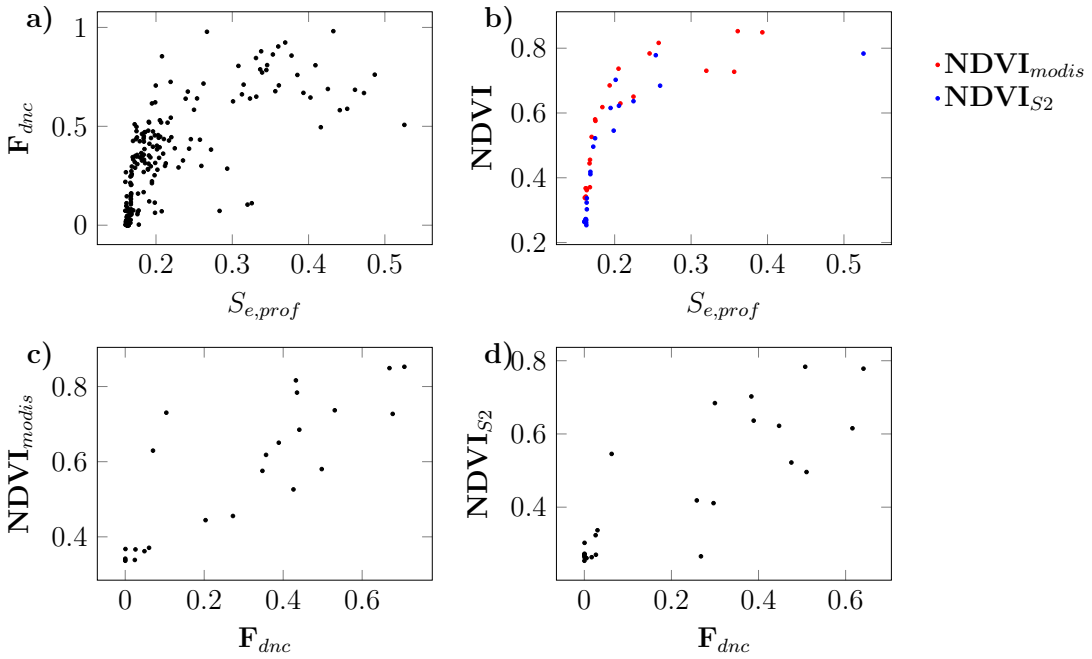

4.4 Discussion

This study explored the sensitivity of remotely sensed indices to measure water use in the Caatinga. Our findings indicate that (i) the water use is highly dependent on soil moisture conditions; (ii) differences in wood characteristics seem to directly affect differences in when species sap flow ceases; (iii) with increasing resolution, from satellites with low resolutions to cameras that allow monitoring of individual tree species, new sources of uncertainties, previously masked by low spatial resolution, reduce correlations between RS indices and individual and community measurements of water use. Notwithstanding, the high resolution of the cameras has the benefit of allowing isolated events, such as the SOS and EOS, to be detected for different species.

It is remarkable how strongly F_{dnc} is related to $S_{e,prof}$, especially when considering daily values (Figure 4.5), which shows relative saturation together with rainfall, as well as greenness and sap flow per species. The strong seasonality, reflected in the highly variable sap flow values observed for all monitored Caatinga plant species, is evident and in agreement with previous studies (LIMA et al., 2012; OLIVEIRA et al., 2014; ALBERTON et al., 2019). Seasonality is particularly evident with regards to the

timing of leaf shedding (EOS) and the drop in soil water storage (S_w) (Figure 4.4d). Moreover, the fact that seasonally varying values of F_{dnc} are only very weakly and negatively related to changes in VPD corroborates the idea that this vegetation is relatively independent of the atmospheric demand when considering intra-annual variation. This is not the case for the diurnal variation of sap flow (data not shown), which remains dependent on VPD as shown by Butz et al. (2018). These findings most likely reflect the fact that we considered a single value of F_{dnc} and VPD for each day, thus the diurnal dependence (where sap flow increases as VPD increases) between these variables was not considered. The same effect occurs between the intra-annual variation of R_n and F_{dn} (Figure 4.4).

The inverse relationship between VPD and ET is also partially caused by the fact that, during the dry season, all trees shed their leaves and water uptake reduces to near-zero, despite the increase in VPD. Furthermore, during leaf-on periods with low atmospheric humidity, it is the strong negative dependence of stomatal opening on VPD that counteracts the concurrent increase in driving force, as mentioned in the introduction. Although the VPD values tend to be lower during the rainy season, thereby reducing potential transpiration, ET is high due to an increased water availability and related presence of leaves. Moreover, there is a strong relationship between VPD and T_{air} (Figure 4.4c), given the temperature depends on the saturated vapour pressure as calculated by Teten's formula (TETENS, 1930); around 57% of the VPD variation is caused by the variation in T_{air}.

F_{dnc} appears to be independent of $S_{e,prof}$ when it reaches values higher than 0.25 (for reasons explained in the Results section, see Figure 4.6b). When $S_{e,prof}$ was below 0.25, there was a clear reduction in sap flow, which became even more pronounced with values below 0.18. When $S_{e,prof}$ values were around 0.16, F_{dnc} became negligible, and NDVI reached its minimum (0.34 for $NDVI_{modis}$ and 0.26 $NDVI_{S2}$), indicating a minimum NDVI for the monitored Caatinga species. Although F_{dnc} was poorly correlated to water availability when $S_{e,prof}$ values were > 0.25 (indicating that the lack of radiation is a stronger driver), values of $S_{e,prof}$ remained below 0.25 for more than 80% of the monitored period, indicating that for at least 80% of the year, water availability was the dominant environmental driver of transpiration. This dependence of F_{dnc} on $S_{e,prof}$ indirectly explains the high correlation between F_{dnc} and NDVI, as shown in Table 4.4, since NDVI also strongly depends on $S_{e,prof}$ (Figure 4.6b).

In the dry season, when F_{dn} was approaching 0, for four of the monitored species

(Figure 4.5) the timing difference seems to be due to differences in wood density, W_d. However, for the species with high F_{dn}, this difference is subtle. As can be surmised from Figure 4.5, the order in which F_{dn} approached 0 was inversely correlated with the order of W_d: *C. leptophloeos* (0.28 g.cm^{-3}) at the end of April; *A. pyrifolium* (0.54 g.cm^{-3}) at the end of June; *A. colubrina* (0.59 g.cm^{-3}) in mid July; *C. nordestinum* (0.66 g.cm^{-3}) in mid to late July. Although this study only compared the W_d of four species, our results indicate that low W_d is a limiting factor for these plants, particularly considering the duration in which they can maintain foliage, since the early senescence observed for low W_d species may be part of the plant's water conservation strategy as is stomatal control, which ultimately prevents the plant from cavitation (SOBRADO, 1993; STRATTON et al., 2000; HACKE et al., 2001). Thus, the high W_d promoted by thick cell walls plays an important role in protecting plants from cavitation, allowing the plant to continue extracting water even from relatively dry soils.

Since W_d is directly related to the capacity of Caatinga plant tissues to store water (LIMA et al., 2012), species with higher wood densities, which have larger stores of water, may be able to survive extremely dry periods. Moreover, the species with the lowest W_d, *C. leptophloeos* has the shortest sap flow period (Figure 4.5) and exhibits a peculiar greenish photosynthetic bark (KILLEEN et al., 1998), which increases plant survival during the dry season (MAHR, 2012). Unfortunately, our data set did not allow us to gather evidence of a higher leaf water potential maintained over a longer period for the species with lower wood density.

C. leptophloeos was not dominant in the monitoring plot and behaved differently, from a phenological perspective, from the other species: leaf flushing began earlier and occured at a slightly faster rate. This species also has a very early onset of senescence (Figure 4.5f), as was previously reported by (LIMA et al., 2012) and attributed to the species low wood density and high water storage characteristics. Despite the fact that the high storage water capacity increases plant survival during dry periods, its low wood density suggests it cannot extract water from soils with very negative water potentials. Therefore, to avoid cavitation, this species shows an early EOS. Furthermore, it is expected that species with considerably different phenologies and low dominance will have a low correlation with the overall phenological timing of the plot-level vegetation. This explains the low correlations of *C. leptophloeos* F_{dn} with the vegetation indices, which reflects the entire plot (Table 4.4).

The GCC_{ns} values of *A. pyrifolium* decreased considerably in the dry period but

did not reach their minimum until the onset of the dry season, contrary to the drop in F_{dn} and its ranking with regards to W_d. However, low GCC values indicate a long leafless period, which was confirmed by the visual inspection of digital imagery and the negligible values of transpiration. The young green leaves of *A. pyrifolium*, with high photosynthetic and transpiration rates, were produced one month after the onset of the rainy season, unlike the other species in which leaf flushing began only a few days after the rains. Moreover, it is worth mentioning that the individuals monitored using GCC were not the same ones monitored with the sap flow sensors, despite the fact that they belong to the same species.

The index adjusted to the soil, $SAVI_{S2}$, showed higher EOS bias (-47 days), compared to $NDVI_{S2}$ (-42 days) (Table 4.5), but a considerable lower SOS bias (-18 days) than $NDVI_{S2}$ (-42 days). Moreover, GCC_{ns} presented a higher correlation with $SAVI_{S2}$ (0.74) than $NDVI_{S2}$ (0.72) (SM, Table S2). Although the differences may seem small, taking into account that the dates for EOS and SOS extracted from GCC_{ns} are the most realistic representation of phenology in this work (since they were confirmed with visual analysis), we can say that $SAVI_{S2}$ better represents phenology in terms of leaf presence. However, regarding plant water use, $SAVI_{S2}$ showed a lower correlation with F_{dnc}, indicating that the best vegetation index representing phenology is not necessarily the best VI representing plant water use.

F_{dnc} exhibited a stronger linear relationship with NDVI derived from MODIS and Sentinel-2 (R^2 0.92 and R^2 0.88, respectively) than the other indices (Table 4.4; Figure 4.6). A plausible explanation for the lower performance of the $NDVI_{S2}$ is that with an increase in the resolution, the pixel heterogeneity and number of pixels per image will increase, which means that the Sentinel-2 images will be noisier. Another explanation is that the MODIS algorithm has already undergone numerous revisions, while Sentinel-2 processing may not be mature enough. In the present work, the automatic cloud detection and cirrus correction filter offered by sen2core was not totally effective, requiring a subsequent visual analysis, suggesting that the algorithm still needs improvement. The last and most likely reason is that the higher temporal resolution of MODIS increases the chance of resulting in a better image composition; therefore, the lower temporal resolution of Sentinel-2 has a higher risk of yielding poor quality images, even when accounting for the filters and quality ratings.

Compared to the near-surface GCC_{ns}, the GCC_{S2} data show a stronger correlation with the sap flow data. Theoretically linked to leaf age, both GCC indices decrease

when senescence occurs for all monitored species, as expected. However, GCC_{ns} displayed a slight increase before the end of the dry season (Figure 4.5). This unexpected rise follows the first sporadic rains and produced a temporary disconnect with F_{dn} and soil water storage, causing the relatively poor correlations (Table 4.4). Other likely explanations for these lower performances include: signal contamination by shrub vegetation, wet/dry terrain, difficulty in selecting pixels, and even the wind causing leaf movements. However, an increase in GCC_{ns} clearly signals the beginning of leaf flushing, thus it could be used in studies investigating when the growing season begins, the rate of leaf establishment, and how long the growing season lasts. Therefore, near-surface GCC data are important as it allows for individual monitoring of tree species.

Our results regarding the transition dates and water use indicate that the $NDVI_{modis}$ provided the best fit and most reliable proxy for the community phenology, but both datasets performed well. The choice of VI is of paramount importance to understand the relation of phenology and plant water use at both the species and community levels (RICHARDSON et al., 2018). Therefore, detection of the near remote phenology through the use of digital cameras (phenocams) can fill the gap between satellite and on-the-ground observations, improving the detection of which VI better represents the vegetation changes observed on the ground (see (RICHARDSON et al., 2018)). On the other hand, phenocam GCC also enhanced our understanding of the sap flow dynamics in individual plants. The fact that the decrease in sap flow is not coupled with the decrease in GCC_{ns} at the end of the rainy season in 2018 (Figure 4.5) indicates that the leaf drop of most species is preceded by the cessation of sap flow. As expected, both sap flow and GCC_{ns} remained low during the dry season. Nevertheless, while GCC_{ns} remained high and at approximately constant values after leaf flushing, the sap flow was variable during the 2018 rainy season. Regardless, the strong correlation between F_{dnc} and both NDVIs shows that the recorded phenological behaviour of the tree vegetation in the plot, as reflected by fluctuations in vegetation indices such as NDVI, represents the overall profile soil moisture conditions well and its effects on the canopy exchange processes for this Caatinga vegetation.

Our findings compare remote sensing products related to vegetation status at different temporal and spatial scales, with the aim to analyse the water use of Caatinga vegetation. Sentinel-2 and MODIS satellite products also provide data from various other spectral bands that have not been used in our analyses. Bands that could be used to generate other indices, for example, which could be explored with advanced

statistical methods, and combined with in-situ data that are complementary to ours or with data from other satellite platforms. Therefore, our study addresses the hypotheses set out at the beginning of the paper, but points to paths in which future work could be further explored.

4.5 Conclusions

Given the hypotheses raised, we can conclude the following:

(1) Soil water availability explained the Caatinga phenology at an ecosystem level, but less so at the species level;

(2) Seasonal signals of vegetation indices GCC and NDVI derived from optical RS data collected for Caatinga vegetation were indeed strongly related to water use, as represented by the late-morning community level sap flow data. However, the individual GCC determined from proximal RS (phenocams) was poorly correlated to individual sap flow.

(3) The sap flow of the monitored species was entirely limited by soil water availability when relative saturation of the soil profile fell below 0.25, a situation that occurred for more than 80% of the observed year.

Our results provide meaningful information about the physiological responses of dry forests in the Caatinga area to environmental variables. They also show the ability of different scales of SR products in detecting variations in plant phenology, which is essential information to interpret and analyse the soil water availability and plant flux density. Moreover, our findings identified when to use SR data as a proxy for phenological and physiologal processes in the Caatinga vegetation.

5 NDVI APPLICABILITY FOR MONITORING VEGETATION AND WATER CONDITIONS IN CAATINGA REGIONS

5.1 Introduction

Remote Sensing (RS) techniques are widely used to monitor many aspect of vegetation (MIRANDA et al., 2017; SANTANA, 2018; SEO et al., 2019; LI et al., 2019; MIRANDA et al., 2020). This monitoring is essential for current strategic planning and forecasting future scenarios (TORRES et al., 2017). Taking into account the large dimensions of the vegetation areas and the continental dimensions of Brazil (MAPBIOMAS, 2019), it is not difficult to see how RS plays an important role in allowing systematic monitoring of large areas of Brazilian forests in near real time. However, the application of these techniques often use models adjusted to the place of application, being limited to a specific vegetation type or location (TEIXEIRA, 2010).

The Caatinga region has diversified savanna vegetation, which can vary from steppe/shrub savanna to more dense forest formations. However, many models that seek to monitor ambient processes related to vegetation (i.e. evapotranspiration and CO_2 exchange) are frequently based on assumptions about the vegetation's properties, combining physical models (i.e. energy balance) with allometric relationships of vegetation, i.e. MOD16, MOD17A2 and MOD17A3 (NATIONAL AERONAUTICS AND SPACE ADMINISTRATION - NASA, 2020b). In such environments, a single type of vegetation is often considered, therefore they assign the same constants for the entire region. These models can have good efficiency in global applications, but their accuracy is greatly compromised when a finer spatial resolution is needed. In order to circumvent these and other problems, some studies seek to independently model the need for vegetation classification (COAGUILA et al., 2017). These models use Vegetation Indices (VIs) as proxies of vegetation status, specially the Normalized Difference Vegetation Index - NDVI. These hybrid models (physic and empiric) are very effective but end up requiring specific calibrations for each application site (TEIXEIRA, 2010)

Despite the need for vegetation descriptors, perhaps the biggest problem faced when seeking to apply orbital RS techniques to monitor vegetation is cloud cover. The availability of satellite images can be highly impaired by clouds (KANDASAMY et al., 2012), requiring the use of other platforms or mixing data from different satellite platforms and sensors.

Despite being the dominant vegetation of northeastern Brazil an area of vegeta-

tion, with an area greater than 844,000 km and more than 60% of native vegetation (MAPBIOMAS, 2019), the Brazilian Caatinga is highly fragmented, anthropized and has only 1.2% of its total extension included within effective protected areas (ANTONGIOVANNI et al., 2020)

The Caatinga dry forest is an example of a vast forest, whose monitoring in all its extension is only possible through RS. However, despite being an environment with relatively little rainfall, it also limits the use of RS techniques due mainly to the presence of clouds. In Figure 5.1, we present the average presence of clouds in a CBERS-4/WFI time series, showing that for the study period, more than 50% of the images, of a total of 257 images, have at least 40% of the area covered by clouds in the study area. This information was provided by the ratio between cloudy pixels and the total amount of pixels in the image calculated by Brazil Data Cube (BCD) (FERREIRA et al., 2020).

Figure 5.1 - Percentage of cloud coverage over CBERS-4/WFI images for the study area of Pernambuco in the study period of March 2018 to May 2019.

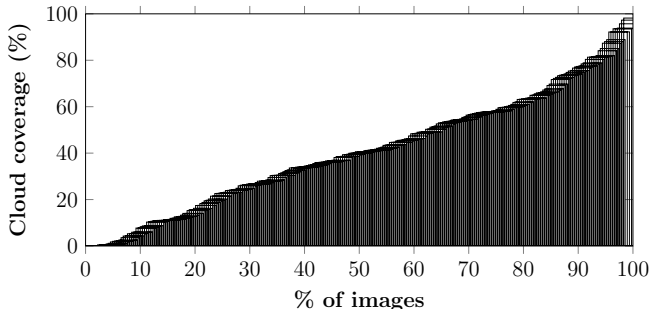

This study seeks to investigate the relationship between the NDVI of different platforms and temporal/spatial resolutions with sweating, represented by the sap flow measured directly in individuals, and test the following hypothesis: the NDVI provided from different satellite platforms is consistent in relation to Caatinga environment over different regions.

5.2 Materials and methods

5.2.1 Study area

Three areas of native Caatinga vegetation were selected, in the Brazilian state of Pernambuco (Figure 3.1), in the municipalities of Lagoa Grande (LGE) (9°02'51"S, 40°19'11"W, 393 m a.s.l.), Serra Talhada (STA) (7°58'12"S, 38°23'06"W, 470 m a.s.l.) and São João (SJO) (8°48'34"S, 36°24'20"W, 683 m a.s.l.). In each site was delimited a monitoring plot of 50 x 100 m (Figure 5.2).

Figure 5.2 - Monitoring plots location: Lagoa Grande (LGE), Serra Talhada (STA) and São João (SJO).

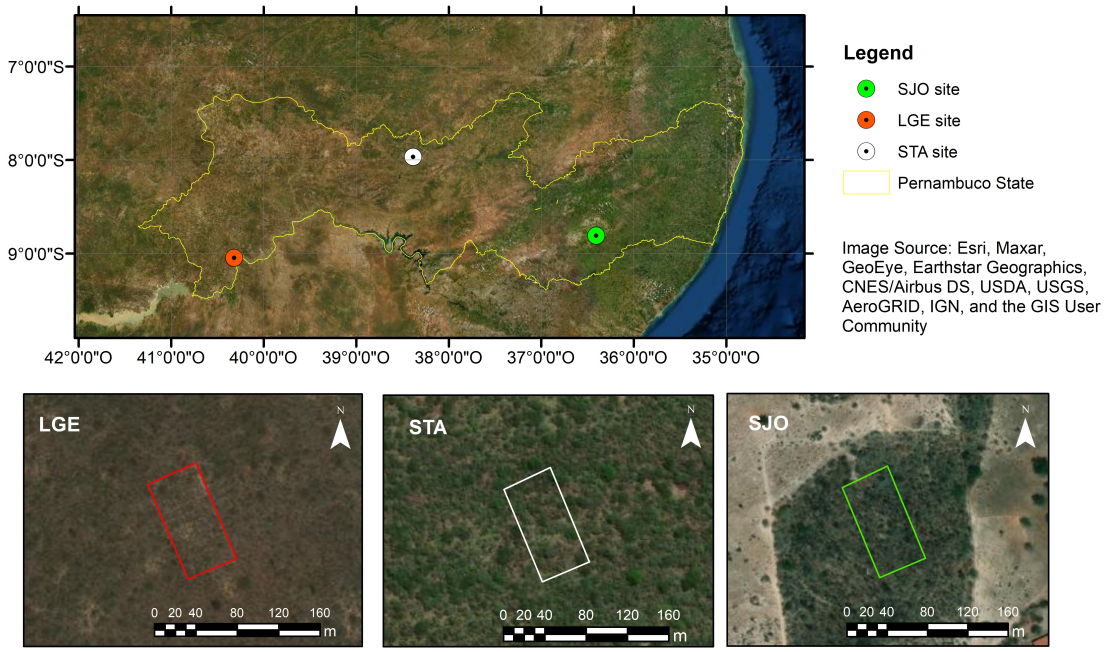

The selected regions are on a climate gradient according to the Köppen classification (BECK et al., 2018). The most arid site, LGE in the center of the Caatinga, having the Bsh (arid steppe hot) climate while STA site is in the transition between the Bsh and Aw (tropical savannah) climates, and the LGE site is under Aw climate (see Literature Figure 2.2).

Regarding the soil type found in each site, according to EMBRAPA soil map classification (EMPRESA BRASILEIRA DE PESQUISA AGROPECUÁRIA - EMBRAPA, 2018),

LGE presents a clayey soil type of acrisols (Argisolo Vermelho-Amarelos Eutroficos), STA presents also main clayey soil of Luvisols (Luvissolos Cromicos Orticos), and SJO o presents a sandy soils of Regosols (Neossolos Regoliticos Eutroficos), see Caatinga soil map in Literature Figure 2.3. A detailed description of SJO soil can be found in Brito et al. (2020), which shows SJO's soil as having more than 80% sand.

The vegetation is xerophile and deciduous in the three sites but each site has a distinct Caatinga vegetation expression. The LGE site vegetation is shrub-tree, with a sparse presence of cacti and an almost constant presence of bromeliads. In the STA monitoring plot, vegetation has and average height of with 5.5 m and an average diameter at breast height (DBH) of 8.2 cm. It's most frequent species in plot are the *Manihot pseudoglaziovii* Pax & K.Hoffm., *Cenostigma microphyllum* (Mart. ex G.Don) Gagnon & G.P.Lewis, *Sapium glandulosum* (L.) Morong, and *Senegalia piauhiensis* (Benth.) Seigler & Ebinger, both with more than 10% of monitoring plot dominance frequency. The STA site vegetation is less surb and the trees are taller (around 10 m heith) with rare presence of cacti or bromeliads (to more details about STA vegetation description please see Chapter 4). The SJO vegetation is a very dense shrub savanah with a expressive presence of large cacti. In relation to the frequency of the sampled species, the cacti *Pilosocereus sp.* presents around 35% of plot dominance and mean DBH of 14.7 cm. The following most dominant plant species in SJO are the woody species: *C. leptophloeos*, *Mimosa ophthalmocentra* Mart. ex Benth, *Sapium sp.*, *Senegalia sp.* and *Spondias tuberosa* Arruda. The average DBH in SJO plant species is 9.7 cm and the average height is 5.2 m.

5.2.2 Experimental strategy

The VIs were obtained from RS sensors which operate at different spatial and temporal scales: MODIS/Terra + Aqua (250 m products MYD13Q1 and MOD13Q1), WFI/CBERS-4 (64 m) and MSI/Sentinel-2A + B (10 m), as presented in Table 5.1.

Table 5.1 - RS data: Variable; Sensor/Satellite, spatial resolution, temporal resolution.

Variable	**Sensor/Satellite**	**S. resol.**	**Temp. resol.**
$NDVI_{modis}$	MODIS/TERRA + AQUA	250m	8 days*
$NDVI_{cbers}$	WFI/CBERS-4	64m	5 days
$NDVI_{S2}$	MSI/Sentinel-2A + 2B	10m	3-10 days

* pixel composition from daily image acquisitions

Regarding cloud detection, Sentinel-2 cloudy images were removed considering cloudy pixel confidence estimated by Sen2cor, subsequent analysis were done to remove cloudy images not recognized by Sen2cor. For CBERS-4 this processing is performed using CMASK by BDC. In addiction to CMASK, $NDVI_{cbers}$ values lower than 0.2 were also removed from valid observations in our analysis. To remove rain direct interference in transpiration and in soil behavior (soil hysteresis effect), the soil moisture was verified and the data corresponding to days with increase on soil moisture, plus 2 days after the event, was also removed from our valid observations.

Sap flow meters were installed in all three sites LGE, STA and SJO. However, due to equipment failures and logistical problems, the flow data of the SJO plot was compromised. Thus, only the STA and LGE sap flow data were considered. The selected plants comprise 20 individuals belonging to five different species found at the each plot area (LGE and STA).

Sap flow study specimens were selected based upon their abundance registered in the inventory of the monitoring plot and the Nordeste project plot network (MOONLIGHT et al., 2020). This inventory includes all plant individuals with a diameter at breast height (DBH) grater than 5cm. Plants were tagged to allow their identification in the field. Abundance of each species was determined by establishing the frequency of individuals belonging to a particular species within the experimental plot (Table 5.2. The total sapwood area to each individual was estimated based on the linear relationship between the radial diameter of the sapwood and the diameter at breast height (DBH) (LUBCZYNSKI et al., 2017). The relative contribution (Table 5.2 and Table 5.3) of the sapwood for each species was calculated based on the proportion between the sums of the sapwood areas of each species.

Table 5.2 - LGE site monitored tree species, dominance of the species in the plot (%), estimated summed sapwood area (cm^2) per species, and a percentage of this sapwood area in relation to the total area of monitored trees in the plot (%).

Species	**Dominance (%)**	**Species sap. area (cm^2)**	**% of total sap. area**
Commiphora leptophloeos	11	95	17
Manihot pseudoglaziovii	26	124	23
Cenostigma microphyllum	8	78	14
Sapium glandulosum	28	168	31
Senegalia piauhiensis	18	83	15
Total	91	548	100

Table 5.3 - STA LGE site monitored tree species, wood density (W_d, g cm^{-3}), dominance of the species in the plot (D., %), estimated summed sapwood area (cm^2) per species, and a percentage of this sapwood area in relation to the total area of monitored trees in the plot (%).

Species	W_d	**D. (%)**	**Species sap. area (cm^2)**	**% of total sap. area**
Anadenanthera colubrina	0.59	4	175	6.2
Aspidosperma pyrifolium	0.54	30	772	27.3
Commiphora leptophloeos	0.28	1	78	2.8
Cenostigma nordestinum	0.66	30	1751	62.0
Senegalia polyphylla	–	15	49	1.7
Total	–	80	2824	100

W_d values by (LIMA et al., 2012)

Sap flux density (F_d, $g\ m^{-2}\ min^{-1}$) for the selected individuals was measured using Granier's TDP method (see Chapter 3). The sap flux density at the tree individual scale (F_d) was first normalized and then scaled-up to the community level, F_{dnc}, considering the relative sapwood area of each species in the both monitoring plot (Table 5.2). F_{dnc} for the sampled species at the scale of the monitoring plot, was calculated as a weighted average, taking into account the relative contribution of the sapwood for each species.

The soil water condition is expressed terms of relative soil water saturation ($S_{e,prof}$, dimensionless) and soil matric potential (Ψ_{prof}, kPa). $S_{e,prof}$ is a fraction, relative to water saturation on soil mean profile; dependent on the actual profile soil moisture, θ_{prof}, the residual profile moisture content, $\theta_{r,prof}$, and the saturated profile moisture content, $\theta_{s,prof}$ (see Chapter **??**). The data were obtained from soil moisture and potential sensors installed along soil profiles. Due to failures in the SJO loggers, only a period equivalent to about 4 months of data was used in the soil analysis (April to August). For more details see Chapter 3. In Table 5.4 is show the $\theta_{r,prof}$, $\theta_{s,prof}$ and Available Water Capacity (AWC)).

Table 5.4 - Sites Soil traits.

Site	$\theta_{r,prof}$	$\theta_{s,prof}$	**AWC (mm)**
LGE	0.088	0.27	97.5
STA	0.035	0.42	300.0
SJO	0.025	0.14	77.5

5.2.3 Data analysis

Data analysis was conducted using chart interpretation and correlation analysis (Pearson and Spearman). In order to establish relationships between the water use and VI, we compared the temporal variability of F_{dnc} from STA and LGE with the NDVI (MODIS, CBERS-4 and Sentinel-2). The same approach was applied to assess the correspondence between the VI and the soil water condition ($S_{e,prof}$ and Ψ_{prof}), but using Spearman correlation due to not linear relation between VI and $S_{e,prof}$.

5.3 Results

The linear regression between sapwood depth parameter and DBH was given by 0.163 * DBH + 0.5, R^2 of 0.51 ($p < 0.05$ for both coefficients) to LGE samples and 0.377 * DBH -1.075, R^2 of 0.67 ($p < 0.05$ for both coefficients) to STA samples (see Appendix A). The total sapwood area estimated for all individuals of STA plot (based on the regression), per species, as well as the percentage contribution to the total active xylem area in the plot for the species monitored (% of total sapwood area), are given in Table 5.2. The total sapwood area estimated for STA individuals as well the selected species and the respective plot dominance be seen on 5.3. The total sapwood area to monitored species on monitoring plot of LGE (548 cm^2 5.2) is five times smaller than in the STA plot (2824 cm^2 5.3); despite the higher dominance of selected species, 91% to STA and 80% to LGE.

The number of total observation considered valid to each source of NDVI is in Table 5.5. The satellite with the most observations was CBERS-4 WFI camera for both sites (STA, LGE and SJO). Regarding the smaller number of valid Sentinel-2 images for SJO, 21 images were available for the period, but only 3 images were not cloudy or shaded.

Table 5.5 - Number of observations considered valid of $NDVI_{modis}$, $NDVI_{s2}$ and $NDVI_{cbers}$ on experiment period.

Plot	Modis	Sentinel-2	CBERS-4	total	days period
LGE	24	26	47	97	371
STA	27	28	48	103	420
SJO	09	03	09	23	111

5.3.1 Vegetation indices and sap flow

NDVI data for the sources Sentinel-2, MODIS and CBERS-4, are in phase with the F_{dnc} (Figure 5.3). There is stability between the different NDVIs throughout the dry season where the F_{dnc} close to 0.0. This period was longer in LGE, lasting approximately 5 months (June to December) and just over two months for STA (September to November). Both VIs seem to be very well aligned in the period of May to November, for this period, there is a greater variability when the Fdnc starts to increase (October for LGE and November for STA). There is also a more pronounced drop in the F_{dnc} compared to VI, this is barely noticeable in the STA graphs (Figure 5.3a and 5.3b), but it is much more noticeable on the LGE site. This fall is even more pronounced when observing the $S_{e,prof}$, mainly for the LGE site (Figure 5.3a), $S_{e,prof}$ appears to be approaching the minimum value a few days after the rain event.

Moreover, $NDVI_{S2}$ has overall lower values (low shift) in relation to $NDVI_{modis}$ and $NDVI_{cbers}$ for both sites; this can be seen most clearly when F_{dnc} is close to 0.0.

Figure 5.3 - a) $NDVI_{modis}$, $NDVI_{S2}$ and $NDVI_{cbers}$ with rainfall and $S_{e,prof}$ for LGE monitoring plot location; b) F_{dnc} of LGE; c) EVI_{modis}, $EVI2_{S2}$, $SAVI_{S2}$ for STA monitoring plot location; d) F_{dnc} of STA.

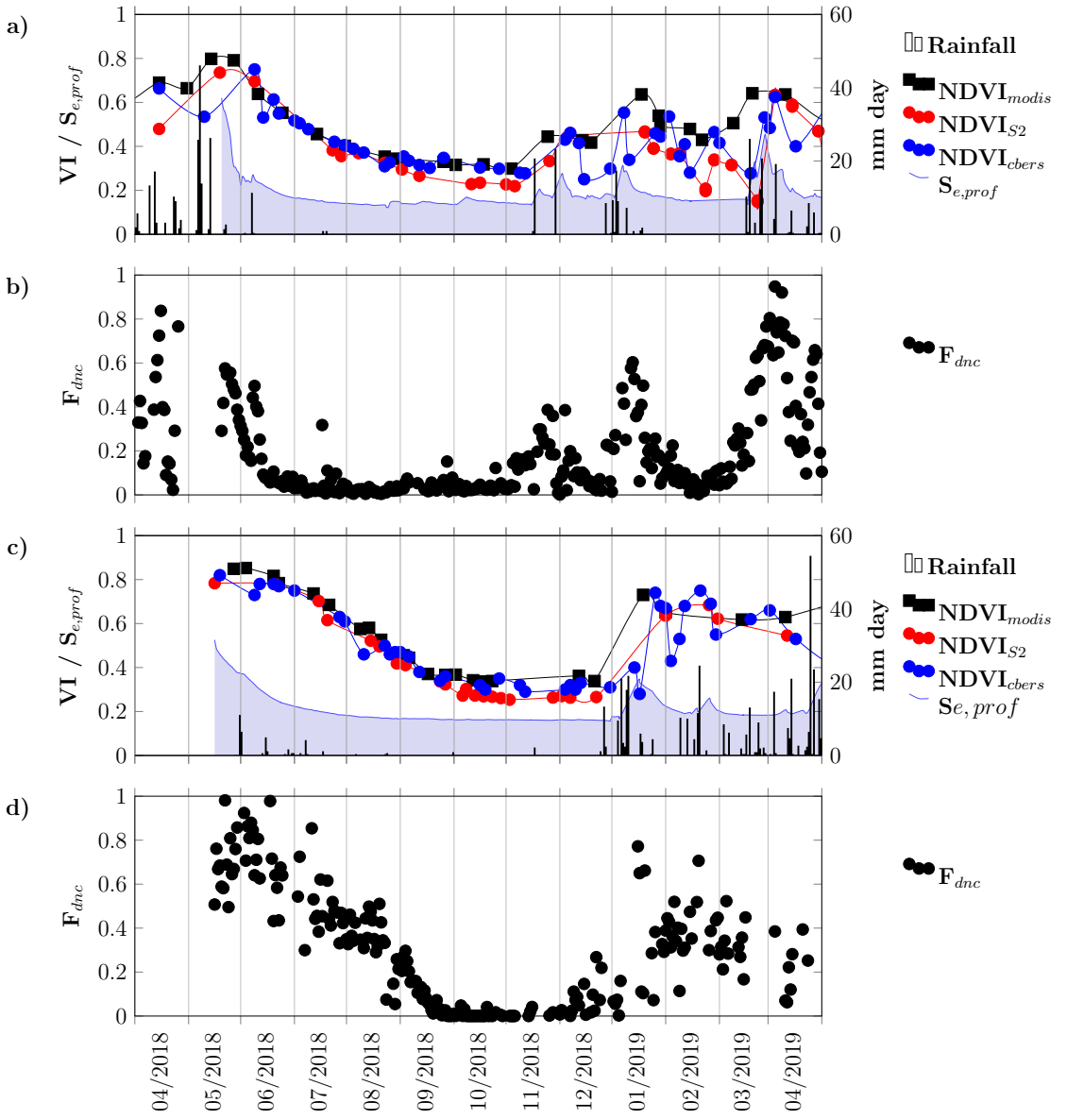

The variation of the three NDVI in relation to the variation of the $\Psi_{prof} \times -1$ (Figure 5.5) shows a linear but quite dispersed relationship and both correlations between them were higher for the STA site than for the LGE site (Table 5.4); The $NDVI_{cbers}$ seems to better follow the variation in the LGE F_{dnc} in relation to the $NDVI_{modis}$ and $NDVI_{sentinel}$ (Figure 5.3 a) and b)), but it has lower correlation.

Figure 5.4 - Scatter plots of F_{dnc} versus $NDVI_{modis}$, $NDVI_{cbers}$ and $NDVI_{sentinel}$ to sites STA plot a) and LGE plot b).

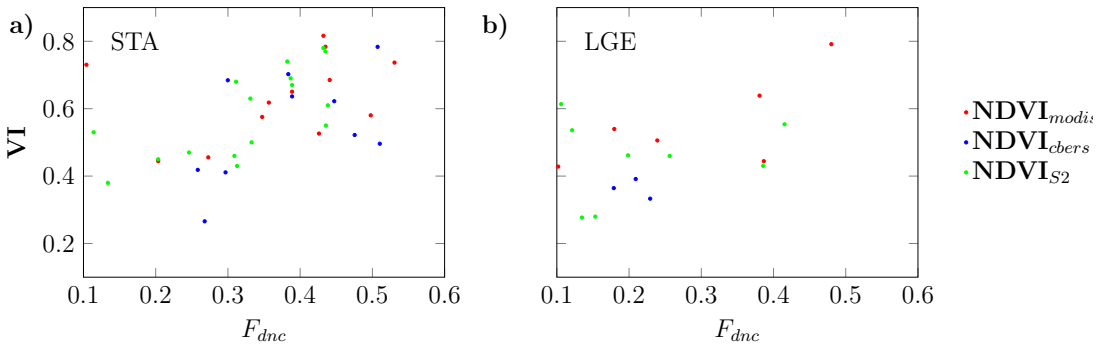

Table 5.6 - Pearson correlation between $NDVI_{modis}$, $NDVI_{s2}$ and $NDVI_{cbers}$ versus LGE F_{dnc} and STA F_{dnc}.

Plot	Modis	Sentinel-2	CBERS-4
LGE F_{dnc}	0.79*	0.77*	0.48*
STA F_{dnc}	0.92*	0.88*	0.85*

5.3.2 Vegetation indices and soil water conditions

The relation between VIs and $S_{e,prof}$ presented the same pattern of behavior analyzed in the Chapter 4 to all monitoring plots (Figure 5.5 a, c and e). Both $NDVI_{modis}$, $NDVI_{cbers}$ and $NDVI_{s2}$ shown a similar behavior and for both sites and NDVI seems to stabilize when $S_{e,prof}$ is greater than 0.2. Regarding Ψ_{prof} (Figures 5.5 b, d and f), NDVI from both satellites and both sites drops when Ψ_{prof} is under -1000 kpa, but for STA and LGE the limit to NDVI values seems to be 1500 kpa, while for SJO site $S_{e,prof}$ values reach -3000 kpa.

Figure 5.5 - Scatter plots of $S_{e,prof}$ and $\Psi_{prof} \times -1$ versus $NDVI_{modis}$, $NDVI_{cbers}$ and $NDVI_{s2}$ to sites: STA plots a) and b); SJO plots b) and c); LGE plots e) and f).

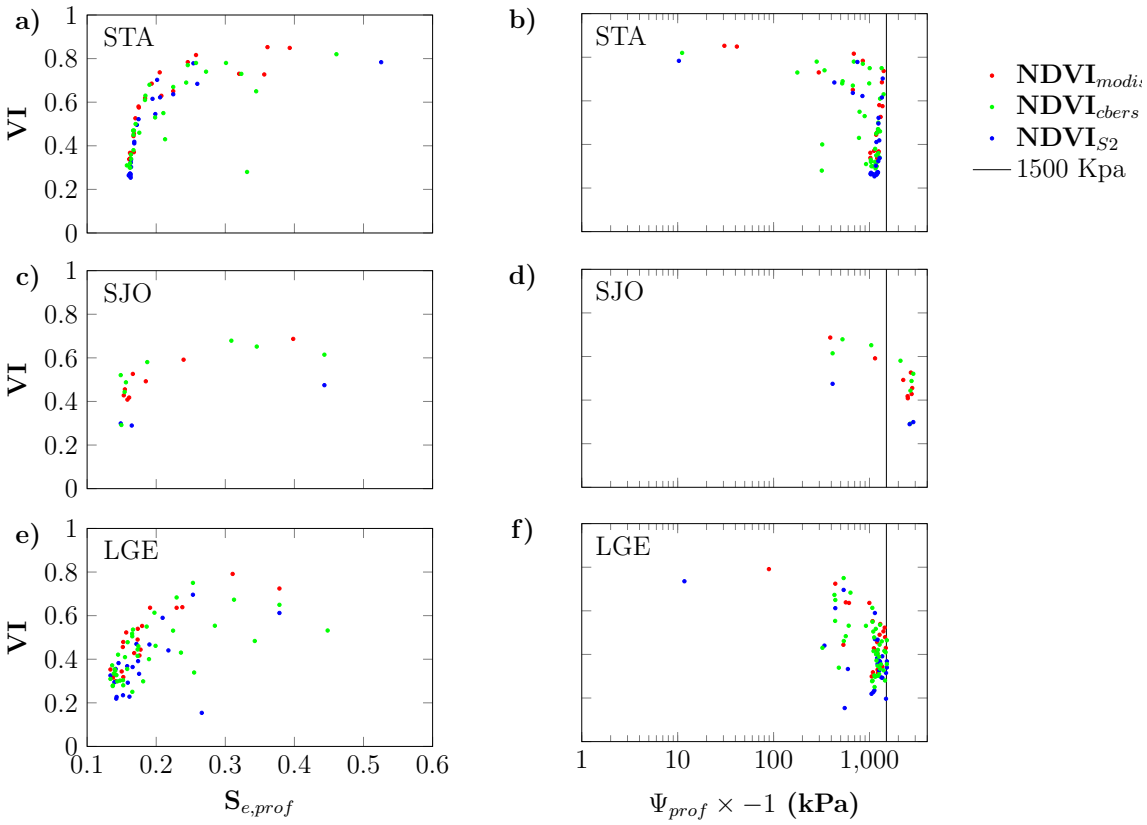

The Spearman posts correlation was very high for the three sites and, in general, both NDVI (Table 5.7). Despite not having a linear relationship, $S_{e,prof}$ is obtained from soil moisture sensors, that doesn't vary much from day to day in comparison to F_{dnc}. The only non-significant correlation was that between SJO $S_{e,prof}$ and $NDVI_{s2}$ due to low number of observations (Table 5.5).

Table 5.7 - Spearman correlation of $NDVI_{modis}$, $NDVI_{s2}$ and $NDVI_{cbers}$ versus $S_{e,prof}$ to plots LGE, STA and SJO.

Plot	**Modis**	**Sentinel-2**	**CBERS-4**
STA $S_{e,prof}$	0.96*	0.92*	0.91*
LGE $S_{e,prof}$	0.86*	0.52*	0.70*
SJO $S_{e,prof}$	0.78*	0.76	0.76*

5.4 Discussion

The periods where there are rain events present greater instability, both in the NDVI ($NDVI_{modis}$, $NDVI_{cbers}$ and $NDVI_{S2}$) and in F_{dnc} signal. In relation to NDVI, this happens due to the greater presence of clouds, cloud shadows and cirrus that can contaminate the image contaminating the signal, even with the cloud filters that have been applied. $NDVI_{modis}$ modis shows better correlation in all comparisons (see Table 5.7 and Table 5.6. Despite presenting a smaller number of observations than $NDVI_{cbers}$ and have the coarsest spatial resolution of the three (250 m versus 64 m from CBERS-4/WFI), MODIS products used are generated from the selection of the best pixels obtained of daily images (see Chapter 2). This seems to have been the factor that most influenced the achievement of the best correlations, which seems to give a great advantage in terms of quality / stability in the NDVI signal evolution.

The $NDVI_{cbers}$ presented a lower correlation with LGE F_{dnc} than $NDVI_{modis}$ and $NDVI_{sentinel}$ (Table 5.6). However, observing that seems to better follow the F_{dnc} variation (Figure 5.3a and 5.3b) it is plausible to consider that this lower correlation is attributed to the daily variation of the F_{dnc} signal and to the greater number of considered observations.

On the other hand, even with a large number of observations, when consider both NDVI from various sources, the evolution of the signal in the rainy season is quite uncertain. In addition, despite not having found many differences between the NDVI in the dry period, it may happen that, due to the difference in spatial resolution, mainly in relation to $NDVI_{modis}$ for the $NDVI_{S2}$, it may happen that in a pixel region there was rain event and in the plot not, which could cause a response in the pixel MODIS and not in the clipping of the plot of Sentinel-2, since the plot is smaller than the pixel.

This type of event is not improbable, quite the opposite, can be seen in in the Figure 5.3, for both LGE and STA, that there are some increases in the $S_{e,prof}$ that do not seem to have an event corresponding rain (see Figure 5.3.a) and some rain events that do not seem to increase the $S_{e,prof}$ (see July Figure 5.3.c). Taking into account that the soil moisture was measured in the monitoring plot, the rain was measured in the tower (about 150 meters away from the respective plot), and the localized and sparse pattern characteristics of Caatinga rainfall, already reported by literature (REIS, 1976; **??**) these events are likely to have occurred. Therefore, filtering the data considering only the rain events recorded by the tower pluviometer was not enough

to remove the influence of soil hysteresis caused by soil water recharge, making it necessary to consider positive changes the values of soil moisture in the monitoring plot also as a rain event.

Regarding instability in F_{dnc}, at least tree factors are involved: First, the flow measurement of the next day is not necessarily related to the previous measurement. In spite of the development of leaf cover, necessary for transpiration, and the leaves senescence to be a process with temporal dependence, other factors directly influence transpiration, for example transpiration ceases almost completely when there are rain events (see Section 5.2.2), for this reason the removal data when the soil were recharging were essential to obtain better correlations. Second, the self made sensors and dataloggers need calibration every 3-4 months, not always possible due to logistical difficulties and the number of sensors installed, as the sensors were degraded, the quality of the data was gradually compromised.

Scatter plots of STA 5.5a and 5.5b presented much more stable relation, while $NDVI_{modis}$ seems to be more sable than $NDVI_{cbers}$ and $NDVI_{s2}$. Despite appearing to be noisier than $NDVI_{modis}$, $NDVI_{cbers}$ presented a high number of valid images (Table 5.5) and, among the three options, was the source with highest number of observations considered valid for the observed period. So being a candidate for a possible $NDVI_{modis}$ substitute, or complement.

Even considering the $S_{e,prof}$ as a comparable measure for the soil water situation between the three sites (since they consider the residual and saturation moisture of each soil), we can see that there is a great difference in the fall rate of the $S_{e,prof}$ when the rain events dry (see Figure 5.3 a and c). The rate drops faster in LGE than STA most due to differences in soil AWC (97.5mm to LGE and 300mm to STA). The greater AWC of STA provides an extension of the F_{dnc} period and allows the vegetation to maintain the foliage for much longer, as can be seen in the NDVI response.

The NDVI response was directly linked to the water condition of the water when $S_{e,prof}$ is below 0.25 for the three sites Figure 5.5. Therefore, the variation in the vegetation indices used is able to reflect the variation in leaf dynamics and transpiration, which is more than 80% of the time limited by water availability. However, the rapid dynamics of vegetation at the beginning of the rainy season, combined with the strong presence of clouds and the spatial variability of rain, impairs the monitoring of vegetation in this period on a small areas, such as the monitored plot areas.

Although it is not possible to evaluate the sap flow for the SJO plot due to the flaws in the sensors, it is possible to infer that the linear relationship between the sap flow and the NDVI applies to this site, since the overall behavior pattern between NDVI and $S_{e,prof}$ also remained (5.5).

5.5 Conclusion

Given the hypotheses raised, we can conclude that the relationships found in the previous hypotheses were confirmed for the other sites. However, the absolute relationship between NDVI signal evolution and these variables changes according to the Caatinga region.

6 GENERAL DISCUSSION

The present work explored Remote Sensing together with several other data acquisition tools in vegetation areas of Caatinga. They were: moisture sensors and soil potential, sap flow sensors, average air temperature, VPD and liquid radiation.

The sap flow sensors allowed to identify differences in the duration of the transpiration periods for different species of the LGE plot and related to the wood density. A relationship that had been indicated using litter data by Lima and Rodal (2010), Lima et al. (2012). However, these authors pointed out that the difference in the timing of low density species could be due to a stronger dependence on the photo period. Our study indicates that the difference is probably due to a stronger control strategy of these species to avoid cavitation, since high wood density promoted by thick cell walls, plays an important role in protecting plants from cavitation (SOBRADO, 1993; STRATTON et al., 2000; HACKE et al., 2001).

The GCC_{ns} was very useful to identify individual species leaf flush and senescence, since it could be obtained from ordinary cameras with daily images. However, on the plot scale, the GCC_{s2} performance was lower than the other tested indices (NDVI and SAVI) in all tests. Regarding transpiration and water condition, NDVI presented the best performance, showing correlations that reach 0.9 (Table 4.4). This corroborates with the high performance (reaching 0.92 R^2) found by Miranda et al. (2017), by using the Simple Algorithm for Retrieving Evapotranspiration (SAFER), method that uses NDVI as a descriptor of vegetation condition, to estimate actual evapotranspiration. Regarding the dynamics of leaf coverage, the SOS and EOS dates estimated with SAVI were the ones that came closest to the dates estimated with the GCC of phenocam (GCC_{ns}), considered as field truth. Indicating that for the Caatinga region SAVI is the best leaf cover descriptor. A result that goes according to the studies of Miranda et al. (2020). Among the tested sources (Sentinel-2, MODIS and CBERS-4), NDVI Modis presented the best correlations, mainly due to being a composition of daily images, which gives it a greater probability of achieving values without interference from clouds, despite the low spatial representativeness resolution, due to its low spatial resolution. What emphasizes the importance of a low revisit time.

The methodology adopted for up-scaling the individual sap flow for the community allowed a direct comparison between the normalized sap flow and remote sensing. The fact that the correlation of IV's with F_{dnc} was higher than with F_{dn} (4.4) shows that the up-scaling method was successful. Although it is not possible to evaluate

the sap flow for the SJO plot due to the flaws in the sensors, it is possible to infer that the linear relationship between the sap flow and the NDVI applies to this site, since the overall behavior pattern between NDVI and $S_{e,prof}$ also remained (5.5).

The variation in the VI's used is able to reflect the variation in leaf dynamics and transpiration, which is more than 80% of the time, period that vegetation is limited by water availability. The VI's used were sufficient to explain the environment dynamics vegetation senescence and soil water condition, in the wet-to-dry period, but the correlation in the wet period is difficult to analyse. The fast dynamics of environment and vegetation response at the beginning of the rainy season, combined with the more frequent clouds cover and the spatial variability of rain, makes very difficult monitor the dynamics of vegetation at the rainy season.

The $NDVI_{cbers}$ obtained from the CBERS-4 satellite proves to be a viable substitute for $NDVI_{modis}$, which, despite performing very well, is reaching the limit of its operational range. This becomes even more plausible if taken into account CBERS program continuation by CBERS-4A, launched on 7 December 2019, whose WFI sensor has 55m spatial resolution, due to lower altitude (INSTITUTO NACIONAL DE PESQUISAS ESPACIAIS - INPE, 2019).

7 CONCLUSION

Given the hypotheses raised: (1) Caatinga phenology at the community scale (represented by RS data) and individual scale (represented by near proximal RS data) are fully explained by soil water availability; (2) time series of optical RS data for the Caatinga vegetation are strongly correlated to variations in individual's species water use; (3) variations in the sap flow signal are fully explained by changes in water availability; (4) the RS data relations with Caatinga environment identified in the previously hypotheses are consistent and applicable over different regions with different rainfall regimes and soil characteristics. We can conclude that:

1) Soil water availability explains the Caatinga phenology at an ecosystem level, but less so on a per-species basis;

2) Seasonal signals of VIs GCC and NDVI derived from optical orbital RS data collected for Caatinga vegetation are indeed strongly related to water use, as represented by late morning community level sap flow data. However, the individual GCC determined from proximal RS (phenocams) is poorly correlated to individual sap flow;

3) The sap flow of the monitored species is entirely limited by soil water availability when relative saturation of the soil profile falls below 0.25, a situation occurring for more than 80% of the observed year;

4) The relationships found in the previous hypotheses were confirmed for the other sites. However, the absolute relationship between NDVI signal evolution and these variables changes according to the Caatinga region.

REFERENCES

AHRENDS, H.; ETZOLD, S.; KUTSCH, W.; STOECKLI, R.; BRUEGGER, R.; JEANNERET, F.; WANNER, H.; BUCHMANN, N.; EUGSTER, W. Tree phenology and carbon dioxide fluxes: use of digital photography for process-based interpretation at the ecosystem scale. **Climate Research**, v. 39, p. 261–274, 9 2009. Available from: <https://doi.org/10.3354/cr00811>. 11, 22

ALBERTON, B.; ALMEIDA, J.; HELM, R.; TORRES, R. da S.; MENZEL, A.; MORELLATO, L. P. C. Using phenological cameras to track the green up in a cerrado savanna and its on-the-ground validation. **Ecological Informatics**, v. 19, p. 62–70, 1 2014. Available from: <https://doi.org/10.1016/j.ecoinf.2013.12.011>. 22

ALBERTON, B.; TORRES, R. da S.; CANCIAN, L. F.; BORGES, B. D.; ALMEIDA, J.; MARIANO, G. C.; SANTOS, J. dos; MORELLATO, L. P. C. Introducing digital cameras to monitor plant phenology in the tropics: applications for conservation. **Perspectives in Ecology and Conservation**, v. 15, n. 2, p. 82–90, 4 2017. Available from: <https://doi.org/10.1016/j.pecon.2017.06.004>. 11, 22, 33

ALBERTON, B.; TORRES, R. da S.; SILVA, T. S. F.; ROCHA, H.; MOURA, M. S. B.; MORELLATO, L. Leafing patterns and drivers across seasonally dry tropical communities. **Remote Sensing**, v. 11, n. 19, p. 2267, 9 2019. Available from: <https://doi.org/10.3390/rs11192267>. 2, 11, 22, 31, 33, 40, 41, 47

ALMEIDA, C. A. de; COUTINHO, A. C.; ESQUERDO, J. C. D. M.; ADAMI, M.; VENTURIERI, A.; DINIZ, C. G.; DESSAY, N.; DURIEUX, L.; GOMES, A. R. High spatial resolution land use and land cover mapping of the brazilian legal amazon in 2008 using landsat-5/TM and MODIS data. **Acta Amazonica**, v. 46, n. 3, p. 291–302, sep. 2016. Available from: <https://doi.org/10.1590/1809-4392201505504>. 12

ANTONGIOVANNI, M.; VENTICINQUE, E. M.; MATSUMOTO, M.; FONSECA, C. R. Chronic anthropogenic disturbance on caatinga dry forest fragments. **Journal of Applied Ecology**, v. 57, n. 10, p. 2064–2074, jul. 2020. Available from: <https://doi.org/10.1111/1365-2664.13686>. 1, 6, 54

ANYIA, A. Water-use efficiency, leaf area and leaf gas exchange of cowpeas under mid-season drought. **European Journal of Agronomy**, v. 20, n. 4, p. 327–339,

04 2004. Available from:
<https://doi.org/10.1016/s1161-0301(03)00038-8>. 13

BAIAMONTE, G.; MOTISI, A. Analytical approach extending the granier method to radial sap flow patterns. **Agricultural Water Management**, v. 231, p. 105988, mar. 2020. Available from:
<https://doi.org/10.1016/j.agwat.2019.105988>. 14

BECK, H. E.; ZIMMERMANN, N. E.; MCVICAR, T. R.; VERGOPOLAN, N.; BERG, A.; WOOD, E. F. Present and future köppen-geiger climate classification maps at 1-km resolution. **Scientific Data**, v. 5, n. 1, oct. 2018. Available from:
<https://doi.org/10.1038/sdata.2018.214>. 7, 55

BEST, M. J.; PRYOR, M.; CLARK, D. B.; ROONEY, G. G.; ESSERY, R. L. H.; MÉNARD, C. B.; EDWARDS, J. M.; HENDRY, M. A.; PORSON, A.; GEDNEY, N.; MERCADO, L. M.; SITCH, S.; BLYTH, E.; BOUCHER, O.; COX, P. M.; GRIMMOND, C. S. B.; HARDING, R. J. The joint UK land environment simulator (JULES), model description – part 1: energy and water fluxes. **Geoscientific Model Development**, v. 4, n. 3, p. 677–699, 9 2011. Available from: <https://doi.org/10.5194/gmd-4-677-2011>. 21

BORGES, C. K.; SANTOS, C. A. C. dos; CARNEIRO, R. G.; SILVA, L. L. da; OLIVEIRA, G. de; MARIANO, D.; SILVA, M. T.; SILVA, B. B. da; BEZERRA, B. G.; PEREZ-MARIN, A. M.; MEDEIROS, S. de S. Seasonal variation of surface radiation and energy balances over two contrasting areas of the seasonally dry tropical forest (caatinga) in the brazilian semi-arid. **Environmental Monitoring and Assessment**, v. 192, n. 8, jul. 2020. Available from:
<https://doi.org/10.1007/s10661-020-08484-y>. 2

BRITO, T. R. do C.; LIMA, J. R. D. S.; OLIVEIRA, C. L. de; SOUZA, R. M. S.; ANTONINO, A. C. D.; MEDEIROS, É. V. de; SOUZA, E. S. de; ALVES, E. M. Mudanças no uso da terra e efeito nos componentes do balanço hídrico no agreste pernambucano. **Revista Brasileira de Geografia Física**, v. 13, n. 2, p. 870, 2020. Available from: <https://doi.org/10.26848/rbgf.v13.2.p870-886>. 56

BURKART, S.; MANDERSCHEID, R.; WEIGEL, H.-J. Design and performance of a portable gas exchange chamber system for CO2- and h2o-flux measurements in crop canopies. **Environmental and Experimental Botany**, v. 61, n. 1, p. 25–34, 09 2007. Available from:
<https://doi.org/10.1016/j.envexpbot.2007.02.007>. 13

BUTZ, P.; HöLSCHER, D.; CUEVA, E.; GRAEFE, S. Tree water use patterns as influenced by phenology in a dry forest of southern ecuador. **Frontiers in Plant Science**, v. 9, 6 2018. Available from: <https://doi.org/10.3389/fpls.2018.00945>. 14, 33

CÁRDENAS, M. F.; RAMÍREZ, C. L.; MEJÍA, J. D.; ESCOBAR, J. F. Design and implementation of a low-cost device for measuring sap flow in woody species. **DYNA**, v. 86, n. 208, p. 214–220, jan. 2019. Available from: <https://doi.org/10.15446/dyna.v86n208.72039>. 15, 26, 27

ČERMÁK, J.; KUČERA, J.; NADEZHDINA, N. Sap flow measurements with some thermodynamic methods, flow integration within trees and scaling up from sample trees to entire forest stands. **Trees**, v. 18, n. 5, p. 529–546, 06 2004. Available from: <https://doi.org/10.1007/s00468-004-0339-6>. 13

CHAVE, J.; COOMES, D.; JANSEN, S.; LEWIS, S. L.; SWENSON, N. G.; ZANNE, A. E. Towards a worldwide wood economics spectrum. **Ecology Letters**, v. 12, n. 4, p. 351–366, 4 2009. Available from: <https://doi.org/10.1111/j.1461-0248.2009.01285.x>. 32

CLIMATE-DATA.ORG. **Clima Serra Talhada**. 2019. Available from: "https://pt.climate-data.org/america-do-sul/brasil/pernambuco/serra-talhada-42488/". Access in 16 Sept. 2019. 18, 34, 35

COAGUILA, D. N.; HERNANDEZ, F. B. T.; TEIXEIRA, A. H. de C.; FRANCO, R. A. M.; LEIVAS, J. F. Water productivity using SAFER - simple algorithm for evapotranspiration retrieving in watershed. **Revista Brasileira de Engenharia Agrícola e Ambiental**, v. 21, n. 8, p. 524–529, 8 2017. Available from: <https://doi.org/10.1590/1807-1929/agriambi.v21n8p524-529>. 2, 33, 53

COSTA, M. H.; BIAJOLI, M. C.; SANCHES, L.; MALHADO, A. C. M.; HUTYRA, L. R.; ROCHA, H. R. da; AGUIAR, R. G.; ARAÚJO, A. C. de. Atmospheric versus vegetation controls of amazonian tropical rain forest evapotranspiration: are the wet and seasonally dry rain forests any different? **Journal of Geophysical Research**, v. 115, n. G4, 11 2010. Available from: <https://doi.org/10.1029/2009jg001179>. 41

DEVICES, I. D. **5TM water content and temperature sensor**. 2017. Available from: "http://manuals.decagon.com/Retired%20and%20Discontinued/Manuals/13441_5TM_Web.pdf". Access in: 22 June 2020. 20

DIDAN, K. **MOD13Q1 MODIS/terra vegetation indices 16-day L3 global 250m SIN grid V006**. NASA EOSDIS Land Processes DAAC, 2015. Available from: <https://lpdaac.usgs.gov/products/mod13q1v006/>. 11, 23

_____. **MYD13Q1 MODIS/aqua vegetation indices 16-day L3 global 250m SIN grid V006**. NASA EOSDIS Land Processes DAAC, 2015. Available from: <https://lpdaac.usgs.gov/products/myd13q1v006/>. 11, 23

DINIZ, J. M. F. de S.; MACIEL, D. A.; GAMA, F. F.; ADAMI, M. A. M. Avaliação do sentinel-2, NDVI e MLME para mapeamento do uso e cobertura da terra. **Anuário do Instituto de Geociências - UFRJ**, v. 43, n. 2, aug. 2020. Available from: <https://doi.org/10.11137/2020_2_381_391>. 12

DUGAS, W.; HEUER, M.; HUNSAKER, D.; KIMBALL, B.; LEWIN, K.; NAGY, J.; JOHNSON, M. Sap flow measurements of transpiration from cotton grown under ambient and enriched CO2 concentrations. **Agricultural and Forest Meteorology**, v. 70, n. 1-4, p. 231–245, sep. 1994. Available from: <https://doi.org/10.1016/0168-1923(94)90060-4>. 13

DURNER, W. Hydraulic conductivity estimation for soils with heterogeneous pore structure. **Water Resources Research**, v. 30, n. 2, p. 211–223, 2 1994. Available from: <https://doi.org/10.1029/93wr02676>. 9, 20

EMPRESA BRASILEIRA DE PESQUISA AGROPECUÁRIA - EMBRAPA. **Brazilian soil classification system**. 2018. Available from: <https://www.embrapa.br/busca-de-publicacoes/-/publicacao/1094001/brazilian-soil-classification-system>. Access in: 14 Jan. 2021. 8, 55

EUROPEAN SPACE AGENCY - ESA. **Sentinel-2 user handbook**. ESA Standard Document, 2015. Available from: <https://sentinel.esa.int/web/sentinel/missions/sentinel-2>. 10

FENG, Y.; HAO, W.; GAO, L.; LI, H.; GONG, D.; CUI, N. Comparison of maize water consumption at different scales between mulched and non-mulched croplands. **Agricultural Water Management**, v. 216, p. 315–324, may 2019. Available from: <https://doi.org/10.1016/j.agwat.2019.02.016>. 13

FERNÁNDEZ, J.; PALOMO, M.; DI

AZ-ESPEJO, A.; CLOTHIER, B.; GREEN, S.; GIRÓN, I.; MORENO, F. Heat-pulse measurements of sap flow in olives for automating irrigation: tests, root flow and diagnostics of water stress. **Agricultural Water Management**, v. 51,

n. 2, p. 99–123, oct. 2001. Available from: <https://doi.org/10.1016/s0378-3774(01)00119-6>. 13

FERREIRA, T. R.; SILVA, B. B. D.; MOURA, M. S. B. D.; VERHOEF, A.; NÓBREGA, R. L. The use of remote sensing for reliable estimation of net radiation and its components: a case study for contrasting land covers in an agricultural hotspot of the brazilian semiarid region. **Agricultural and Forest Meteorology**, v. 291, p. 108052, 9 2020. Available from: <https://doi.org/10.1016/j.agrformet.2020.108052>. 2, 32, 33, 41, 54

FRANCESCONI, W.; SRINIVASAN, R.; PéREZ-MIñANA, E.; WILLCOCK, S. P.; QUINTERO, M. Using the soil and water assessment tool (swat) to model ecosystem services: a systematic review. **Journal of Hydrology**, v. 535, p. 625 – 636, 2016. ISSN 0022-1694. Available from: <http://www.sciencedirect.com/science/article/pii/S0022169416000524>. 1, 31

GOLDSTEIN, G.; MEINZER, F. C.; BUCCI, S. J.; SCHOLZ, F. G.; FRANCO, A. C.; HOFFMANN, W. A. Water economy of Neotropical savanna trees: six paradigms revisited. **Tree Physiology**, v. 28, n. 3, p. 395–404, 03 2008. ISSN 1758-4469. Available from: <https://doi.org/10.1093/treephys/28.3.395>. 33

GONÇALVES, N. B.; LOPES, A. P.; DALAGNOL, R.; WU, J.; PINHO, D. M.; NELSON, B. W. Both near-surface and satellite remote sensing confirm drought legacy effect on tropical forest leaf phenology after 2015/2016 ENSO drought. **Remote Sensing of Environment**, v. 237, p. 111489, 2 2020. Available from: <https://doi.org/10.1016/j.rse.2019.111489>. 2

GRANIER, A. Une nouvelle méthode pour la mesure du flux de sève brute dans le tronc des arbres. **Annales des Sciences Forestères**, v. 42, p. 193–200, 1985. 14, 25, 33

_____. Evaluation of transpiration in a douglas-fir stand by means of sap flow measurements. **Tree Physiology**, v. 3, p. 309–319, 1987. 33

GROSSIORD, C.; CHRISTOFFERSEN, B.; ALONSO-RODRíGUEZ, A. M.; ANDERSON-TEIXEIRA, K.; ASBJORNSEN, H.; APARECIDO, L. M. T.; BERRY, Z. C.; BARALOTO, C.; BONAL, D.; BORREGO, I.; BURBAN, B.; CHAMBERS, J. Q.; CHRISTIANSON, D. S.; DETTO, M.; FAYBISHENKO, B.; FONTES, C. G.; FORTUNEL, C.; GIMENEZ, B. O.; JARDINE, K. J.; KUEPPERS, L.; MILLER, G. R.; MOORE, G. W.; NEGRON-JUAREZ, R.;

STAHL, C.; SWENSON, N. G.; TROTSIUK, V.; VARADHARAJAN, C.; WARREN, J. M.; WOLFE, B. T.; WEI, L.; WOOD, T. E.; XU, C.; MCDOWELL, N. G. Precipitation mediates sap flux sensitivity to evaporative demand in the neotropics. **Oecologia**, v. 191, n. 3, p. 519–530, 9 2019. Available from: <https://doi.org/10.1007/s00442-019-04513-x>. 33

HACKE, U. G.; SPERRY, J. S.; POCKMAN, W. T.; DAVIS, S. D.; MCCULLOH, K. A. Trends in wood density and structure are linked to prevention of xylem implosion by negative pressure. **Oecologia**, v. 126, n. 4, p. 457–461, 2 2001. Available from: <https://doi.org/10.1007/s004420100628>. 32, 49, 67

HUETE, A. A soil-adjusted vegetation index (savi). **Remote sensing of Environment**, v. 25, p. 295–309, 1988. 12

HUETE, A.; DIDAN, K.; MIURA, T.; RODRIGUEZ, E.; GAO, X.; FERREIRA, L. Overview of the radiometric and biophysical performance of the MODIS vegetation indices. **Remote Sensing of Environment**, v. 83, n. 1-2, p. 195–213, nov. 2002. Available from: <https://doi.org/10.1016/s0034-4257(02)00096-2>. 11

HUETE, A.; JUSTICE, C.; LIU, H. Development of vegetation and soil indices for MODIS-EOS. **Remote Sensing of Environment**, v. 49, n. 3, p. 224–234, sep. 1994. Available from: <https://doi.org/10.1016/0034-4257(94)90018-3>. 11

INSTITUTO BRASILEIRO DE GEOGRAFIA E ESTATÍSTICA - IBGE. **Biomas e sistema costeiro-marinho do brasil**. 2019. Available from: <https://www.ibge.gov.br/>. Access in: 14 Jan. 2021. 5

INSTITUTO NACIONAL DE PESQUISAS ESPACIAIS - INPE. **CBERS-3 e 4**. 2018. Available from: <http://www.cbers.inpe.br/sobre/cbers3-4.php>. Access in: 30 nov. 2020. 10

_____. **Câmeras imageadoras CBERS 04A**. 2019. Available from: <http://www.cbers.inpe.br/sobre/cameras/cbers04a.php>. Access in: 30 Nov. 2020. 68

JABLOUN, M.; SAHLI, A. Evaluation of FAO-56 methodology for estimating reference evapotranspiration using limited climatic data. **Agricultural Water Management**, v. 95, n. 6, p. 707–715, 06 2008. Available from: <https://doi.org/10.1016/j.agwat.2008.01.009>. 13

JACOMINE, P. K. T.; CAVALCANTI, A. C.; BURGOS, N.; PESSO, S. C. P.; SILVEIRA, C. O. **Levantamento exploratório-reconhecimento de solos do Estado de Pernambuco**. Recife: SUDENE, 1973., 1973. 34

JOHN, A.; SKELTON, R.; XU, K.; XU, A.; CANTILLO, J. New, open-source miniature external sap flow gauges for capturing plant water use. **Acta Horticulturae**, n. 1300, p. 47–54, dec. 2020. Available from: <https://doi.org/10.17660/actahortic.2020.1300.7>. 15

KANDASAMY, S.; BARET, F.; VERGER, A.; NEVEUX, P.; WEISS, M. A comparison of methods for smoothing and gap filling time series of remote sensing observations: application to MODIS LAI products. **Biogeosciences Discussions**, v. 9, n. 12, p. 17053–17097, 12 2012. Available from: <https://doi.org/10.5194/bgd-9-17053-2012>. 33, 53

KILLEEN, T. J.; JARDIM, A.; MAMANI, F.; ROJAS, N. Diversity, composition and structure of a tropical semideciduous forest in the chiquitanía region of santa cruz, bolivia. **Journal of Tropical Ecology**, v. 14, n. 06, p. 803–827, 11 1998. Available from: <https://doi.org/10.1017/s0266467498000583>. 49

KOTTEK, M.; GRIESER, J.; BECK, C.; RUDOLF, B.; RUBEL, F. World map of the köppen-geiger climate classification updated. **Meteorologische Zeitschrift**, v. 15, n. 3, p. 259–263, 7 2006. Available from: <https://doi.org/10.1127/0941-2948/2006/0130>. 34

KUME, T.; OTSUKI, K.; DU, S.; YAMANAKA, N.; WANG, Y.-L.; LIU, G.-B. Spatial variation in sap flow velocity in semiarid region trees: its impact on stand-scale transpiration estimates. **Hydrological Processes**, v. 26, n. 8, p. 1161–1168, 7 2011. Available from: <https://doi.org/10.1002/hyp.8205>. 13

LEMOS, J. R.; RODAL, M. J. N. Fitossociologia do componente lenhoso de um trecho da vegetação de caatinga no parque nacional serra da capivara, piauí, brasil. **Acta Botanica Brasilica**, v. 16, n. 1, p. 23–42, 1 2002. Available from: <https://doi.org/10.1590/s0102-33062002000100005>. 32

LI, C.; LI, H.; LI, J.; LEI, Y.; LI, C.; MANEVSKI, K.; SHEN, Y. Using NDVI percentiles to monitor real-time crop growth. **Computers and Electronics in Agriculture**, v. 162, p. 357–363, jul. 2019. Available from: <https://doi.org/10.1016/j.compag.2019.04.026>. 12, 53

LIMA, A. L. A.; RODAL, M. J. N. Phenology and wood density of plants growing in the semi-arid region of northeastern Brazil. **Journal of Arid Environments**, v. 74, p. 1363–1373, 11 2010. 1, 32, 67

LIMA, A. L. A. d.; SAMPAIO, E. V. de S. B.; CASTRO, C. C. de; RODAL, M. J. N.; ANTONINO, A. C. D.; MELO, A. L. de. Do the phenology and functional stem attributes of woody species allow for the identification of functional groups in the semiarid region of brazil? **Trees**, v. 26, n. 5, p. 1605—1616, 10 2012. ISSN 0931-1890. Available from: <https://doi.org/10.1007/s00468-012-0735-2>. 1, 31, 32, 33, 36, 47, 49, 58, 67

LOPEZ, J. G. **Construction of heat dissipation probes to estimate sap flow**. 2015. Available from: <http://rgdoi.net/10.13140/RG.2.1.1181.2004>. 15, 25, 26

LOUIS, J.; DEBAECKER, V.; PFLUG, B.; MAIN-KNORN, M.; BIENIARZ, J.; MüLLER-WILM, U.; CADAU, E.; GASCON, F. Sentinel-2 sen2cor: L2a processor for users. In: LIVING PLANET SYMPOSIUM. Prague, Czech Republic: ESA, 2016. p. 9–13. 24

LUBCZYNSKI, M. W.; CHAVARRO-RINCON, D. C.; ROSSITER, D. G. Conductive sapwood area prediction from stem and canopy areas-allometric equations of kalahari trees, botswana. **Ecohydrology**, v. 10, n. 6, p. e1856, 4 2017. Available from: <https://doi.org/10.1002/eco.1856>. 29, 57

MACHADO, I. C. S.; BARROS, L. M.; SAMPAIO, E. V. S. B. Phenology of caatinga species at serra talhada, PE, northeastern brazil. **Biotropica**, v. 29, n. 1, p. 57–68, 03 1997. Available from: <https://doi.org/10.1111/j.1744-7429.1997.tb00006.x>. 31

MAHR, D. Commiphora: an introduction to the genus. **Cactus and Succulent Journal**, v. 84, n. 3, p. 140–154, 5 2012. Available from: <https://doi.org/10.2985/0007-9367-84.3.140>. 49

MAPBIOMAS. **Caatinga: evolução anual da cobertura e uso da terra (1985-2019**. 2019. Available from: <https://mapbiomas-br-site.s3.amazonaws.com/Infograficos/Colecao5/MBI-Infografico-caatinga-5.0-BR.jpg>. Access in: 20 nov. 2020. 1, 5, 6, 53, 54

MARQUES, T. V.; MENDES, K.; MUTTI, P.; MEDEIROS, S.; SILVA, L.; PEREZ-MARIN, A. M.; CAMPOS, S.; LÚCIO, P. S.; LIMA, K.; REIS, J. dos;

RAMOS, T. M.; SILVA, D. F. da; OLIVEIRA, C. P.; COSTA, G. B.; ANTONINO, A. C.; MENEZES, R. S.; SILVA, C. M. S. e; BEZERRA, B. Environmental and biophysical controls of evapotranspiration from seasonally dry tropical forests (caatinga) in the brazilian semiarid. **Agricultural and Forest Meteorology**, v. 287, p. 107957, jun. 2020. Available from: <https://doi.org/10.1016/j.agrformet.2020.107957>. 2

MENDES, K. R.; CAMPOS, S.; SILVA, L. L. da; MUTTI, P. R.; FERREIRA, R. R.; MEDEIROS, S. S.; PEREZ-MARIN, A. M.; MARQUES, T. V.; RAMOS, T. M.; VIEIRA, M. M. de L.; OLIVEIRA, C. P.; GONÇALVES, W. A.; COSTA, G. B.; ANTONINO, A. C. D.; MENEZES, R. S. C.; BEZERRA, B. G.; SILVA, C. M. S. e. Seasonal variation in net ecosystem CO2 exchange of a brazilian seasonally dry tropical forest. **Scientific Reports**, v. 10, n. 1, jun. 2020. Available from: <https://doi.org/10.1038/s41598-020-66415-w>. 2

MESQUITA, D. O.; COSTA, G. C.; GARDA, A. A.; DELFIM, F. R. Species composition, biogeography, and conservation of the caatinga lizards. In: **Caatinga**. [s.n.], 2017. p. 151–180. Available from: <https://doi.org/10.1007/978-3-319-68339-3_6>. 6

MINER, G. L.; HAM, J. M.; KLUITENBERG, G. J. A heat-pulse method for measuring sap flow in corn and sunflower using 3d-printed sensor bodies and low-cost electronics. **Agricultural and Forest Meteorology**, v. 246, p. 86–97, 11 2017. Available from: <https://doi.org/10.1016/j.agrformet.2017.06.012>. 13, 14, 15

MIRANDA, R. de Q.; GALVÍNCIO, J. D.; MOURA, M. S. B. de; JONES, C. A.; SRINIVASAN, R. Reliability of MODIS evapotranspiration products for heterogeneous dry forest: a study case of caatinga. **Advances in Meteorology**, v. 2017, p. 1–14, 2017. Available from: <https://doi.org/10.1155/2017/9314801>. 53, 67

MIRANDA, R. de Q.; NÓBREGA, R. L. B.; MOURA, M. S. B. de; RAGHAVAN, S.; GALVÍNCIO, J. D. Realistic and simplified models of plant and leaf area indices for a seasonally dry tropical forest. **International Journal of Applied Earth Observation and Geoinformation**, v. 85, p. 101992, 3 2020. Available from: <https://doi.org/10.1016/j.jag.2019.101992>. 2, 12, 32, 33, 53, 67

MOONLIGHT, P.; BANDA-R, K.; PHILLIPS, O.; DEXTER, K.; PENNINGTON, R.; BAKER, T.; LIMA, H. C. de; FAJARDO, L.; GONZÁLEZ-M, R.;

LINARES-PALOMINO, R.; LLOYD, J.; NASCIMENTO, M.; PRADO, D.; QUINTANA, C.; RIINA, R.; M., G. R.; VILLELA, D.; AQUINO, A.; ARROYO, L.; BEZERRA, C.; BRUNELLO, A. T.; BRIENEN, R.; CARDOSO, D.; CHAO, K.-J.; COUTINHO, I. C.; CUNHA, J.; DOMINGUES, T.; SANTO, M. do E.; FELDPAUSCH, T.; FERNANDES, M. F.; GOODWIN, Z.; JIMÉNEZ, E.; LEVESLEY, A.; LOPEZ-TOLEDO, L.; MARIMON, B.; MIATTO, R.; MIZUSHIMA, M.; MONTEAGUDO, A.; MOURA, M. de; MURAKAMI, A.; NEVES, D.; CHEQUÍN, R.; OLIVEIRA, T. de S.; OLIVEIRA, E. de; QUEIROZ, L. de; PILON, A.; RAMOS, D.; REYNEL, C.; RODRIGUES, P.; SANTOS, R.; SÄRKINEN, T.; SILVA, V. da; SOUZA, R.; VASQUEZ, R.; VEENENDAAL, E. Expanding tropical forest monitoring into dry forests: the dryflor protocol for permanent plots. **Plants, People, Planet**, April 2020. Available from: <http://eprints.whiterose.ac.uk/159622/>. 34, 36, 57

MURPHY, P. G.; LUGO, A. E. Ecology of tropical dry forest. **Annual Review of Ecology and Systematics**, v. 17, n. 1, p. 67–88, 11 1986. Available from: <https://doi.org/10.1146/annurev.es.17.110186.000435>. 31

NATIONAL AERONAUTICS AND SPACE ADMINISTRATION - NASA. **Moderate resolution imaging spectroradiometer**. 2020. Available from: <https://modis.gsfc.nasa.gov/about/design.php>. Access in: 29 nov. 2020. 10

_____. **Moderate resolution imaging spectroradiometer Data Products**. 2020. Available from: <https://modis.gsfc.nasa.gov/data/dataprod/>. Access in: 29 nov. 2020. 53

OLIVEIRA, C. C. de; ZANDAVALLI, R. B.; LIMA, A. L. A. de; RODAL, M. J. N. Functional groups of woody species in semi-arid regions at low latitudes. **Austral Ecology**, v. 40, n. 1, p. 40–49, 7 2014. Available from: <https://doi.org/10.1111/aec.12165>. 47

OLIVEIRA, G. F.; GARCIA, A. C. L.; MONTES, M. A.; JUCÁ, J. C. L. D. A.; VALENTE, V. L. D. S.; ROHDE, C. Are conservation units in the caatinga biome, brazil, efficient in the protection of biodiversity? an analysis based on the drosophilid fauna. **Journal for Nature Conservation**, v. 34, p. 145–150, dec. 2016. Available from: <https://doi.org/10.1016/j.jnc.2016.10.006>. 5

PARKINSON, C. L.; GUIT, W. J. **Status of the Aqua Mission**. 2019. Available from: <https://modis.gsfc.nasa.gov/about/design.php>. Access in: 29 nov. 2020. 10

PASQUALOTTO, G.; CARRARO, V.; MENARDI, R.; ANFODILLO, T. Calibration of granier-type (TDP) sap flow probes by a high precision electronic potometer. **Sensors**, v. 19, n. 10, p. 2419, 5 2019. Available from: <https://doi.org/10.3390/s19102419>. 1, 2, 13, 14, 33

PATAKI, D. E.; MCCARTHY, H. R.; LITVAK, E.; PINCETL, S. Transpiration of urban forests in the los angeles metropolitan area. **Ecological Applications**, v. 21, n. 3, p. 661–677, 04 2011. Available from: <https://doi.org/10.1890/09-1717.1>. 13

PENNINGTON, R. T.; LAVIN, M.; OLIVEIRA-FILHO, A. Woody plant diversity, evolution, and ecology in the tropics: Perspectives from seasonally dry tropical forests. **Annual Review of Ecology, Evolution, and Systematics**, v. 40, n. 1, p. 437–457, 12 2009. Available from: <https://doi.org/10.1146/annurev.ecolsys.110308.120327>. 31

PENNINGTON, R. T.; LEHMANN, C. E.; ROWLAND, L. M. Tropical savannas and dry forests. **Current Biology**, v. 28, n. 9, p. R541–R545, 05 2018. Available from: <https://doi.org/10.1016/j.cub.2018.03.014>. 31

PICOLI, M. C. A.; SIMOES, R.; CHAVES, M.; SANTOS, L. A.; SANCHEZ, A.; SOARES, A.; SANCHES, I. D.; FERREIRA, K. R.; QUEIROZ, G. R. Cbers data cube: a powerful technology for mapping and monitoring brazilian biomes. **ISPRS Annals of Photogrammetry, Remote Sensing and Spatial Information Sciences**, V-3-2020, p. 533–539, aug. 2020. Available from: <https://doi.org/10.5194/isprs-annals-v-3-2020-533-2020>. 2, 25

PING, L.; LAYRENT, U.; PING, Z. Granier's thermal dissipation probe (tdp) method for measuring sap flow in trees: theory and practice. **Acta Botanica Sinica**, v. 46, p. 631–646, 2004. 1, 2, 14, 15, 26, 27, 33

PUGNAIRE, F. I.; MORILLO, J. A.; PEÑUELAS, J.; REICH, P. B.; BARDGETT, R. D.; GAXIOLA, A.; WARDLE, D. A.; PUTTEN, W. H. van der. Climate change effects on plant-soil feedbacks and consequences for biodiversity and functioning of terrestrial ecosystems. **Science Advances**, v. 5, n. 11, p. eaaz1834, 11 2019. Available from: <https://doi.org/10.1126/sciadv.aaz1834>. 1, 31

QUEIROZ, L. P. de; CARDOSO, D.; FERNANDES, M. F.; MORO, M. F. Diversity and evolution of flowering plants of the caatinga domain. In: **Caatinga**.

Springer International Publishing, 2017. p. 23–63. Available from: <https://doi.org/10.1007/978-3-319-68339-3_2>. 5, 8

R CORE TEAM. **R: a language and environment for statistical computing**. Vienna, Austria, 2019. Available from: <https://www.R-project.org/>. 19

RAFI, Z.; MERLIN, O.; DANTEC, V. L.; KHABBA, S.; MORDELET, P.; ER-RAKI, S.; AMAZIRH, A.; OLIVERA-GUERRA, L.; HSSAINE, B. A.; SIMONNEAUX, V.; EZZAHAR, J.; FERRER, F. Partitioning evapotranspiration of a drip-irrigated wheat crop: Inter-comparing eddy covariance-, sap flow-, lysimeter- and FAO-based methods. **Agricultural and Forest Meteorology**, v. 265, p. 310–326, feb. 2019. Available from: <https://doi.org/10.1016/j.agrformet.2018.11.031>. 13

REDDY, S. Climatic classification: the semi-arid tropics and its environment — a review. **Pesquisa Agro**, v. 18, p. 823–847, 1983. 32

REICH, P. B.; WRIGHT, I. J.; CAVENDER-BARES, J.; CRAINE, J. M.; OLEKSYN, J.; WESTOBY, M.; WALTERS, M. B. The evolution of plant functional variation: traits, spectra, and strategies. **International Journal of Plant Sciences**, v. 164, n. S3, p. S143–S164, 5 2003. Available from: <https://doi.org/10.1086/374368>. 32

REIS, A. C. Clima da caatinga. **Anais da Academia Brasileira de Ciências**, v. 48, p. 325–335, 1976. 1, 64

REN, R.; CRONE, J. von der; HORTON, R.; LIU, G.; STEPPE, K. An improved single probe method for sap flow measurements using finite heating duration. **Agricultural and Forest Meteorology**, v. 280, p. 107788, 1 2020. Available from: <https://doi.org/10.1016/j.agrformet.2019.107788>. 1, 2, 13, 33

RESTREPO-COUPE, N.; ROCHA, H. R. da; HUTYRA, L. R.; ARAUJO, A. C. da; BORMA, L. S.; CHRISTOFFERSEN, B.; CABRAL, O. M.; CAMARGO, P. B. de; CARDOSO, F. L.; COSTA, A. C. L. da; FITZJARRALD, D. R.; GOULDEN, M. L.; KRUIJT, B.; MAIA, J. M.; MALHI, Y. S.; MANZI, A. O.; MILLER, S. D.; NOBRE, A. D.; RANDOW, C. von; SÁ, L. D. A.; SAKAI, R. K.; TOTA, J.; WOFSY, S. C.; ZANCHI, F. B.; SALESKA, S. R. What drives the seasonality of photosynthesis across the amazon basin? a cross-site analysis of eddy flux tower measurements from the brasil flux network. **Agricultural and Forest Meteorology**, v. 182-183, p. 128–144, 12 2013. Available from: <https://doi.org/10.1016/j.agrformet.2013.04.031>. 11

RICHARDSON, A. D. Tracking seasonal rhythms of plants in diverse ecosystems with digital camera imagery. **New Phytologist**, v. 222, n. 4, p. 1742–1750, 12 2019. Available from: <https://doi.org/10.1111/nph.15591>. 2, 11

RICHARDSON, A. D.; BRASWELL, B. H.; HOLLINGER, D. Y.; JENKINS, J. P.; OLLINGER, S. V. Near-surface remote sensing of spatial and temporal variation in canopy phenology. **Ecological Applications**, v. 19, n. 6, p. 1417–1428, 9 2009. Available from: <https://doi.org/10.1890/08-2022.1>. 11, 22

RICHARDSON, A. D.; HUFKENS, K.; MILLIMAN, T.; AUBRECHT, D. M.; CHEN, M.; GRAY, J. M.; JOHNSTON, M. R.; KEENAN, T. F.; KLOSTERMAN, S. T.; KOSMALA, M.; MELAAS, E. K.; FRIEDL, M. A.; FROLKING, S. Tracking vegetation phenology across diverse north american biomes using PhenoCam imagery. **Scientific Data**, v. 5, n. 1, 03 2018. Available from: <https://doi.org/10.1038/sdata.2018.28>. 2, 32, 33, 39, 51

RUBEL, F.; BRUGGER, K.; HASLINGER, K.; AUER, I. The climate of the european alps: Shift of very high resolution köppen-geiger climate zones 1800–2100. **Meteorologische Zeitschrift**, v. 26, n. 2, p. 115–125, 4 2017. Available from: <https://doi.org/10.1127/metz/2016/0816>. 34

SAMPAIO, E. V. Overview of the brazilian caatinga. In: BULLOCK S. H.; MOONEY, H. A. E. (Ed.). **Seasonally Dry Tropical Forests**. Cambridge University Press, 1995. p. 35–63. Available from: <https://doi.org/10.1017/cbo9780511753398.003>. 32

SÁNCHEZ-CARRILLO, S.; ÁLVAREZ-COBELAS, M.; BENÍTEZ, M.; ANGELER, D. G. A simple method for estimating water loss by transpiration in wetlands. **Hydrological Sciences Journal**, v. 46, n. 4, p. 537–552, 08 2001. Available from: <https://doi.org/10.1080/02626660109492849>. 13

SANTANA, N. Fire recurrence and normalized difference vegetation index (NDVI) dynamics in brazilian savanna. **Fire**, v. 2, n. 1, p. 1, dec. 2018. Available from: <https://doi.org/10.3390/fire2010001>. 12, 53

SANTOS, C. A. C. dos; MARIANO, D. A.; NASCIMENTO, F. das Chagas A. do; DANTAS, F. R. da C.; OLIVEIRA, G. de; SILVA, M. T.; SILVA, L. L. da; SILVA, B. B. da; BEZERRA, B. G.; SAFA, B.; MEDEIROS, S. de S.; NEALE, C. M. Spatio-temporal patterns of energy exchange and evapotranspiration during an intense drought for drylands in brazil. **International Journal of Applied**

Earth Observation and Geoinformation, v. 85, p. 101982, mar. 2020. Available from: <https://doi.org/10.1016/j.jag.2019.101982>. 2

SÄRKINEN, T.; IGANCI, J. R.; LINARES-PALOMINO, R.; SIMON, M. F.; PRADO, D. E. Forgotten forests - issues and prospects in biome mapping using Seasonally Dry Tropical Forests as a case study. **BMC Ecology**, v. 11, n. November, 2011. ISSN 14726785. 31

SEKI, K. Swrc fit - a nonlinear fitting program with a water retention curve for soils having unimodal and bimodal pore structure. **Hydrology and Earth System Sciences Discussions**, v. 4, p. 407–437, 2007. Available from: <https://www.hydrol-earth-syst-sci-discuss.net/4/407/2007/>. 20

SEO, B.; LEE, J.; LEE, K.-D.; HONG, S.; KANG, S. Improving remotely-sensed crop monitoring by NDVI-based crop phenology estimators for corn and soybeans in iowa and illinois, USA. **Field Crops Research**, v. 238, p. 113–128, 5 2019. Available from: <https://doi.org/10.1016/j.fcr.2019.03.015>. 12, 53

SIDHU, N.; PEBESMA, E.; CÂMARA, G. Using google earth engine to detect land cover change: Singapore as a use case. **European Journal of Remote Sensing**, v. 51, n. 1, p. 486–500, jan. 2018. Available from: <https://doi.org/10.1080/22797254.2018.1451782>. 2

SILVA, M. A. O.; ANDRADE, A. C. de. Geração de imagens de reflectância de um ponto de vista geométrico. **Revista Brasileira de Geomática**, v. 1, p. 23–30, 2013. Available from: <https://periodicos.utfpr.edu.br/rbgeo/article/view/5434>. 25

SILVA, P. F. da; LIMA, J. R. d. S.; ANTONINO, A. C. D.; SOUZA, R.; SOUZA, E. S. de; SILVA, J. R. I.; ALVES, E. M. Seasonal patterns of carbon dioxide, water and energy fluxes over the Caatinga and grassland in the semi-arid region of Brazil. **Journal of Arid Environments**, v. 147, p. 71–82, dec 2017. 5, 19, 41

SOBRADO, M. A. Trade-off between water transport efficiency and leaf life-span in a tropical dry forest. **Oecologia**, v. 96, n. 1, p. 19–23, 10 1993. Available from: <https://doi.org/10.1007/bf00318025>. 32, 49, 67

SOIL-SURVEY-STAFF. **Soil taxonomy: a basic system of soil classification of making and interpreting soil surveys**. Washington, D.C.: Natural Resources Conservation Service, 1999. 869 p. (USDA. Agriculture Handbook, 436). 34

SOUZA, L. S. B. de; MOURA, M. S. B. de; SEDIYAMA, G. C.; SILVA, T. G. F. da. Carbon exchange in a caatinga area during an unusually drought year. **Agrometeoros**, v. 25, n. 1, 11 2018. Available from: <https://doi.org/10.31062/agrom.v25i1.26265>. 2

SOUZA, M. J. N. de; OLIVEIRA, J. G. B. de; LINS, R. C.; JATOBá, L. Overview of the brazilian caatinga. **Revista Ciência & Trópico**, v. 20, n. 1, p. 173–198, 1992. 32

STANLEY, F. C.; MERCANTI, E. P.; BECKER, M. A. **Third Earth resources technology satellite-1 symposium. Volume 1 technical presentations, section A**. Washington, D.C, 1973. Volume 1: Technical Presentations Section A. Available from: <https://ntrs.nasa.gov/citations/19740022592>. Access in: 07 nov. 2020. 9, 12

STRATTON, L.; GOLDSTEIN, G.; MEINZER, F. C. Stem water storage capacity and efficiency of water transport: their functional significance in a hawaiian dry forest. **Plant, Cell & Environment**, v. 23, n. 1, p. 99–106, 1 2000. Available from: <https://doi.org/10.1046/j.1365-3040.2000.00533.x>. 32, 49, 67

SWENSON, N. G.; ENQUIST, B. J. Ecological and evolutionary determinants of a key plant functional trait: wood density and its community-wide variation across latitude and elevation. **American Journal of Botany**, v. 94, n. 3, p. 451–459, 3 2007. Available from: <https://doi.org/10.3732/ajb.94.3.451>. 32

TEIXEIRA, A. de C.; BASTIAANSSEN, W.; AHMAD, M.; MOURA, M.; BOS, M. Analysis of energy fluxes and vegetation-atmosphere parameters in irrigated and natural ecosystems of semi-arid brazil. **Journal of Hydrology**, v. 362, n. 1-2, p. 110–127, 11 2008. Available from: <https://doi.org/10.1016/j.jhydrol.2008.08.011>. 13

TEIXEIRA, A. H. de C. Determining regional actual evapotranspiration of irrigated crops and natural vegetation in the são francisco river basin (brazil) using remote sensing and penman-monteith equation. **Remote Sensing**, v. 2, n. 5, p. 1287–1319, 5 2010. Available from: <https://doi.org/10.3390/rs0251287>. 2, 12, 33, 53

TETENS, O. Uber einige meteorologische begriffe. **z. Geophys**, v. 6, p. 297–309, 1930. 48

TOPP G.C.AND DAVIS, J.; P.ANNAN, A. Electromagnetic determination of soil water content: Measurment in coaxial transmission lines. **Water Resources Research**, v. 16, p. 574–582, 1980. 20

TORRES, R. R.; LAPOLA, D. M.; GAMARRA, N. L. R. Future climate change in the caatinga. In: SILVA J. M. C.; LEAL, I. R. T. M. E. (Ed.). **Caatinga**. Springer International Publishing, 2017. p. 383–410. Available from: <https://doi.org/10.1007/978-3-319-68339-3_15>. 1, 7, 53

TROVÃO, D. M. de B. M.; FERNANDES, P. D.; ANDRADE, L. A. de; NETO, J. D. Variações sazonais de aspectos fisiológicos de espécies da caatinga. **Revista Brasileira de Engenharia Agrícola e Ambiental**, v. 11, n. 3, p. 307–311, jun. 2007. Available from: <https://doi.org/10.1590/s1415-43662007000300010>. 1

VAJSOVÁ, B.; FASBENDER, D.; WIRNHARDT, C.; LEMAJIC, S.; DEVOS, W. Assessing spatial limits of sentinel-2 data on arable crops in the context of checks by monitoring. **Remote Sensing**, v. 12, n. 14, p. 2195, 07 2020. Available from: <https://doi.org/10.3390/rs12142195>. 38

VELOSO, A. L. **Ecorregiões propostas para o Bioma Caatinga: resultados do Seminário de Planejamento Ecorregional da Caatinga**. Recife: Associação Plantas do Nordeste, 2001. 80 p. 1, 5, 6

VERHOEF, A.; EGEA, G. Modeling plant transpiration under limited soil water: Comparison of different plant and soil hydraulic parameterizations and preliminary implications for their use in land surface models. **Agricultural and Forest Meteorology**, v. 191, p. 22–32, 6 2014. Available from: <https://doi.org/10.1016/j.agrformet.2014.02.009>. 9, 21

WILLIAMS, D.; CABLE, W.; HULTINE, K.; HOEDJES, J.; YEPEZ, E.; SIMONNEAUX, V.; ER-RAKI, S.; BOULET, G.; BRUIN, H. de; CHEHBOUNI, A.; HARTOGENSIS, O.; TIMOUK, F. Evapotranspiration components determined by stable isotope, sap flow and eddy covariance techniques. **Agricultural and Forest Meteorology**, v. 125, n. 3-4, p. 241–258, oct. 2004. Available from: <https://doi.org/10.1016/j.agrformet.2004.04.008>. 13

WOEBBECKE, D. M.; MEYER, G. E.; BARGEN, K. V.; MORTENSEN, D. A. Color indices for weed identification under various soil, residue, and lighting conditions. **Transactions of the ASAE**, v. 38, n. 1, p. 259–269, 1995. Available from: <https://doi.org/10.13031/2013.27838>. 11, 22

WOLFE, R.; THOME, K.; TSAY, S.-C. **Status of the Terra Mission**. 2019. Available from: <https://modis.gsfc.nasa.gov/sci_team/meetings/201911/presentations/plenary/wolfe.pdf>. Access in: 29 nov. 2020. 10, 11

WUTZLER, T.; REICHSTEIN, M.; MOFFAT, A. M.; MIGLIAVACCA, M. **REddyProc: Post Processing of (Half-)Hourly Eddy-Covariance Measurements**. [S.l.], 2019. R package version 1.2. Available from: <https://CRAN.R-project.org/package=REddyProc>. 19

YAN, L.; ROY, D.; LI, Z.; ZHANG, H.; HUANG, H. Sentinel-2a multi-temporal misregistration characterization and an orbit-based sub-pixel registration methodology. **Remote Sensing of Environment**, v. 215, p. 495–506, 09 2018. Available from: <https://doi.org/10.1016/j.rse.2018.04.021>. 39

APPENDIX A - SAPWOOD ESTIMATION

In this section is presented variance analysis (ANOVA) used to calculate the parameters used in the estimation of sapwood in the chapters presented. The regression parameters was estimated using the Diameter at Breast Height (DBH), at 1.3m of height, referred in the figures as "Total" (total trunk diameter including bark, xylem, sapwood and hardwood). The analysis discounting the bark (not included here) showed no significant difference.

The Figure A.1 contains the ANOVA considering only the individuals of Petrolina site. The Figure A.2 contains the scatter plot Scatter-plot between sapwood and DBH of these Petrolina individuals.

Figure A.1 - Analysis of sapwood predicted by DBH for Petrolina site.

```
Residuals:
    Min      1Q  Median      3Q     Max
-4.4712 -2.1135 -0.6937  1.5691  6.0527

Coefficients:
            Estimate Std. Error t value Pr(>|t|)
(Intercept)  4.42469    1.88515   2.347   0.0321 *
total        0.15871    0.02481   6.396 8.85e-06 ***
---
Signif. codes:  0 '***' 0.001 '**' 0.01 '*' 0.05 '.' 0.1 ' ' 1
Residual standard error: 2.892 on 16 degrees of freedom
Multiple R-squared:  0.7189,    Adjusted R-squared:  0.7013
F-statistic: 40.91 on 1 and 16 DF,  p-value: 8.853e-06

Confidence interval
                2.5 %    97.5 %
(Intercept) 0.4283571 8.4210178
total       0.1061090 0.2113116
```

Figure A.2 - Scatter-plot between sapwood and DBH (total) for Petrolina site.

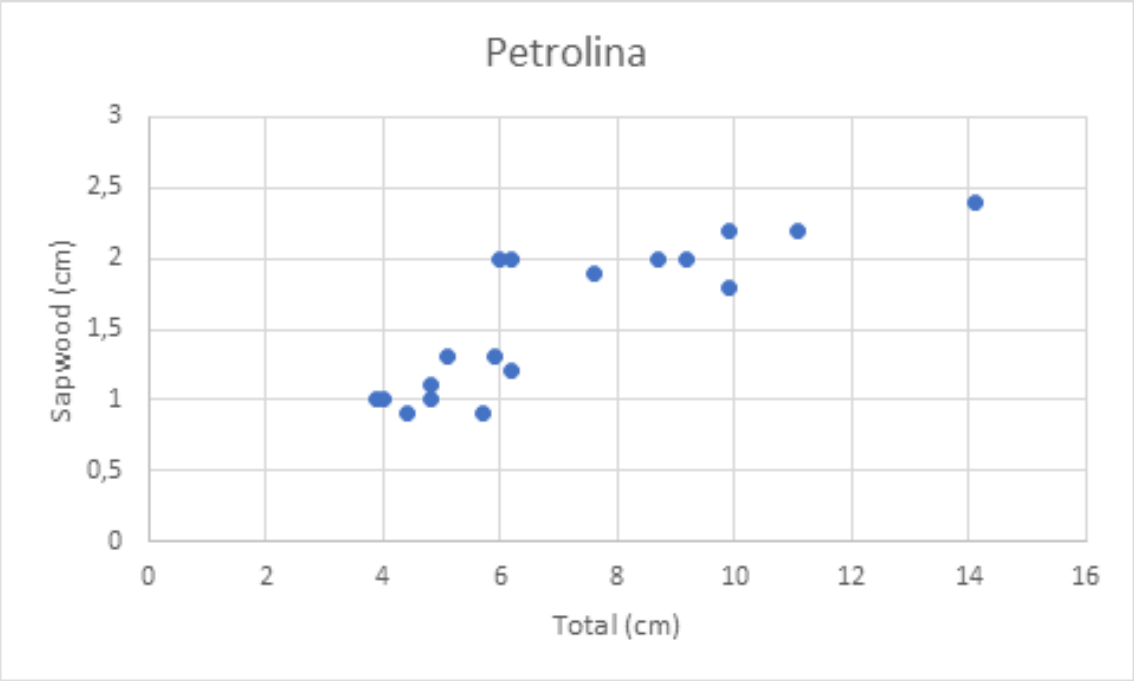

The Figure A.3 contains the ANOVA considering only the individuals of Serra Talhada site. The Figure A.4 contains the scatter plot Scatter-plot between sapwood and DBH of these Serra Talhada site individuals.

Figure A.3 - Analysis of sapwood predicted by DBH for Petrolina site.

```
Residuals:
     Min       1Q   Median       3Q      Max
-1.67208 -0.46267  0.07502  0.50101  1.42991

Coefficients:
             Estimate Std. Error t value Pr(>|t|)
(Intercept)  0.60969    0.36891   1.653 0.113272
total        0.15902    0.03799   4.186 0.000416 ***
---
Signif. codes:  0 '***' 0.001 '**' 0.01 '*' 0.05 '.' 0.1 ' ' 1

Residual standard error: 0.8006 on 21 degrees of freedom
Multiple R-squared:  0.4549,    Adjusted R-squared:  0.429
F-statistic: 17.53 on 1 and 21 DF,  p-value: 0.0004161

Confidence interval
                2.5 %    97.5 %
(Intercept) -0.15750653 1.3768937
total        0.08002611 0.2380165
```

Figure A.4 - Scatter-plot between sapwood and DBH (total) for Serra Talhada site.

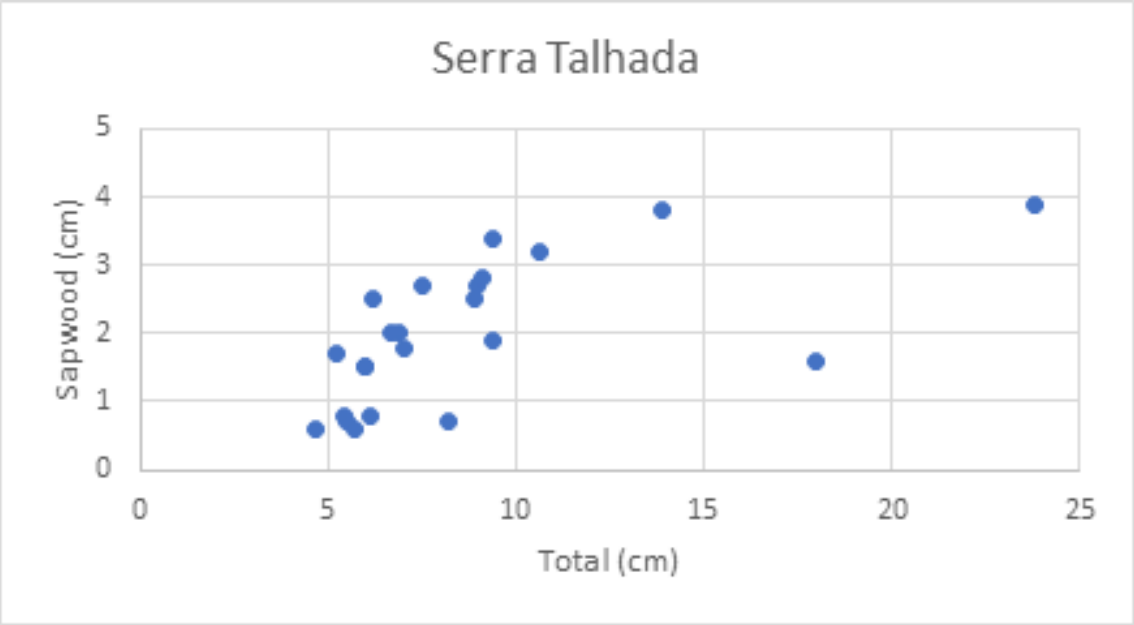

The Figure A.5 contains the ANOVA considering both individuals of Serra Talhada

and Petrolina site. The Figure A.6 contains the scatter plot Scatter-plot between sapwood and DBH of these individuals. In this case, as in Serra Talhada, the intercept was considered not significant, so the model was generated considering the intercept equal to 0.

Figure A.5 - Analysis of sapwood predicted by DBH for Petrolina and Serra Talhada site.

```
Residuals:
    Min      1Q  Median      3Q     Max
-1.6417 -0.3135 -0.1142  0.3048  1.4783

Coefficients:
            Estimate Std. Error t value Pr(>|t|)
(Intercept)  0.50033    0.22357   2.238    0.031 *
Total          0.16341    0.02527   6.466 1.17e-07 ***
---
Signif. codes:  0 '***' 0.001 '**' 0.01 '*' 0.05 '.' 0.1 ' ' 1

Residual standard error: 0.6217 on 39 degrees of freedom
Multiple R-squared:  0.5174,    Adjusted R-squared:  0.505
F-statistic:  41.8 on 1 and 39 DF,  p-value: 1.17e-07

Confidence interval:

                2.5 %    97.5 %
(Intercept) 0.0481085 0.9525508
Total       0.1122903 0.2145323
```

Figure A.6 - Scatter-plot between sapwood and DBH (total) for Petrolina and Serra Talhada site.

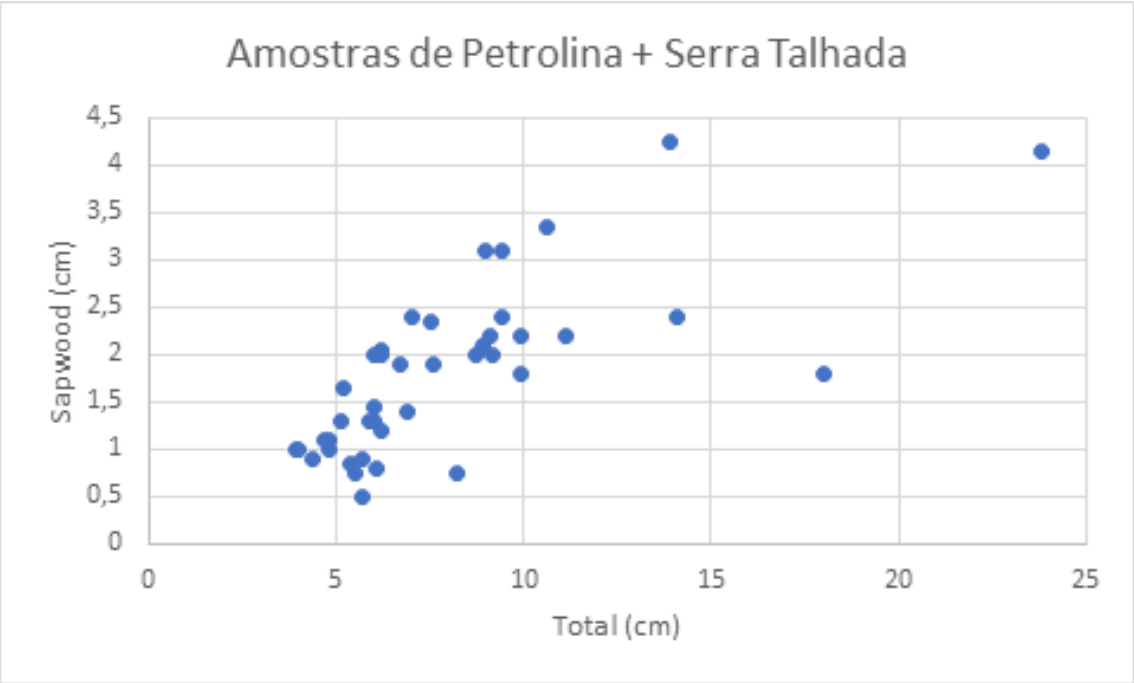

APPENDIX B - SAP FLOW AND SOIL SENSOR DATALOGGER

This Appendix contains the electronic schematic, circuits and the component lists of the loggers built and uses in this work. For the construction of these loggers, the Arduino platform was used.

Figure B.1 - Electronic schematic of soil sensor logger.

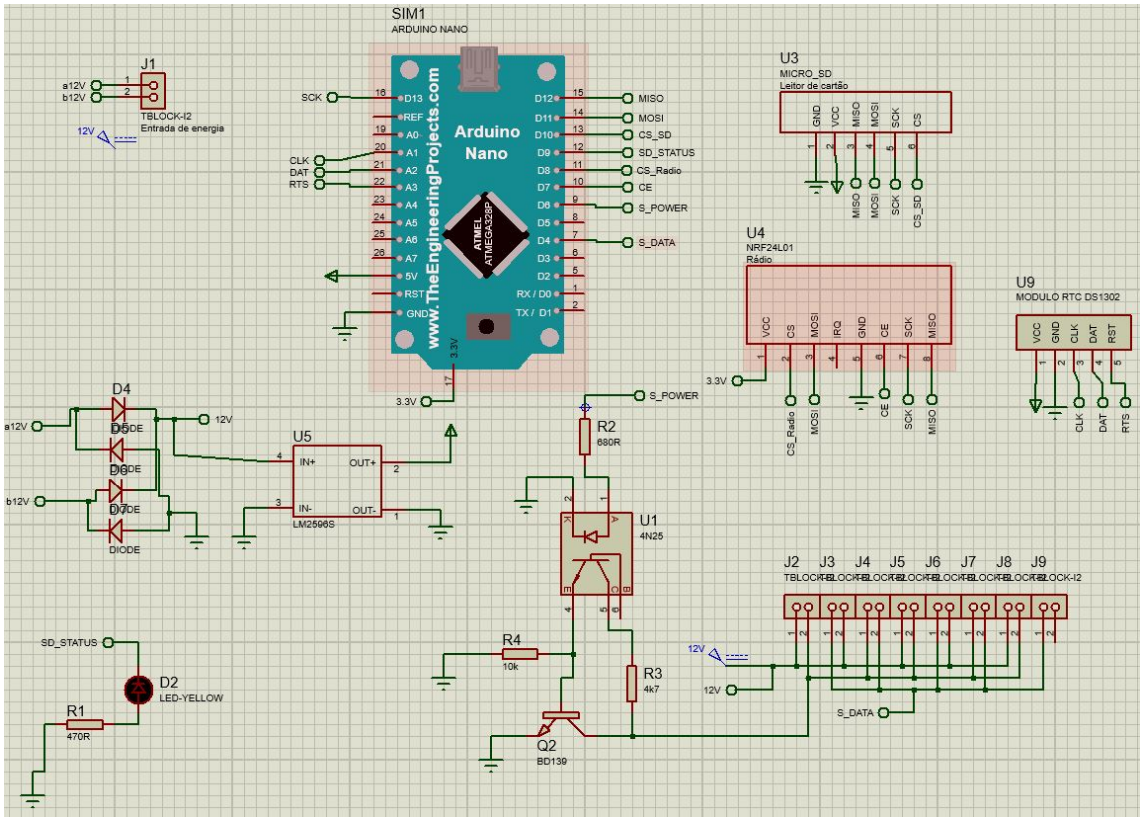

Figure B.2 - Electronic board of soil sensor logger.

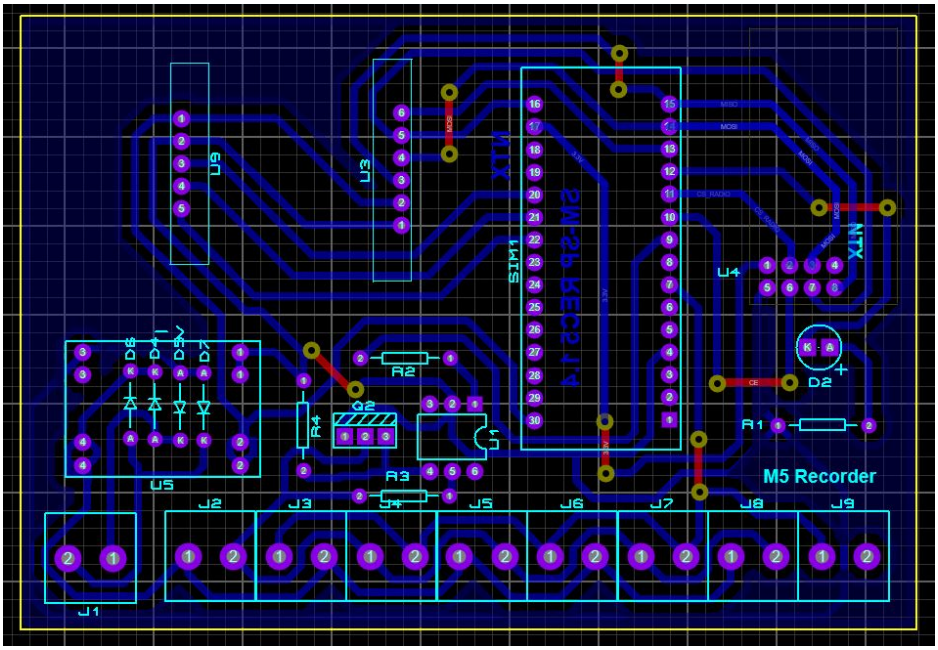

Figure B.3 - Component list of soil sensor logger.

Category	Quantity	References	Value
Transistors	1	Q2	BD139
Resistors	1	R1	470R
Resistors	1	R2	680R
Resistors	1	R3	4k7
Resistors	1	R4	10k
Miscellaneous	9	J1,J2,J3,J4,J5,J6,J7,J8,J9	Terminal
Miscellaneous	1	SIM1	ARDUINO NANO
Integrated Circuits	1	U1	4N25
Integrated Circuits	1	U3	MICRO_SD
Integrated Circuits	1	U4	NRF24L01
Integrated Circuits	1	U5	LM2596S
Integrated Circuits	1	U9	MODULO RTC DS1302
Diodes	1	D2	LED-YELLOW
Diodes	4	D4,D5,D6,D7	DIODE

Figure B.4 - Electronic schematic of sap flow logger.

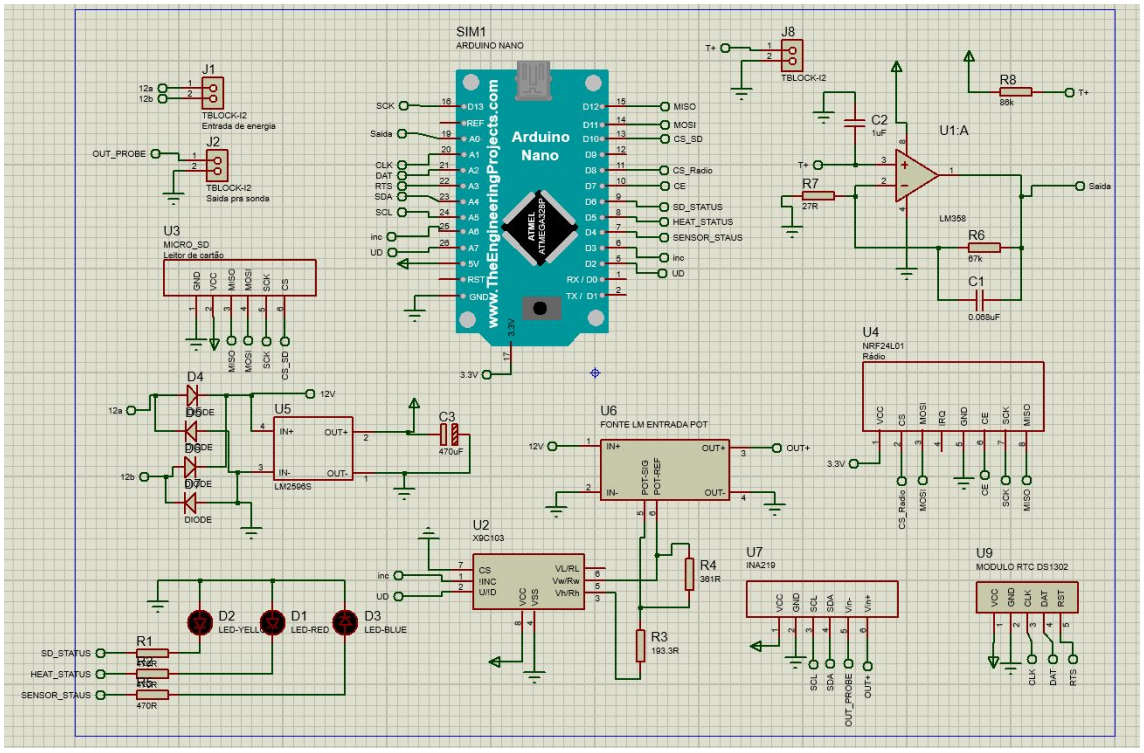

Figure B.5 - Electronic board of sap flow logger.

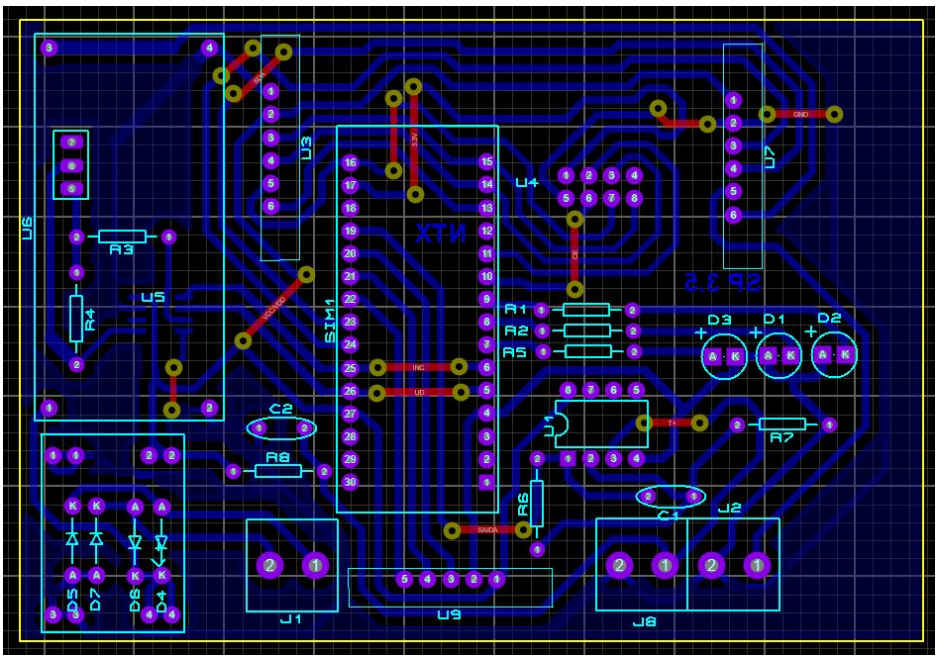

Figure B.6 - Component list of sap flow logger.

Category	Quantity	References	Value
Resistors	3	R1,R2,R5	470R
Resistors	1	R3	193.3R
Resistors	1	R4	361R
Resistors	1	R6	67k
Resistors	1	R7	27R
Resistors	1	R8	86k
Miscellaneous	3	J1,J2,J8	TERMINAL
Miscellaneous	1	SIM1	ARDUINO NANO
Integrated Circuits	1	U1	LM358
Integrated Circuits	1	U2	CI X9C103
Integrated Circuits	1	U3	MICRO_SD
Integrated Circuits	1	U4	NRF24L01
Integrated Circuits	1	U5	LM2596S
Integrated Circuits	1	U6	Power LM ENTRADA POT
Integrated Circuits	1	U7	INA219
Integrated Circuits	1	U9	MODULO RTC DS1302
Diodes	1	D1	LED-RED
Diodes	1	D2	LED-YELLOW
Diodes	1	D3	LED-BLUE
Diodes	4	D4,D5,D6,D7	DIODE
Capacitors	1	C1	0.068uF
Capacitors	1	C2	1uF
Capacitors	1	C3	470uF

APPENDIX C - LGE SAP FLOW DATA PER SPECIES

In this Appendix is shown the sap flow (F_{dn} per species (Figure C.1) to Lagoa Grande (LGE) site.

Figure C.1 - a) Rainfall (mm day^{-1}) and soil water profile relative saturation (S_w, dimensionless); Species averaged sap flow density, F_{dn} (dimensionless) together with S_w for: b) *C. nordestinum*; (c *S. polyphylla*; f) *A. colubrina* and; g) *C. leptophloeos*.

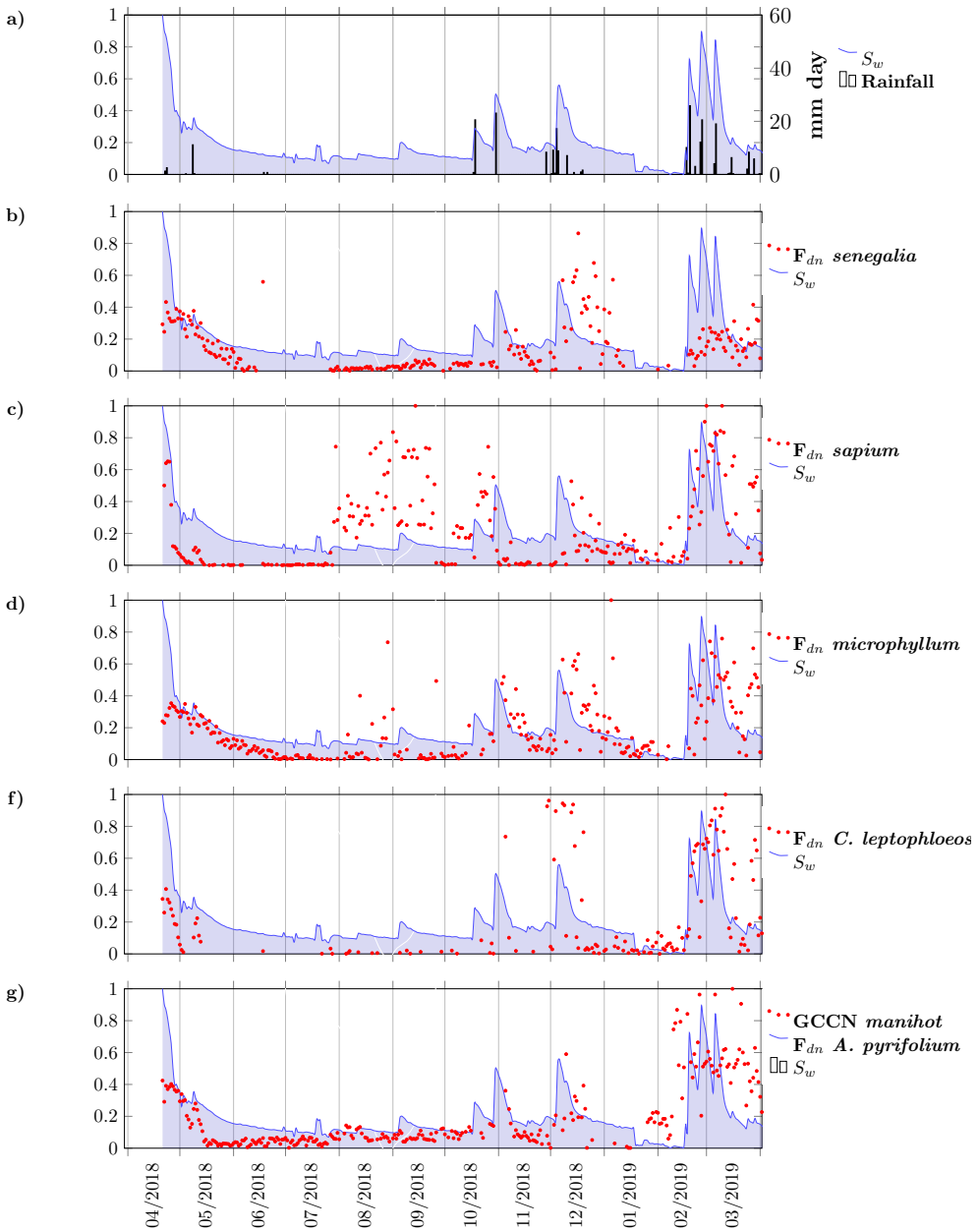

PUBLICAÇÕES TÉCNICO-CIENTÍFICAS EDITADAS PELO INPE

Teses e Dissertações (TDI)

Teses e Dissertações apresentadas nos Cursos de Pós-Graduação do INPE.

Notas Técnico-Científicas (NTC)

Incluem resultados preliminares de pesquisa, descrição de equipamentos, descrição e ou documentação de programas de computador, descrição de sistemas e experimentos, apresentação de testes, dados, atlas, e documentação de projetos de engenharia.

Propostas e Relatórios de Projetos (PRP)

São propostas de projetos técnico-científicos e relatórios de acompanhamento de projetos, atividades e convênios.

Publicações Seriadas

São os seriados técnico-científicos: boletins, periódicos, anuários e anais de eventos (simpósios e congressos). Constam destas publicações o Internacional Standard Serial Number (ISSN), que é um código único e definitivo para identificação de títulos de seriados.

Pré-publicações (PRE)

Todos os artigos publicados em periódicos, anais e como capítulos de livros.

Manuais Técnicos (MAN)

São publicações de caráter técnico que incluem normas, procedimentos, instruções e orientações.

Relatórios de Pesquisa (RPQ)

Reportam resultados ou progressos de pesquisas tanto de natureza técnica quanto científica, cujo nível seja compatível com o de uma publicação em periódico nacional ou internacional.

Publicações Didáticas (PUD)

Incluem apostilas, notas de aula e manuais didáticos.

Programas de Computador (PDC)

São a seqüência de instruções ou códigos, expressos em uma linguagem de programação compilada ou interpretada, a ser executada por um computador para alcançar um determinado objetivo. Aceitam-se tanto programas fonte quanto os executáveis.